N°d'ordre NNT : 2018LYSEC030

THESE de DOCTORAT DE L'UNIVERSITE DE LYON opérée au sein de l'Ecole Centrale de Lyon

Ecole Doctorale : Matériaux – ED 034

Spécialité : Matériaux

Date de soutenance prévue le 08/11/2018, par :

Jian ZHANG

Orthogonal chemical functionalization of titanium tungsten (TiW) based multimaterial surfaces

Fonctionnalisation chimique de surface de substrats de TiW. Application au dévelopement de la fonctionnalisation chimique orthogonale de substrats composés de TiW/Au/SiO_2

Thèse préparée à l'Institut des Nanotechnologies de Lyon
sous la direction de Jean-Pierre Cloarec et Yann Chevolot

Devant le jury composé de:

Pr. Claude Jolivalt, Professeure UPMC, LRS UMR 7197, Paris	Présidente (Rapporteure)
Dr. Luc Vellutini, Maître de conférence-HDR Université de Bordeaux, ISM UMR 5255, Bordeaux	Rapporteur
Dr. Stéphane Monfray, Ingénieur STMicroelectonics, Grenoble	Invité
Pr. Jean-Pierre Cloarec, Professeur ECL, INL UMR 5270, Lyon	Directeur de thèse
Dr. Yann Chevolot, DR-CNRS-HDR, INL UMR 5270, Lyon	Co-directeur de thèse

Acknowledgements

Firstly, I would like to thank all the committee members for their time and consideration, especially Pr. Claude Jolivalt and Dr. Luc Vellutini for the evaluation of this dissertation. I thank Dr. Stéphane Monfray to review my thesis. The thesis would not have been completed without their cooperation and constructive suggestions.

Secondly, I am so grateful for the PhD fellowship from China Scholarship Council (CSC), which gave me financial aids to carry out my thesis work in France.

Thirdly, I thank Dr. Catherine Bru-Chevallier and Dr. Christian Seassal, director and vice director of Institut des Nanotechnologies de Lyon, as well as Dr. Jean-Yves Buffière, director of École Doctorale Matériaux de Lyon.

Fourth, I thank my PhD my supervisors Pr. Jean-Pierre Cloarec and Dr. Yann Chevolot. It has been a pleasure to work under their supervision. They brought me into the field of surface chemistry, and gave me continuous guidance, encouragement, and advices during the last three years. I am deeply grateful of their help in the completion of this thesis.

I would like to express my appreciation to my colleagues at Chemistry and Nanobiotechnology group. I appreciate to Dr. Christelle Yeromonahos for the favours of XPS measurements and patterned substrates fabrication. Dr. Virginie Monnier, thank you very much for the favours of SEM measurements. Dr. Thomas Gehin showed me a lot of experimental instruments in our lab, thank you very much. Dr Magali Phaner-Goutorbe and Dr. Emmanuelle Laurenceau are very nice, thank you very much for the every help and supporting. Isabel Nabeth, we were in the same office during the last three years, thanks very much for your accompany and excellent coffee. I have been extremely lucky and blessed with many friendly colleagues who are working or once worked in the group: Dr. Salome Ansanay-Alex, Dr. Lucie Dupin, Dr. Francesca Zuttion, Dr. Maxime Boksebeld, Dr. Mathieu Caillau, Dr. Muchen Li, Dr. Xiaofei Bai, Dr. Feixiong Chen, Rachael Taitt, Solène Lecot, Olya Sysova, Bryan Chan, Nicolas Martinez Rodriguez, Zihua Yang, etc. I would like to thank the former PhD student Dr. Francisco Palazon for his helps on the scientific problems.

I would like to thank other colleagues at Institut des Nanotechnologies de Lyon. Among them I would like to thank Mr. Claude Botella and Dr. Geneviève Grenet respectively for XPS analysis. I thank Mr. Aziz Benamrouche for the favours of AFM measurements and Dr. José Penuelas for the favours of XRD measurements. I thank Dr. Radoslaw Mazurczyk for the favours of patterned substrates fabrication. Technical supports of NanoLyon are appreciated for all the infrastructures.

I thank Dr. Stéphane Monfray from STMicroelectonics for providing the substrates to me. Here, I would like to express my special thanks to Pr. Didier Leonard from Institut des Sciences Analytiques (ISA) UMR 5280 for the help of ToF-SIMS measurements and analysis.

I would like to thank all the Chinese PhD students for the great times we have spent together in the past three years in Lyon: Zehua Fu, Haohao Ding, Xin Guan, Dong Han, Han Meng, Qinjie Ju, Yu Zhang, Yue Ma, Xiao Li, He Ding, Fei Zheng, Guang Zhu, Wenqi Chai, Mingyang Lou, Kaijun Yi, Lei Jiang, Peng Wang, Jianzhao Wu, Weizhen You, etc.

At last, I thank all my friends and family for their support and love, who have helped me and shared with me my worries, frustrations, and happiness.

Table of contents

List of figures

List of tables

Acronymes

AFM Atomic Force Microscopy

APDMES 3-ethoxydimethylsilylpropylamine

APPA 3-aminopropylphosphonic acid

ATR Attenuated Total Reflectance

DA Dopamine

DCM Dichloromethane

DFT Density Functional Theory

DPN Dip Pen Lithography

EBL Electron-Beam Lithography

F-thiol 1H,1H,2H,2H-Perfluorodecanethiol

F-phosphonic acid 1H, 1H,2H,2H-Perfluorooctanephosphonic acid

F-silane H,1H,2H,2H-Perfluorodecyldimethyl- chlorosilane

FTIR Fourier-Transform Infrared Spectroscopy

IR Infrared

IRRAS Infrared Reflection Absorption Spectroscopy

ITO Indium-Tin Oxide

LSPR Localized Surface Plasmon Resonance

MUAM 11-amino-undecanethiol hydrochloride

NMR Nuclear Magnetic Resonance

PBS Phosphate Buffered Saline

PEG Poly (Ethylene Glycol)

PEM Photo Elastic Modulator

PLL Poly-L-Lysine

PM-IRRAS Polarization-Modulation Infrared Reflection Absorption Spectroscopy

RMS Root Mean Square

SAM Self-Assembled Monolayer

SEM Scanning Electron Microscopy

SERS Surface-Enhanced Raman Spectroscopy

SPR Surface Plasmon Resonance

SMAP Selective Molecular Assembly Patterning

SSP Substrate Selective Patterning

STM Scanning Tunneling Microscopy

T-BAG Tethering by Aggregation and Growth

TERS Tip-Enhanced Raman Spectroscopy

TiW Titanium Tungsten

ToF-SIMS Time-of-Flight Secondary Ion Mass Spectroscopy

UV Ultraviolet

XPS X-ray Photoelectron Spectroscopy.

XRD X-Ray Diffraction.

General introduction

Introduction générale

A Mise en contexte et problématique

Le développement actuel des nanotechnologies implique de plus en plus des surfaces nanostructurées avec différents matériaux. A titre d'exemple, des capteurs (bio)chimiques classiques tels que les capteurs à résonance de plasmon de surface et les capteurs à base de transistors à effet de champ, ont été atteint leur limite intrinsèque de sensibilité, et ne sont pas utilisables pour détecter des traces de substances chimiques ou d'espèces biomoléculaires. Depuis des années, les nanotechnologies permettent de faire évoluer les performances de ces capteurs, en réduisant les dimensions des éléments de détection (transducteurs) utilisés dans ces capteurs (Figure G.1). Les capteurs SPR classiques s'appuyaient sur la fabrication d'une couche mince d'or continu d'environ 48 nm d'épaisseur. En structurant la couche métallique pour former des ilots d'or 2D ou 3D, il est possible d'augmenter l'intensité du champ électromagnétique par unité de surface sondée, et de rendre le capteur plus sensible[1], [2] ou plus versatile[3], [4]. De même, les structures nanoélectroniques développées avec les technologies actuelles permettent d'être sensible à des variations de quelques centaines de charges électriques seulement. Ces performances sont par exemple explorées avec les structures FDSOI 28 nm de la société STMicrolectronics[5]–[7].

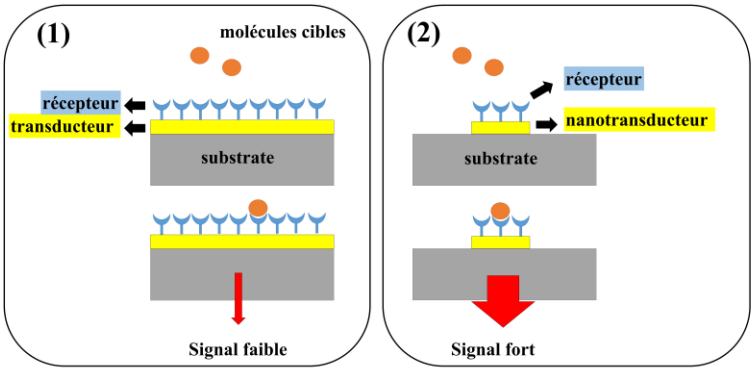

Figure I.1 Influence théorique de la dimension d'un transducteur sur l'intensité des signaux d'un biocapteur.

Pourtant, alors que ces nanotransducteurs semblent intrinsèquement plus performants que des transducteurs de plus grande taille, leur utilisation n'est utile que si les molécules cibles à détecter sont capturées sur les zones sensibles du capteur. Toute molécule cible adsorbée en un autre site du dispositif (substrat, canal fluidique…) ne peut pas contribuer au signal et apporter d'information utile pour la détection des cibles. Pour bénéficier de l'amplification physique potentiellement apportée par l'échelle nanométrique d'un transducteur, et détecter des cibles présentes à faible concentration dans un milieu de mesure, il est nécessaire de maximiser la capture de cibles (Figure G.2). Cette maximisation peut passer par plusieurs

approches, comme par exemple le transport actif des cibles vers le transducteur (ex: fluidique, ondes acoustiques, diélectrophorèse)[8] ou la fonctionnalisation sélective de surfaces.

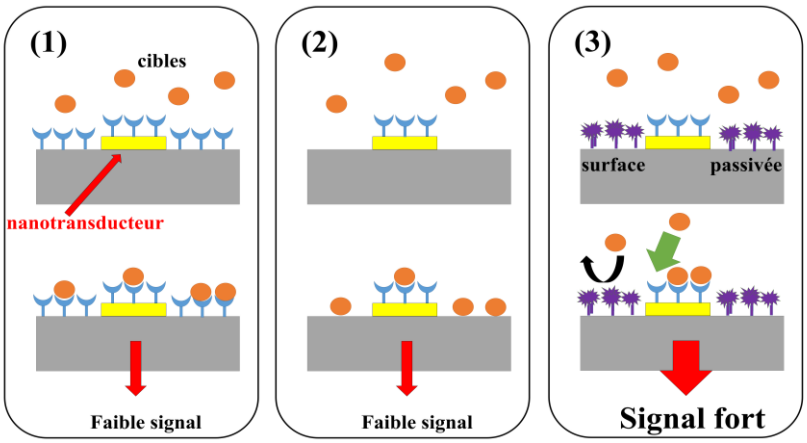

Figure I.2 Influence des interactions moléculaires sur les performances globales d'un biocapteur comportant un nanotransducteur.

Le présent travail est centré sur la question de la fonctionnalisation sélective (ou « orthogonale » de surfaces composées de différents matériaux. L'objectif central est d'étudier dans quelle mesure il est possible de modifier des matériaux différents d'un même substrat, avec des réactions de surfaces spécifiques de chacun des matériaux, en vue de conférer à chaque matériau des propriétés particulières. Dans notre exemple lié aux nanotransducteurs, on souhaite par exemple pouvoir immobiliser une couche de molécules sonde formant un récepteur sur le nanotransducteur, tout en conférant aux autres matériaux à repousser les cibles moléculaires de façon efficace : il est donc nécessaire de fixer des fonctions chimiques et/ou des molécules organiques différentes sur les différents matériaux de la surface, et si possible avec le moins de mélanges possibles entre les molécules mises en œuvre.

Des travaux sur la fonctionnalisation sélective de surfaces ont déjà été menés dans l'équipe Chimie & Nanobiotechnologies de l'INL, pour explorer comment cette approche peut contribuer à améliorer les performances de capteurs, mais aussi être employée pour fabriquer de nanodispositifs avec de nouvelles propriétés, non fabricables en s'appuyant uniquement sur de la nanofabrication descendante (lithographie + lift-off)[9], [10]. La fonctionnalisation chimique de surfaces a été d'abord étudiée pour des matériaux homogènes, tels que la silice ou l'or[11]–[14]. La fonctionnalisation de surfaces composées de différents matériaux a été explorée dès 1989 dans le groupe de George M. Whitesides, à l'échelle macroscopique[15].

En vue de fabriquer différents capteurs et biopuces, l'équipe Chimie & Nanobiotechnologies a étudié différentes voies de modification de matériaux homogène (verre, silice)[16], [17]. Par la suite, en vue de fabriquer des systèmes de manière plus souples, l'équipe a commencé à étudier le comportement de dispositifs multimatériaux, par exemple à base de silice et d'or, ou de silice et nitrure[18].

Les travaux sur la fonctionnalisation orthogonale de surfaces à deux matériaux ont été lancés dans l'équipe avec la thèse de Francisco Palazon (Fonctionnalisations orthogonales de surface: rappel des travaux dans l'équipe Chimie & Nanobiotechnologies)[19], qui s'est appuyé sur deux réactions maîtrisées séparément dans l'équipe : la silanisation de la silice (1) et la formation de couche d'alkylthiol sur or (2) (Figure G.3).

Il a d'abord été possible de vérifier que des silanes n'interagissent pas significativement avec de l'or (3), et que des alkylthiols ne se fixent pas de manière stable à de la silice (4) (Figure G.3).

Dans un deuxième temps, il a été démontré qu'il est possible de faire réagir simultanément, en une étape, un mélange de silanes et de thiols, sur un substrat composé d'or et de silice : dans les conditions adéquates, les silanes se greffent spécifiquement à la silice et les thiols spécifiquement à l'or (Figure G.3).

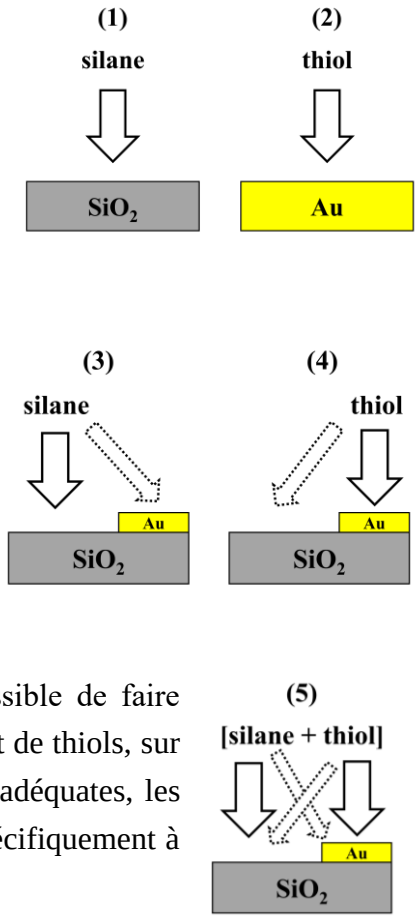

Figure I.3 Fonctionnalisation orthogonale de *substrats or + silice: résumé des acquis déjà étudiés dans l'équipe.*

Ces études ont été menées d'abord sur des substrats macroscopiques, ensuite sur des substrats de silice avec des motifs d'or micrométriques, et enfin des substrats de silice avec des motifs de quelques centaines de nanomètres de taille caractéristique[20], [21].

L'efficacité de la fonctionnalisation a été mesurée à la fois par analyses spectroscopiques (ex: imagerie ToF-SIMS, imagerie XPS), et par capture sélective de nanoparticules sur des motifs, avec analyse des particules capturées par microscopie électronique à balayage. La présente thèse a été menée dans la continuité du travail ci-dessus. Les savoir-faire pour fonctionnaliser sélectivement silice et or ont été utilisés, et un troisième matériau a été ajouté : le titanate de tungstène (TiW). Il a été choisi pour enrichir notre bibliothèque car TiW est un matériau fortement utilisé et maitrisé dans la fabrication de composants nanoélectroniques[22]–[25]. Il est possible d'obtenir des wafers de TiW fabriqués de manière répétable, et le TiW présente un comportement stable. La société STMicrolectronics, qui explore avec l'INL de nouveaux capteurs chimiques, a mis à la disposition de l'équipe un wafer de TiW, pour explorer le comportement de ce matériau en termes de fonctionnalisation de surface.

B Questions de recherche

Le travail réalisé au cours de ce doctorat est centré sur les questions suivantes :

(1) Comment se comporte le TiW vis-à-vis de différentes molécules organiques, en termes de fonctionnalisation chimique de surface ?

(2) Est-il possible de procéder à des fonctionnalisations chimiques orthogonal d'un substrat comportant du TiW et d'autres matériaux en surface : TiW et or ; TiW, or et silice.

C Objectifs du projet de recherche

Les travaux menés pendant les trois années de cette thèse ont impliqué les sujets résumés ci-dessous :

Etudier le comportement d'un substrat de TiW planaire et homogène, vis-à-vis de trois classes de molécules organiques : silane, catéchol (dopamine), acide phosphonique (AP). Caractériser la formation des couches organiques formées avec ces trois molécules, ainsi que leur stabilité respective (Figure G.4).

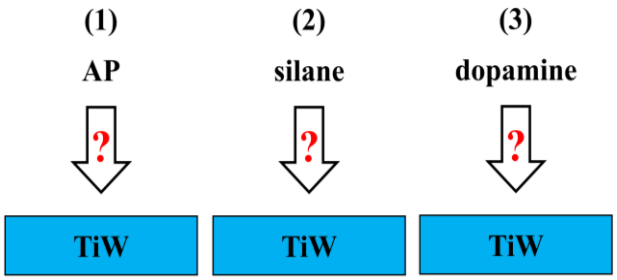

Figure I.4 Fonctionnalisation de TiW avec différentes molécules organiques.

Sur un substrat à deux matériaux TiW + or, étudier dans quelles conditions il est possible de greffer les acides phosphoniques (AP) sur TiW, des thiols sur l'or, sans que les thiols ne se fixent sur TiW ni les acides phosphoniques sur TiW (Figure G.5).

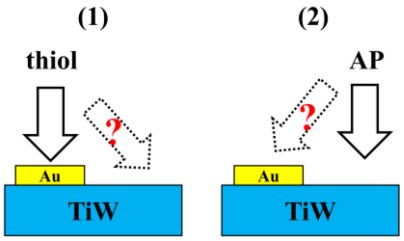

Figure I.5 Fonctionnalisation orthogonale de surfaces or + TiW.

Sur un substrat à trois matériaux TiW + or + SiO_2, étudier dans quelles conditions il est possible de fonctionnaliser sélectivement TiW, or et silice avec respectivement Acide Phosphonique (AP), thiol et silane. Evaluer les contaminations croisées, et identifier la manière la plus appropriée d'obtenir trois réactions de fonctionnalisation orthogonales (Figure G.6).

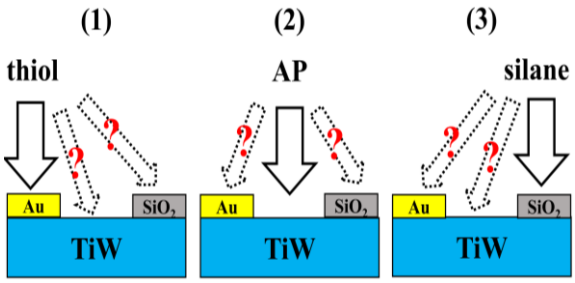

Figure I.6 Fonctionnalisation orthogonale de substrats or + silice + TiW.

D Plan du mémoire de thèse

Le présent mémoire de thèse est structuré en quatre chapitres :

Le **chapitre 1** présente un état de l'art sur différentes approches de fonctionnalisation chimique *localisée* à la surface de matériaux inorganiques. Nous montrons comment il est possible de localiser des fonctions chimiques souhaitées en des zones spatialement définies à la surface d'un substrat, en s'appuyant par exemple sur l'irradiation de la surface avec un faisceau de particules, sur la lithographie souple (« microcontact printing »), les technologies en champ proche (microscopie à force atomique ou champ proche optique), et l'approche par fonctionnalisation chimique orthogonale. Nous comparons ces différentes stratégies notamment en termes de débit de fabrication, de résolution des motifs, de précision du positionnement absolu des motifs sur un substrat, et de souplesse d'utilisation. Le travail réalisé dans la présente thèse est centré sur l'approche par fonctionnalisation orthogonale. Nous présentons les quelques réalisations de fonctionnalisation chimique orthogonale décrites dans la littérature pour des substrats composés de deux matériaux différents : silice et or. Nous rappelons notamment les points les plus importants du travail de Francisco Palazon sur ce sujet, dans l'équipe Chimie et Nanobiotechnologie de l'INL.

Le chapitre 2 présente une étude de la fonctionnalisation chimique de substrats homogènes planaires de TiW avec les trois molécules suivantes 1) l'acide 3-aminopropylphosphonique (3-aminopropylphosphonic acid ou APPA) ; 2) le silane 3-ethoxydimethylsilylpropylamine (APDMES) ; et le catéchol dopamine (DA). La formation de couches homogènes d'APPA, APDMES et DA a été étudiée. Les substrats ont été analysés par diffraction X, microscopie à force atomique (AFM), spectroscopie XPS, spectrométrie de masse d'ion secndaire à temps de vol (Time-of-flight secondary Ion mass spectrometry ou ToF-SIMS), et spectroscopie infra-rouge en mode réflexion totale atténuée (ATR-FTIR). Nous avons exploré l'état chimique des surfaces après fonctionnalisation avec ces différentes molécules, ainsi que l'évolution des surfaces fonctionnalisées en fonction de la durée de lavages. Il s'agit à notre connaissance de la première étude sur la fonctionnalisation chimique de surface du TiW.

Le **chapitre 3** présente une étude de la fonctionnalisation chimique orthogonale de substrats de TiW comportant des motifs d'or de dimensions microniques. En nous appuyant des caractérisations XPS PM-IRRAS, et imagerie ToF-SIMS nous montrons comment les motifs d'or peuvent être fonctionnalisés avec un thiol, tandis que le TiW peut être fonctionnalisé avec un acide phosphonique. Le travail expérimental montre dans quelles conditions il est possible de rendre ces deux réactions orthogonales. Les surfaces sont ensuite utilisées pour capturer par interactions électrostatiques des carboxy-nanoparticules. Nous utilisons la microscopie électronique à balayage pour vérifier comment les nanoparticules sont capturées sur les zones de TiW et les zones d'or. Cette approche nous permet de comparer

quantitativement la capture des nanoparticules sur or et l'adsorption non spécifique de nanoparticules sur TiW.

Dans le **chapitre 4**, nous étudions le comportement d'un substrat de TiW recouvert de motifs d'or et de silice, vis-à-vis de trois réactions de fonctionnalisation de surface : la structure est séquentiellement fonctionnalisée avec un silane, un thiol et un acide phosphonique puis lavée. Les silanes, comme les acides phosphoniques, possèdent une affinité pour les surfaces de TiW présentant un oxyde natif. Nous explorons dans quelles conditions obtenir une orthogonalité entre les trois réactions mises en jeu : silanisation de la silice, dépôt du thiol sur l'or, dépôt d'acide phosphonique sur TiW. Les surfaces sont caractérisées par XPS, imagerie ToF-SIMS, ATR-FTIR et mesure d'angle de contact.

E Références

[1] X. D. Hoa, A. G. Kirk, M. Tabrizian. Enhanced SPR response from patterned immobilization of surface bioreceptors on nano-gratings. *Biosens. Bioelectron.*, **2009**, *24*, 3043–3048.

[2] X. D. Hoa, A. G. Kirk, M. Tabrizian. Towards integrated and sensitive surface plasmon resonance biosensors: a review of recent progress. *Biosens. Bioelectron.*, **2007**, *23*, 151–160.

[3] F. A. Banville, J. Moreau, M. Sarkar, M. Besbes, M. Canva, P. G. Charette. Spatial resolution versus contrast trade-off enhancement in high-resolution surface plasmon resonance imaging (SPRI) by metal surface nanostructure design. *Opt. Express*, **2018**, *26*, 10616–10630.

[4] M. Sarkar, M. Besbes, J. Moreau, J. F. Bryche, A. Olivéro, G. Barbillon, A. L. Coutrot, B. Bartenlian, M. Canva. Hybrid plasmonic mode by resonant coupling of localized plasmons to propagating plasmons in a kretschmann configuration. *ACS Photonics*, **2015**, *2*, 237–245.

[5] G. T. Ayele, S. Monfray, S. Ecoffey, F. Boeuf, J. P. Cloarec, D. Drouin, A. Souifi. Ultrahigh-sensitive CMOS pH sensor developed in the BEOL of standard 28 nm UTBB FDSOI. *IEEE J. Electron Devices Soc.*, **2018**, *6*, 1026–1032.

[6] L. Rahhal, G. T. Ayele, S. Monfray, J. P. Cloarec, B. Fornacciari, E. Pardoux, C. Chevalier, S. Ecoffey, D. Drouin, P. Morin, P. Garnier, F. Boeuf, A. Souifi. High sensitivity pH sensing on the BEOL of industrial FDSOI transistors. *Solid-State Electron.*, **2017**, *134*, 22–29.

[7] G. T. Ayele, S. Monfray, F. Boeuf, J. P. Cloarec, S. Ecoffey, D. Drouin, E. Puyoo, A. Souifi. Development of ultrasensitive extended-gate Ion-sensitive-field-effect-transistor

based on industrial UTBB FDSOI transistor. *47th European Solid-State Device Research Conference (ESSDERC)*, **2017**, 264–267.

[8] S. Toru, M. Frenea-Robin, N. Haddour, F. Buret. Tunable and label-free bacteria alignment using standing surface acoustic waves. *Annual International Conference of the IEEE Engineering in Medicine and Biology Society (EMBC)*, **2012**, 4998–5001.

[9] F. Palazon, V. Monnier, Y. Chevolot, É. Souteyrand, J. P. Cloarec. Nanotraps: different approaches for the precise placement of micro and nano-objects from a colloidal dispersion onto nanometric scale sites of a patterned macroscopic surface. *J. Colloid Sci. Biotechnol*. **2013**, *2*, 249–262.

[10] F. Palazon, P. R. Romeo, A. Belarouci, C. Chevalier, H. Chamas, É. Souteyrand, A. Souifi, Y. Chevolot, J. P. Cloarec. Site-selective self-assembly of nano-objects on a planar substrate based on surface chemical functionalization. *Nanopackaging: From Nanomaterials to the Atomic Scale, Springer*, **2015**, 93–112.

[11] A. Ulman. Formation and structure of self-assembled monolayers. *Chem. Rev.*, **1996**, *96*, 1533–1554.

[12] D. E. Leyden, W. T. Collins. Silylated Surfaces. *CRC Press*, **1980**.

[13] K. M. R. Kallury, U. J. Krull, M. Thompson. X-ray photoelectron spectroscopy of silica surfaces treated with polyfunctional silanes. *Anal. Chem.*, **1988**, *60*, 169–172.

[14] H. Engelhardt, P. Orth. Alkoxy silanes for the preparation of silica based stationary phases with bonded polar functional groups. *J. Liq. Chromatogr.*, **1987**, *10*, 1999–2022.

[15] P. E. Laibinis, J. J. Hickman, M. S. Wrighton, G. M. Whitesides. Orthogonal self-assembled monolayers: alkanethiols on gold and alkane carboxylic acids on alumina. *Science*, **1989**, *245*, 845–847.

[16] P. G. Charette, J. P. Cloarec, J. Moreau, G. Barbillon, M. Canva. Plasmonic imaging systems and dedicated functionalized biochips for biosensing, *Handbook of Enhanced Spectroscopy*, *CRC Press*, **2015**, 50-115.

[17] J. P. Cloarec, Y. Chevolot, E. Laurenceau, M. Phaner-Goutorbe, É. Souteyrand. A multidisciplinary approach for molecular diagnostics based on biosensors and microarrays. *IRBM*, **2008**, *29*, 105–127.

[18] J. P. Cloarec, C. Chevalier, J. Genest, J. Beauvais, H. Chamas, Y. Chevolot, T. Baron, A. Souifi. pH driven addressing of silicon nanowires onto Si_3N_4/SiO_2 micro-patterned surfaces. *Nanotechnology*, **2016**, *27*, 295602.

[19] F. Palazon. Fonctionnalisation de surfaces hétérogènes or/silice pour l'ancrage sélectif de biomolécules et colloïdes sur biocapteurs LSPR. *Ecole centrale de Lyon*, **2014**.

[20] F. Palazon, P. Rojo-Romeo, C. Chevalier, T. Géhin, A. Belarouci, A. Cornillon, F. Zuttion, M. Phaner-Goutorbe, É. Souteyrand, Y. Chevolot, J. P. Cloarec. Nanoparticles selectively immobilized onto large arrays of gold micro and nanostructures through surface chemical functionalizations. *J. Colloid Interface Sci.*, **2015**, *447*, 152–158.

[21] F. Palazon, D. Léonard, T. L. Mogne, F. Zuttion, C. Chevalier, M. Phaner-Goutorbe, É. Souteyrand, Y. Chevolot, J. P. Cloarec. Orthogonal chemical functionalization of patterned gold on silica surfaces. *Beilstein J Nanotechnol.*, **2015**, *6*, 2272–2277.

[22] C. K. Wang, S. J. Chang, Y. K. Su, C. S. Chang, Y. Z. Chiou, C. H. Kuo, T. K. Lin, T. K. Ko, J. J. Tang. GaN MSM photodetectors with TiW transparent electrodes. *Mater. Sci. Eng. B*, **2004**, *112*, 25–29.

[23] H. C. Chiua, C. H. Chen, C. W. Yang, H. L. Kao, F. H. Huang, S. W. Peng. Highly thermally stable in situ SiN_X passivation AlGaN/GaN enhancement-mode high electron mobility transistors using TiW refractory gate structure. *J. Vac. Sci. Technol. B*, **2013**, *31*, 051212 1-4.

[24] A. Roshanghias, G. Khatibi, R. Pelzer, J. Steinbrenner. On the effects of thickness on adhesion of TiW diffusion barrier coatings in silicon integrated circuits. *Surf. Coat. Technol.*, **2014**, *259*, 386–392.

[25] F. Battegay, M. Fourel, Barrier material selection for TSV last, flipchip & 3D-UBM & RDL integrations. *ECTC*, **2015**, 1183–1192.

Chapter 1

State of the art

1 State of the art

1.1 Introduction

Surface chemical functionalization of inorganic materials has been developed for various applications, such as surface patterning fabrication[1], tissue engineering[2], biosensors[3], localization of colloidal nano-objects[4] and corrosion inhibition[5]. It can be done in several ways, for instance:

(1) By electron or ion beams.

(2) Polymers coating.

(3) Formation of an organolayer thanks to the covalent grafting of low molecular weight molecules.

The molecules that form the organolayer have two main elements: a substrate-binding head group, and a hydrocarbon chain (spacer). Eventually an additional functional head group is present at the other end of the spacer allowing the coupling of a molecule or a nano-object. This terminal function can also limit nonspecific adsorption of undesired molecular species. The organolayer can be formed from liquid or gas phase onto the solid surface (Figure 1.1).

The most reported reactions are the ones of thiols on gold surfaces and ones of silanes on silica surfaces though the formation of Au-S bond and Si-O bond, respectively[6]–[9]. Under well control experimental conditions, the attachment of these molecules can give raise to self-organized monolayers called self-assembled monolayer (SAM). However, in the literature, thin layers of low molecular weight molecules are often referred as SAM despite the lack of proof of self-organization. Here, we call “organolayers” formed from low molecular weight molecules with a thickness below 5 nm, whether they are organized or not. We focus on the discussion about the covalent binding of organolayers on oxides and gold in section 1.3.

In parallel, efforts have been devoted to developing localized chemical surface functionalization allowing for the patterning of surface chemical functionalization. To this aim, various approaches, such as beam irradiation, microcontact printing, near field technologies, and electrochemistry have been explored. Alternatively, localized chemical functionalization of multi-materials patterned substrate can be obtained using selected grafting reactions to grow different organolayers on the different materials. Such approach will be called later “orthogonal chemical functionalization” in this thesis.

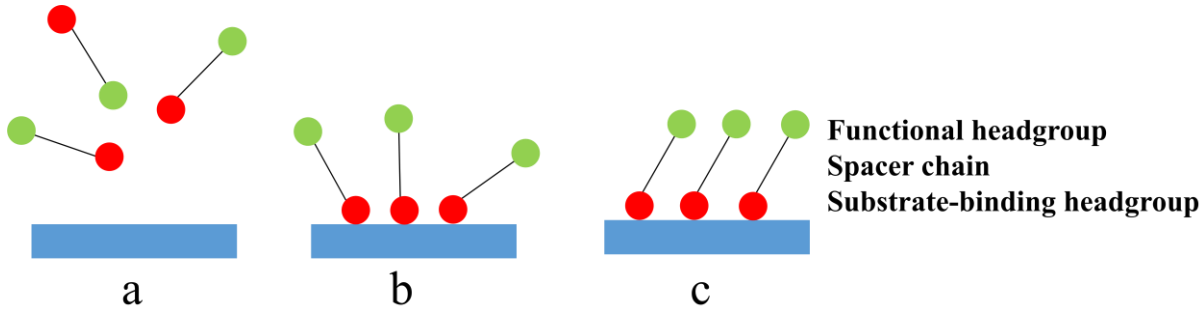

Figure 1.1 Ideal representation of organolayers on a solid surface. Molecules from a liquid or gas phase (a) are chemically bonded onto the substrate by their substrate-specific headgroup (b) and self-arrange through Van der Waals interactions to form a pseudo-crystalline monolayer (c).

In the following we will first review different methodologies that have been explored to achieve localized surface modification. Orthogonal functionalization is based on material specific reactions. Therefore, formation of organolayers on various individual materials is first discussed and then, the different methods reported for orthogonal surface modifications of multi-material substrates is reviewed. Finally, we will recall the state of the art of the chemical functionalization of titanium tungsten alloy (TiW). Its orthogonal functionalization on multi-material substrates is discussed.

1.2 Localized chemical functionalization approaches

In the following we focus mainly on the local formation of organolayers. Among the various processes allowing for local surface functionalization, writing of chemical features on the substrate seems a straightforward approach. These can be achieved either by the introduction of reacting groups at the surface of the material allowing for the subsequent grafting reaction (for example local introduction of silanol groups for silinization) or the local promotion or degradation of the organolayers by irradiation, mechanical removal or photochemistry.

Among the different techniques employed to these aims one can consider the use of focused incident particle beam (ions, electrons) or photons (lasers or masking techniques). Substrate modifications can also be triggered locally by near field techniques (SNOM, AFM lithography, nanoimprint, thermolithography) or microcontact printing. In the following, we will review these techniques. Localized electrochemical reactions such as polypyrrole formation on metallic electrodes will not be detailed here, since it implies know how (see Roupioz's group at SYMMES) that are too far from our research group's knowledge to invest energy and work for being implemented correctly. It is considered out of scope of the present work.

1.2.1 Beam irradiation

Focused ion or electron beams can be used to write patterns directly on a substrate to either “pre-functionalize” the substrate (introduce reaction groups) or to remove locally an already-

formed organolayer. Incident particles are generally electrons with incident energies ranking typically in the 10eV~100KeV range. Indeed, in this range of energies, the electron beams lithography has to be compared with bond energies and the abilities of such electron to promote the formation or destruction of chemical bonds.

For the substrates pre-functionalized by organolayers, electron-beam lithography (EBL) techniques are promising for directly writing patterns on the organolayers through removing the molecules from the surface. EBL patterns process on organolayers is shown in Figure 1.2. Patterning is either due to the destruction of the functional group at the terminus of the molecules in the organolayers, thereby preventing subsequent binding of a target molecule to the exposed area, or to backfilling an exposed area with a chemically active molecule in an otherwise inert molecules, thereby creating local binding sites.

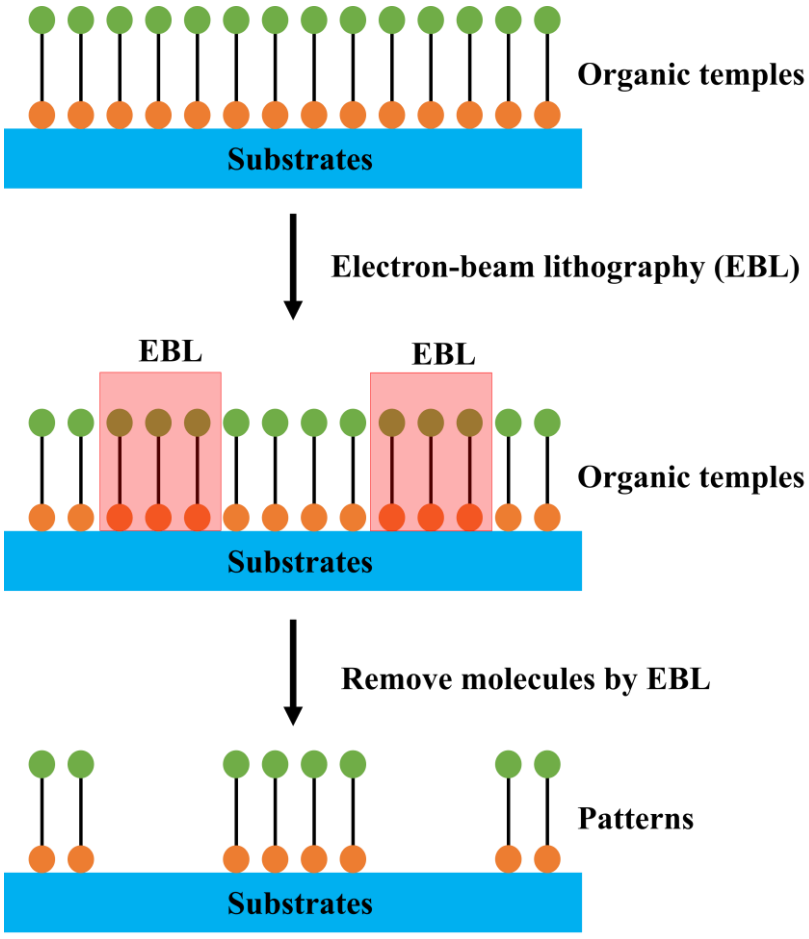

Figure 1.2 Ideal representation of electron-beam lithography (EBL) process.

Electron beam technique has been used for fabrication of organosilane patterns on silica with ultrahigh resolution (from 10 nm to a single molecule scale)[10]–[14]. On thiols functionalized gold surfaces, nanometer scale patterns have also be obtained[15], [16]. It is worth noting that A. Gölzhäuser *et al.* reported the local conversion of nitro terminated organolayers to amino groups thanks to electron beam allowing for their subsequent coupling with carboxylic functions[17]–[20].

1.2.2 Micro-contact printing

Microcontact printing method was first developed by G. M. Whitesides *et al*. in 1993[21]. Microcontact printing uses a stamp to print molecules with sub-micrometric resolution onto a substrate. The stamp, usually made of polydimethyl siloxane (PDMS) or polyacrylamide (PAA), is first coated with the desired molecules (ink) and then brought into contact with the substrate. If the molecular ink interact more strongly with the substrate than with the stamp, it is transferred at the contact regions from the stamp to the substrate (Figure 1.3)[22], [23]. The resolution and periodicity achievable by microcontact printing are dependent on the young modulus of the stamp and can range in the few tens of nanometers scale with hard polymers [24], [25]. For example, microcontact printing of thiols on gold or silanes on glass have been reported[21], [26]. In addition, this process has also been successfully described for the printing of proteins[27], [28], polymers[29], [30] and particles[31].

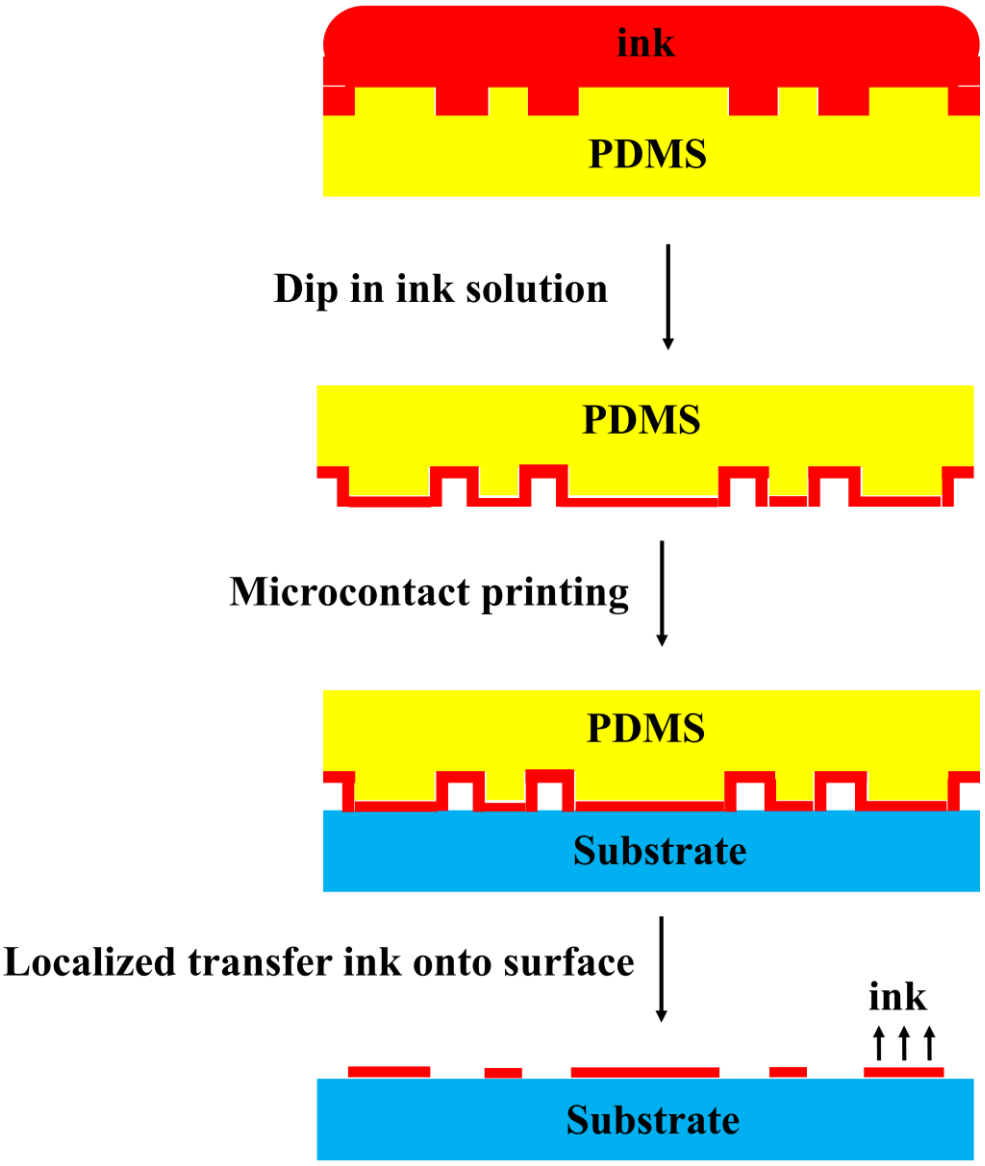

Figure 1.3 Ideal representation of microcontact printing process.

1.2.3 Near-Field technologies

Similarly to microcontact printing dip pen nanolithography (DPN)[32] can use an AFM tip to locally deposit the molecules. Thanks to a water meniscus that is formed between AFM tip and solid substrate, the molecular ink is transported from the tip to the surface, as shown in Figure 1.4.

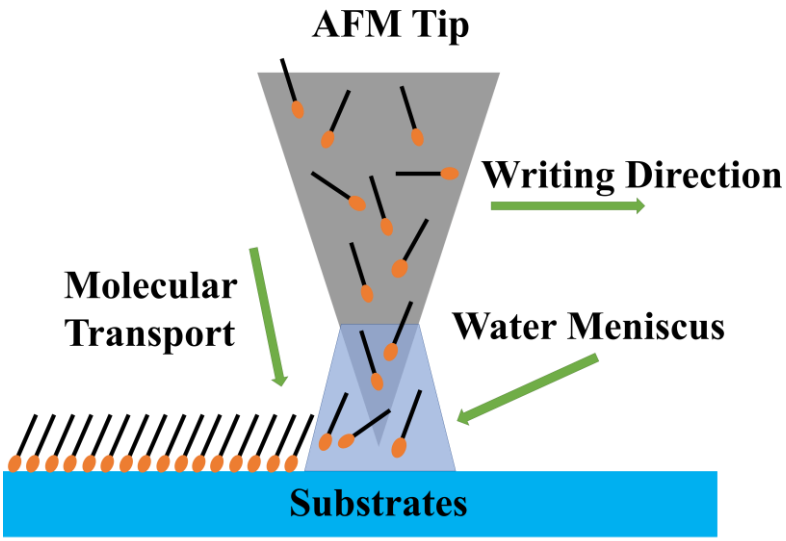

Figure 1.4 Ideal representation of AFM dip pen nanolithography process.

Alkane thiolates features obtained by DPN onto a gold surface has been reported in the literature [33]–[35]. For example, F. Stellacci et al. wrote thin lines of mercaptohexadecanoic acid of nearly 100 nm on gold. The resulting carboxylated functionalized lines allowed for the attachment of aminated functionalized gold nanoparticles by covalent binding[25]. C. A. Mirkin *et al*. reported a similar strategy for the lithography of silazane onto Si/SiO_x and oxidized GaAs substrates. They obtained 100 nm wide lines[36]. DPN can be used to construct arrays of proteins on functionalized gold and silica substrates[37]–[39]. In addition, AFM based nanolithography technique can be used to mechanically erase/scratch an organolayer. Eventually, new molecules can be simultaneously introduced on the "new formed" areas by either pre-coating the tip or by diffusion of the new molecules from the medium[40]–[42].

Besides of AFM dip pen lithography, scanning near-field photolithography is another powerful near-field technology for nanoscale molecular patterns, in which a near-field scanning optical microscope (SNOM) coupled to a UV laser. Because of the wide range of photochemical methods available for surface derivatization, scanning near-field photolithography appears poised to fulfill its promise by combining the power of photolithography with nanometric spatial resolution for single molecular immobilization and detection[43], [44].

1.2.4 Orthogonal chemical functionalization

The above methods aimed mainly at localizing an organolayer at defined areas of a homogeneous surface. However, if the substrate consists of patterns of different materials, these materials can be functionalized independently, by choosing molecules with the appropriate substrate binding head groups. This approach combines top down and bottom-up approaches. Indeed, the creation of the patterned material substrate is commonly obtained via conventional technological processes (top-down process: lithography, physical vapor deposition, chemical vapor deposition, plasma etching…). These materials are selected for the physical and chemical orthogonal properties. Their specific chemical functionalization is obtained by taking advantage of the affinity of certain molecular groups toward given materials (bottom-up process). The method has been termed as ‘‘orthogonal self-assembly monolayers” by G. M. Whitesides *et al*.[45], “selective molecular assembly patterning” (SMAP) by M. Textor *et al*.[46] and “substrate selective patterning” (SSP) by M. Bergkvist *et al*.[47]. Herein, we will use “orthogonal chemical functionalization” to name the method. Various chemical compounds and substrates have been used:

(1) Metal oxide/silica templates modified with phosphonate and silanes[48].

(2) Au/metal oxide templates functionalized with thiols and phosphonate, amine or carboxylic acids[49].

(3) Au/silica templates modified with thiol and silanes[50].

Gold micro and nanostructures on silica is quite common as it may have different applications in optics and electronics[47]. For example, on plasmonic devices, orthogonal chemical functionalization may enable the gold structures to trap a target (i.e. nanoparticles, biomolecules…) from solution while avoiding non-specific adsorption on the rest of the surface. In our group, F. Palazon *et al*. developed a single-step orthogonal chemical functionalization procedures for micro and nanoscale gold features on a silica surfaces[51]. This approach was used to trap streptavidin-coated nanoparticles onto the biotin functionalized gold nano-antennas structures. The capture yield relative to the nanoantenna was 68.8% without mixing, while nonspecific adsorption was less than 1%[4].

1.2.5 Comparison of different chemical patterning approaches

We have presented different approaches for localized functionalization on homogeneous or multi-materials surfaces. These methods can be compared in terms different criteria: implementation (parallel or serial), resolution (minimum possible feature size), throughput (total patterned area per unit time), location precision (minimum distance for precise positioning of a desired feature on a substrate) and versatility (available possibility), as shown in Table 1.1. In the columns a rough criteria indicator (+, ++, +++) is given of the different localized methods. Of course, the indicator is dependent on the perspective and goals, and

includes features such as materials selection, structural organization and ease of use. Hopefully the summary might help you to grasp a method for your own purposes.

Implementation: Microcontact printing could achieve parallel inking of a stamp followed by a single printing step on a substrate to form periodic array. Near-field technique (e.g. DPN, NSOM photochemistry) and photoelectric beam irradiation mainly carry out in serial mode to pattern the surface step by step. However, new DPN developments have reached massively parallel patterning with different inks on each tip[52]. For orthogonal chemical functionalization on multi-materials, the organolayers could be serial or parallel functionalized on each material.

Throughput: Microcontact printing probably presents highest throughput compared with other above mentioned techniques as an area of several cm^2 can be functionalized in quite short time. The throughput of EBL is about 10-10^4 μm^2/h[53]. Multi-tip AFM DPN can have a considerable higher throughput than EBL, which could allow high throughput fabrication and integration on the cm^2 scale[52]. For orthogonal chemical functionalization the throughput could be high, which is mainly based on the size and materials for creating the patterned substrate.

Resolution: The resolution is related to the throughput. The microcontact printing technique with higher throughput can hardly reach nanometer features, when the goal is to deposit molecules on a planar substrate. However, microcontact printing may be used to stamp molecules on thick patterns implemented on a substrate. In this case, thickness may be more determinant than the feature characteristic size, and one can imagine it is possible to stamp very small patterns. EBL can generate periodic patterns with very high resolution under 10 nm. The resolution of orthogonal chemical functionalization is lower than near-field techniques and EBL in most cases.

Location precision: Near-field technologies can exhibit a location precision defined by the curvature radius of the tip for DPN, provided that marks have been implemented on substrate. Microcontact printing location precision may limited by the precision of mechanical positioning of the stamp, when it is used to stamp molecules on a planar substrate. This difficulty is overridden when stamp is to be positioned on predefined thick patterns (e.g. implemented by any lithographic technique), since molecules are expected to be stamped on the patterned higher surface and not on the underlying substrate. Orthogonal functionalization location precision is expected to mainly rely on the quality of the different materials patterns that have been implemented. The main constraint is related to the quality of the different surface materials, and the orthogonality of the targeted reactions.

Versatility: Microcontact printing have relatively low versatility, as the same defined stamp is used on the whole surface for one time. Of course, different stamps having different patterns or inks can be printed many times onto the whole substrate, which can achieve multi-

functional surface. EBL and DPN techniques have higher versatility as different shapes and sizes can be defined directly on the whole substrate. Orthogonal chemical functionalization could modify a wide range of inorganic materials integrated systems due to the available functional groups and complex interaction between different surfaces.

	Implement	Resolution	Throughput	Location precision	Versatility
Microcontact printing	Parallel	+	+ + +	+	+
Near-field techniques	Serial/Parallel	+ + +	+ +	+ + +	+ + +
Beam irradiation	Serial/Parallel	+ + +	+	+ + +	+ + +
Orthogonal chemical functionalization	Serial/Parallel	+ +	+ + +	+ +	+ + +

Table 1.1 Comparisons among different chemical patterning approaches (+++ is highest, + is lowest).

1.3 Organolayers functionalization of inorganic surface

Organolayers can be built on a wide range of solid surfaces to tune their physicochemical properties, or to immobilize molecules for sensing applications. The layer has a 2D structure and is composed of organic molecules that are spontaneously bound from a liquid or gas environment onto a solid surface, usually by a covalent bond or a non-covalent bond between one of the molecule's headgroups and the surface. The remaining available headgroups, separated from the former by a spacer chain can be chosen to fulfill a specific function. This process is therefore referred to as chemical surface functionalization.

1.3.1 Oxides

Oxides can be symbolized as MO_x, where M can be a metal (e.g. Al, Ti) or a semiconductor (e.g. Si). It can also refer to materials that forms native oxides or (-OH) groups upon activation reactions. In principle, activation (increase of the surface density of metal oxide moieties) can be obtained in a variety of ways, such as piranha solution, UV/ozone irradiation and plasma activation. Oxides are appealing, as they are typically not only easily accessible and thermodynamically stable, but also many of them share the potential for surface functionalization through the reactivity of surface bound -OH groups as anchoring points for the formation of densely packed layers (Figure 1.5). The reactions have recently been reviewed in details[54]. Here we will focus on silane, phosphonate and catechol that have been used to covalently attach organolayers onto oxides.

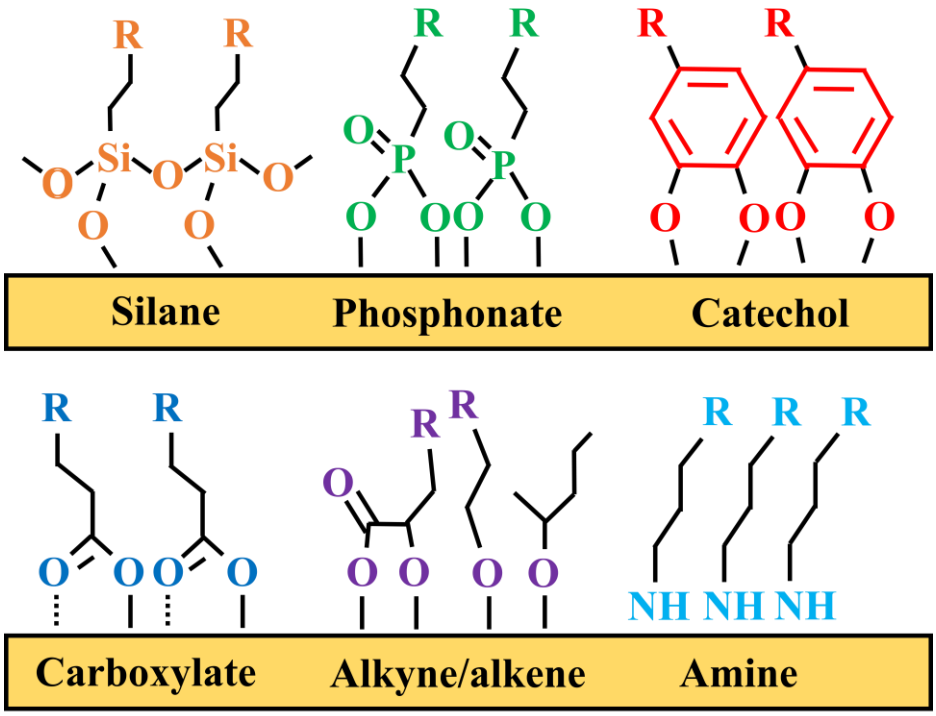

Figure 1.5 Attachment methods and the resulting modified oxide surfaces.

Table 1.2 undertakes a summary on the use of these three reactions on various substrates. In the first column, the different types of oxide surfaces are indicated. In the remaining columns, the corresponding references are given for the substrate–organolayer combination. The quality of the layers includes features such as structural order and long-term stability. It might be helpful to select an optimal oxide surface-organolayers combination for own purposes.

Oxide Surface	Silanes	Phosphonates	Catechols
Glass	[55]–[58]	-	[59]
SiO_2	[58], [60], [61]	[62], [63]	[64]
TiO_2	[65]–[68]	[67], [69]–[71]	[72]–[79]
WO_3	-	[80]	-
Al_2O_3	[81]–[84]	[85]–[88]	[89], [90]
ZnO	[91]–[94]	[95]–[98]	-
SnO_2	[99]–[102]	-	-
ITO	[103]–[106]	[107]–[110]	[111]
Co/Cr/steel	[112]–[115]	[112], [116]–[118]	[119]

Table 1.2 Overview of reported substrates–organolayers combinations.

1.3.1.1 Phosphonic acids

1.3.1.1.1 Phosphonic acids presentation

H. D. Cook *et al*. reported on the use of phosphonic acids and phosphonates molecule for the formation of organolayers in 1954[120]. Since, phosphonic acids, phosphonates and phosphonate esters have become attractive anchoring groups for hydroxylated surfaces, especially for oxides. The common surface-binding phosphonic groups reported in the literature to bind onto a metal oxide surface are shown in Table 1.3.

Name and formula	Mechanism
Phosphonic acid[107], [121] 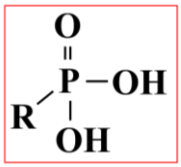	Phosphonic acid are soluble in a wide variety of solvent including water. Depending on the alkyl chain length, their solubility in water can be limited. Short chain are highly soluble in water while longer chain are not. The reaction mechanism is described below.
Ester phosphonate[122]–[124] 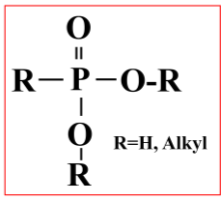	Phosphonate esters permit to perform the layer formation even with short alkyl chain in organic solvent when water should be avoided. This is the case with oxides that are soluble in water for example. Furthermore, the electron donating effect of the alkyl groups, favors the coordination of the phosphoryl oxygen by an acidic titanium dioxide site.
Phosphonic dichloride[80] 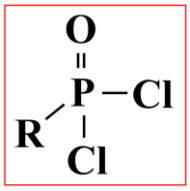	Condensation between phosphonic dichloride and tungsten eliminates HCl and forms covalent bonds between the phosphonate and substrates. 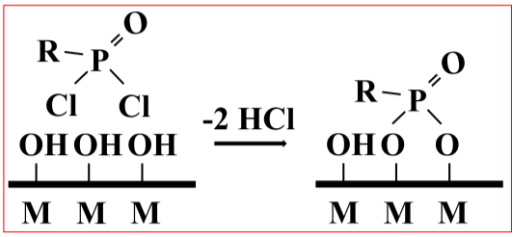

Table 1.3 Different phosphonates surface-binding groups.

On Lewis acidic metal oxide surfaces (Figure 1.6, route1), binding originates from initial coordination of the phosphoryl oxygen atom (P=O) to a Lewis acidic site. Then the P atom becomes more electrophilic and induces the consecutive heterocondensation with the neighboring surface hydroxyl groups, resulting in strong covalent P-O-M anchoring. On metal oxide lacking Lewis acidity the mechanism follow route 2 in Figure 1.6.

The coordination of phosphoryl oxygen is minimal and the heterocondensation is promoted by hydrogen bonding between for instance metal hydroxyl and phosphono's hydroxyl or [(alkoxy)hydroxyphosphoryl]oxy-'s alkoxy. Heating may accelerate the covalent coupling by favoring alcohol or water condensation.

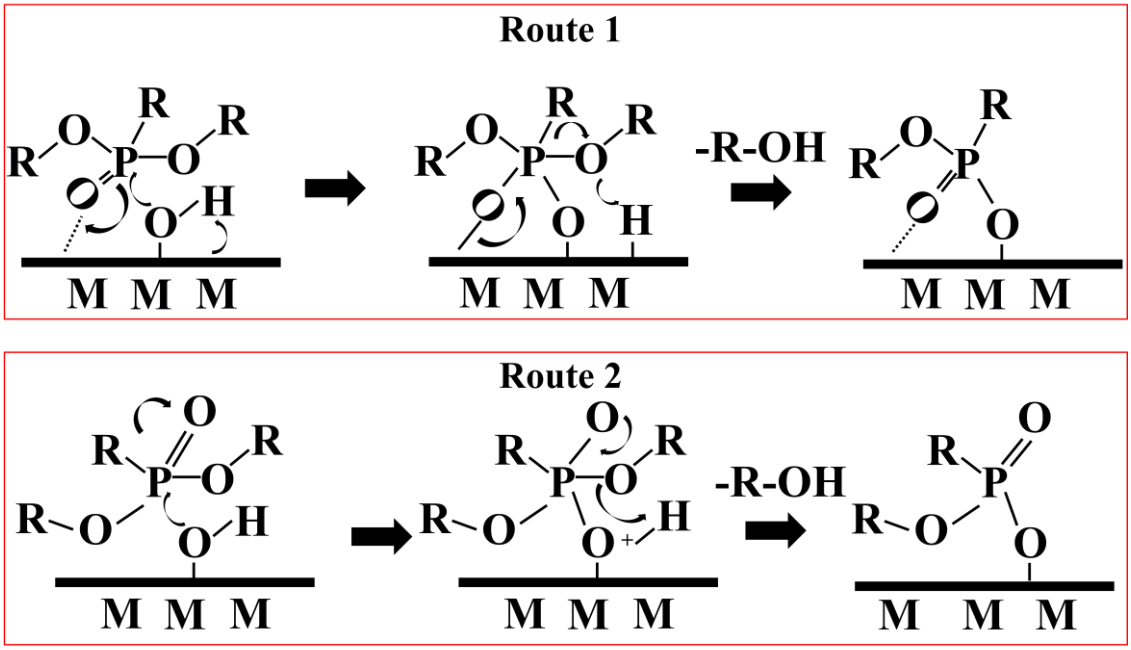

Figure 1.6 Mechanism of phosphonic acid attachment 1) to Lewis acidic metal oxides and 2) to poorly Lewis acidic metal oxides.

The presence of the three oxygen atoms of the phosphonates allow monodentate, bidentate, or tridentate binding modes in combination with possible electrostatic and hydrogen-bonding interactions (Figure 1.7)[107], [124].

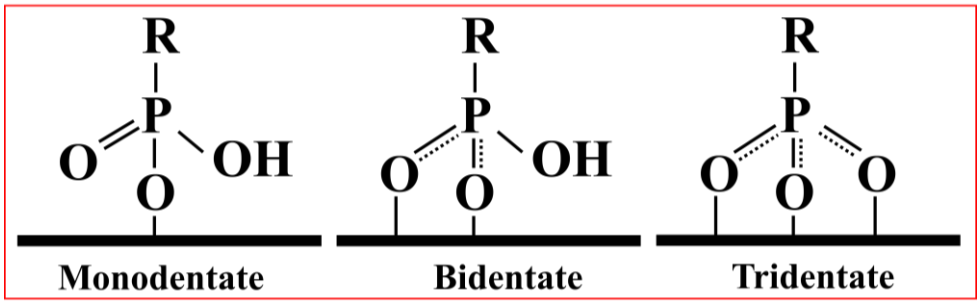

Figure 1.7 Different bonding modes of a phosphonate unit to a metal oxide surface.

It is difficult to unambiguously identify any single one binding mode present in a system. However, it is possible to distinguish the presence or absence of some of the binding modes. Different analysis methods such as nuclear magnetic resonance (NMR) spectroscopy, time-of-flight secondary mass spectroscopy (TOF-SIMS), polarization modulation-infrared reflection-adsorption spectroscopy (PM-IRRAS), X-ray photoelectron spectroscopy (XPS), density functional theory (DFT), were used to better understand the binding modes (Table 1.4).

M-O-P bond	The M-O-P bond was evidenced by ToF-SIMS and ^{17}O MAS NMR in particular in the case of titania. A resonance signal at δ=185 ppm provided direct evidence for the formation of P-O-Ti linkage. Furthermore, using ToF-SIMS, characteristic fragments (TiP_2O_6, TiP_2O_7H, and $TiP_3O_6H_2$) confirmed the formation of P-O-Ti bonds on Ti90/Al6/V4 substrate[125]. XPS O1s peak also suggest that some of the P-O-H bonds (533 eV) are transformed into P-O-Ti bonds (531.5 eV)[67].
Binding mode	On titania, using ^{17}O MAS NMR, free residual P=O and P-OH functionalities were also detected at δ=113/85ppm suggesting the existence of mono and bidentate binding mode[126]. Using PM-IRRAS, the presence of strong peaks corresponding to $\nu_{(P=O)}$ vibrations in the 1230cm^{-1} region, along with the diminished peaks between 955 and 930cm^{-1} (P-OH stretching vibrations), indicated the presence of mainly bidentate bound octadecylphosphonic acid (ODPA) on ITO surface[127]. However on phenylphosphonic acid (PPA)-indium zinc oxide (IZO), the absence of $\nu_{(P-OH)}$ mode (925 and 939 cm^{-1}) and $\nu_{(P=O)}$ mode (1220 cm^{-1}) indicated that bidentate or tridentate binding were preferred.[128] On ZnO, the observed shifts of the P=O and P−O stretches on IR spectrum after surface anchoring have been modeled by DFT. A multi-dentate bonding involving the formation of two P−O−Zn bonds and a strong P=O-H linkage between the phosphonic head and the surface seems possible.[129]
Hydrogen bonding	The H-bonding interactions in adsorbed carboxyalkylphosphonates on TiO_2 and ZrO_2 were measured by ^{1}H MAS NMR. The hydrogen-bonding network in multilayers of the diacids is more ordered but highly perturbed from the bulk state with the formation of heterodimers rather than homodimers[130].

Table 1.4 Different analysis methods of binding modes.

1.3.1.1.2 Phosphonic acid layer formation: experimental parameters

Phosphonic acid layers can also be formed by adsorption from a vapor-phase reaction or solution phase. The vapor-phase reaction maybe easily lead to the multilayers formation[131], [132]. The most common techniques to obtain phosphonate-based monolayers are immersion or dip coating, from a solution. Immersion times span from a few minutes to a couple of hours or even days. The concentrations of the phosphonates solution range from 1 mM to 10 mM and a wide variety of solvents of polar and non-polar have been used: water[133]–[136], methanol[135]–[137], acetonitrile[136], ethanol[127], [138], [139], THF[63], [117], [125], [129], [136], acetone[130], [136], TCE[140], pyridine[136], dimethyl sulfoxide[136], dichloromethane[123], chloroform[140] and toluene[67], [126]. Whether one is preferable to another seems to depend on which molecule and substrate are used as well as which

characteristic is desired. First, the solvents employed for functionalization are dictated by the solubility of the phosphonate. For example, phosphonic acids with different lengths of alkyl spacer have different solubility in water and organic solvent. On the other hand, the oxide should not be dissolved by the solvent. In particular some oxides can be dissolved by aqueous media. In addition, it has been reported that the nonpolar solvents seems to favor the interaction between the hydrophilic phosphonate and the hydrophilic oxide. For example, a study of solvent effects during alkyl phosphonic acid layers on ITO concluded that weak or negligible interactions of the solvent with the surface promote denser, more stable monolayers[136]. However phosphonic acids and phosphonates layers formation protocols on metal oxides involve an annealing process to promote the stable covalent bonding with the TiO_2, Al_2O_3 and ITO as in the particular case of silica [80], [98], [126], [128], [136], [141], [142]. The annealing temperature range is from tens to 200 °C. The annealing time is from a few minutes to many hours.

E. L. Hanson *et al*. have developed a technique for grafting phosphonic acid films, referred to as tethering by aggregation and growth (T-BAG) method[62]. The approach includes self-assembly of weakly physical adsorbed phosphonate on a vertical substrate by slow evaporation of solvent, and a subsequent thermal annealing step at 140 °C under low humidity conditions to induce chemisorption of the phosphonic acids onto the substrate. The T-BAG procedure appears to benefit from some organized aggregation of the dissolved phosphonic acid at the air-solvent interface and appears to ensure robust chemical bonding in a heating step. This approach has been used on SiO_2, ITO or TiO_2[125], [127].

1.3.1.1.3 Phosphonic acid layer stability

The stability of phosphonic acids and phosphonates organolayers is crucial for successfully using these layers to coat medical implants substrates and other biomedical applications. In general, phosphonic acid surface modifications lead to reproducible and stable layers on a wide variety of oxides. However, their grafting on SiO_2 seems to be governed by weak physical interactions, such as van der Waals interactions and hydrogen bonding, unless an annealing step is performed. In fact the T-BAG procedure was developed with the aim to form stable phosphonic acid layers on SiO_2.

The solvent and its polarity seems also to be crucial for enhancing the interaction between the polar phosphonate head group and the hydrophilic oxide surface and therefore for favoring the condensation reaction. The annealing step favors the condensation between the phosphonate and the hydroxyls. Indeed, the formation of the P-O-M bond is compulsory for the layer stability. Its energy is in the 3.5 eV/bond range. For comparison, the S-Au bond is 1.7 eV/bond[67].

However, the stability of the phosphonic acid layer is still a matter of debate as it seems to depend on the oxide to be modified. Different phosphonic acid layers on ZrO_2[143], ITO[110],

[144] cobalt chromium alloys[117], [118] and Al_2O_3[86] surfaces were found to be stable. Different reports show that the layers even on the above oxides are not as stable as claimed. This discrepancy may results from the experimental conditions under which the layer is formed (solvent, annealing) and from the conditions under which the stability is evaluated.

For example, H. Yang *et al*. showed that the stability of phosphonate monolayers on ITO were affected by the experimental conditions. Monolayers prepared using the dipping method followed by baking at 140 °C for 2 hours were as good as or even better than those prepared using T-BAG method in terms of stability. It has been shown that phosphonate monolayers are more stable in either PBS solution or ambient air condition than pure water[110], [144].

The stability of the adsorption of octadecylphosphonic acid on Al_2O_3 surfaces is based on different types of interfacial bonding, which strongly depends on the present surface crystallographic orientation and thereby local geometries. Adhesion free energies as well as the local atomic arrangements at the surface play a crucial role for the formation of a stable film on aluminum oxide[86].

Generally, phosphonic acid layers are described as stable on TiO_2. However, several authors reported that their stability could be weaken. J. Ralston *et al.* showed that the stability of ODPA monolayers on titania surface is influenced by the dielectric constants of the solvent used during the layer formation[70]. C. M. Agrawal *et al*. investigated the stability of phosphonic acid monolayers on titanium in tris-buffered saline (TBS 37 °C), ambient air and ultraviolet (UV) light after modification in the solvent of doubly distilled water without annealing. In TBS, a significant proportion of phosphonic acid molecules were desorbed from the titanium surface within 1 day. In ambient air, their phosphonic acid monolayer was stable for up to 14 days. It has also been found that under UV-radiation exposure, the alkyl chains of the phosphonic acid molecules were decomposed, leaving only the phosphonate groups on the titanium surface after 12 hours[67].

1.3.1.2 Silane

1.3.1.2.1 Silanes presentation

Surface modification with alkylsilanes is one of the most commonly used methods to prepare organolayers on oxides. The grafting involves hydroxyl groups at the surface, which can form Si-O-Si or Si-O-metal bridges. This reaction is often referred to as silanization. Silanes has been used extensively for the functionalization of silica or other bioanalytical platforms as its role in surface modification has been intensively investigated and well understood[145]–[148]. Alkyl silanes are composed of one to four leaving groups leading to the formation of one to four bridges. For surface functionalization, monofunctional, bifunctional and trifunctional are mainly used. Multifunctional silanes can in principle bind to a greater extent on oxide surfaces while monofunctional silanes may yield sub-monolayer coverages. The leaving groups can be a hydride, halide (generally chloride) or an alkoxide: Silanization with R_3SiH, $RSiH_3$, $RSiCl_3$,

$RSi(OCH_3)_3$ and $RSi(OEt)_3$ have been reported on various oxides including metal oxides (or their native oxide layer such as aluminum oxide, zinc oxide, titanium oxide, chromium oxide and nicked alloy)[149]–[154]. Silane organolayer formation on oxides is attributed to either one-step reaction or two-step reaction mechanisms[9], [155]. In the one-step mechanism, the direct condensation of pendant hydroxyls from the surface of the oxide with the silane occurs at an appreciable rate for temperature above 300-400 °C with chlorosilanes and above 100-200 °C with alkoxy silanes (Figure 1.8).

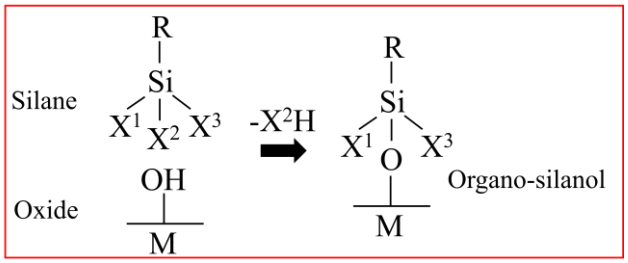

Figure 1.8 One-step mechanism of silanes organolayer formation.

At room temperature, a more complex mechanism firstly involves the hydrolysis of the leaving group of the organosilane; leading to an organo-silanol. This organo-silanol binds with pendant surface hydroxyl groups through hydrogen bonds. Then, dehydration of the silanol with pendant hydroxyl groups from the substrate lead to the formation of a Si-O-Si or Si-O-M bond. The yield of this dehydration is weak at room temperature, leading to poorly attached silane layers; it is usually necessary to use thermal annealing or catalysis (e.g. amine catalysis) to condense water and transform a significant amount of hydrogen bonds into covalent siloxane bonds[9], [156]. In the case of multifunctional silane (e.g. multichloro or multialkoxy), lateral crosslinking can take place between silanes. Under uncontrolled experimental conditions cross linking reactions can lead to 3D polysiloxane network, as presented in Figure 1.9.

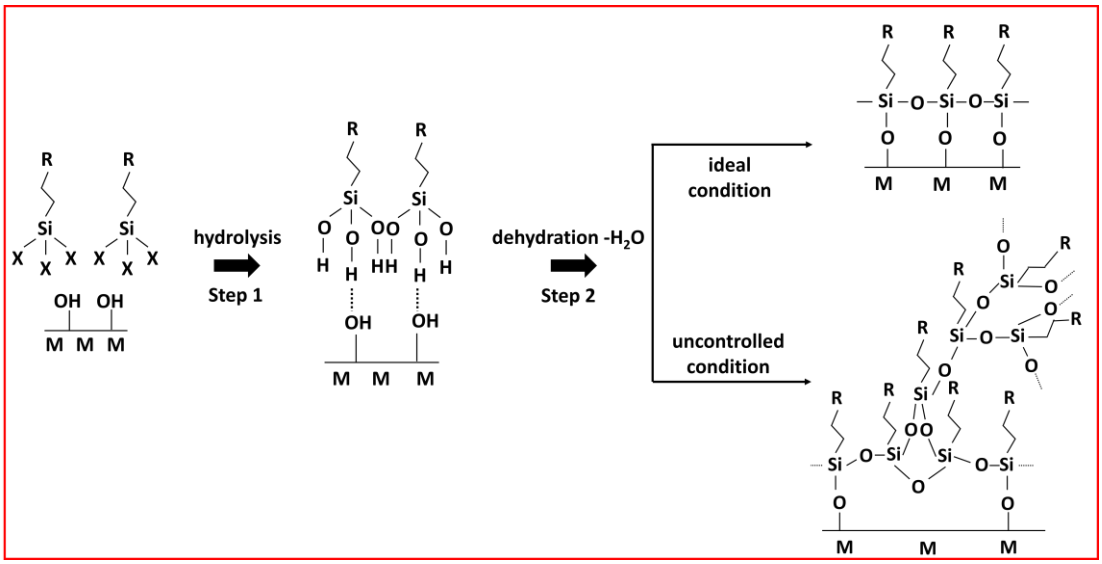

Figure 1. 9 Two-step mechanism of silanes organolayer formation.

As mentioned above, monofunctional organosilane (R_3SiX, where X=H, Cl or OEt) having only one hydrolysable group (leaving group), only one siloxane bond can be formed either between the silanes and the surface or between two silanes. Thus, polymerization reaction is avoided. The modification of silanes on oxides have been demonstrated by various characterization techniques such as ToF-SIMS, AFM, ellipsometry, IR, and XPS.

For silanes functionalization on silica, the nature of the organolayers can be further explored by deconstructing the high-resolution XPS spectra of Si2p peaks to determine the contributions from different SiOx moieties. M. R. Alexander et al. demonstrate that the Si2p component peaks in SiO_x films can be resolved and quantitative peak fitting can be performed based on two assumptions: (1) each Si atom has a valence of four, resulting in four component peaks within the Si2p envelope and (2) the shift of the Si binding energies depends primarily on the number of oxygen atoms attached to the Si[157]. The four component peaks of the Si2p envelope are abbreviated as $Si(O)_1$, $Si(O)_2$, $Si(O)_3$ and $Si(O)_4$ with binding energies at 101.5 eV, 102.1 eV, 102.8 eV, and 103.4 eV, respectively. The oxygen subscript indicates how many oxygen atoms are attached to the Si atom. The $Si(O)_4$ designation indicates a tetrahedral SiO_2 network. The $Si(O)_1$ designation indicates only one oxygen atoms are attached to the Si atom. For example, E. Laurenceau et al. reported monofunctional silane (APDMES) grafted silica. There are two contributions at 103.6 eV and 101.6 eV, which was assigned to the $Si(O)_4$ and $Si(O)_1$ component peak, which was indicative of the $Si(O)_1$ of APDMES bonded to the silica surface[158]. H. J. Martin et al. reported multifunctional silane (APTES) grafted titanium. There is no contribution of $Si(O)_1$ component peak[65]. This deconvolution is widely used to characterize the SiO_x containing films on solid surfaces[159]–[164].

For the direct observation of Si-O bond formation, IR spectroscopy has previously been used for the silica silanization studies for monitoring Si-O-Si bond formation. Silanes layers formation on SiO_2 can be monitored by the longitudinal optical (LO) absorption band that arises from the vibrations perpendicular to the surface of Si-O bonds at the organolayers and SiO_2 interface[165], [166]. However, from the broad absorption peaks at 950 cm^{-1} - 1250 cm^{-1}, the modes of Si-O bonds from silica, silane/silica interface, and silane-silane cross-linking overlap. It is quite difficult to determine whether the newly formed organosilanes are parts of the silica network or just attached through one bond. J. Gao et al. reported that detection of the LO phonon mode of thin SiO_2 films makes it possible to characterize the newly formed Si-O bonds at the SAM/(SiO_2/Si) interface[167]. Y. J. Chabal et al. reported that the APTES layer obtained on SiO_2 by pre-annealing the solution at 70 °C exhibits a better stability in deionized water than the one prepared at room temperature using in situ IR absorption spectroscopy[168]. For silanization functionalization, combination of different technologies have been used to investigate the organolayers formation. C. M. Agrawal et al. studied the formation and stability of self-assembled monolayers (SAMs) on Co–Cr–W–Ni alloy surface

for the first time. OTS SAM coated alloy specimens were characterized using contact angle goniometry, FTIR, XPS and AFM. The study shows that Co–Cr alloys can be surface modified using SAMs for potential biomedical applications[152]. S. Boujday et al. reported that the mechanism of APTES interaction with silicon surfaces was investigated using IR in grazing angle attenuated total reflection mode, atomic force microscopy, and contact angle measurements. It suggests the mechanism follows a nucleation-growth model on a chemically heterogeneous surface[169].

It is noteworthy that PM-IRRAS is a sensitive and nondestructive way of acquiring molecular information on these bidimensional systems, such as the formation of chemical bonds with substrates, the hydrogen-bonded structures, and the conformation of the alkyl chains and the orientation of the functional groups. L. Vellutini et al. have reported the silanization of different molecules on SiO_2/Au substrates, which were monitored by PM-IRRAS for the first time. It allows to monitor easily the chemical modification of the terminal function of monolayers grafted onto SiO_2 surfaces[170]–[174].

1.3.1.2.2 Silane layers formation: experimental parameters

Silane organolayers can be formed from solutions, from gas phase or by spin coating. J. Sagiv et al. first reported on the preparation of silane monolayers from the solution phase[175]. Silanization is usually carried out by immersing the sample surface into a dilute solution of silanes in an organic solvent. In solution-phase reactions, critical factors are the solvent viscosity and polarity, and the amount of water in the liquid medium to hydrolyze the silane molecules[57], [61], [176]. Organic solvents used for silanization include: ethanol[177], acetone[178], [179], dioxane[57], benzene[57], toluene[57], [180]–[182], xylene[183], pentane[57], bicyclohexyl[184], cyclooctane[57], hexadecane[57], octane[57], cyclohexane[57], hexane[57], CCl_4[57], [183] and dichloromethane[57]. Anhydrous solvents or solvents with controlled water content are typically required to obtain a smooth monolayer. Indeed, the water content will affect the hydrolysis of the leaving group of the organosilane in the first step, as incomplete hydrolysis or excessive hydrolysis result in incomplete monolayers or formation of polysiloxanes on the surface, respectively[58], [185]–[187]. Before functionalization, the solvents are either dried[188], used in normal conditions (neither dried nor mixed with added water) or mixed with ultrapure water[178], [179]. In addition, post-formation annealing and pre-annealing of the silicon oxide produce significant improvements in the quality of the film and a smaller number of unreacted sites[9], [168], [183], [188]. Indeed, the amount and the location of water (on the substrate surface, in the solvent and even as adsorbed water on the glassware) takes a major role in the behavior of the finalized silane layer[166], [189]. Silanes layers can also be formed by adsorption from a vapor-phase medium[190]–[193].

1.3.1.2.3 Silane layers stability

The stability of silane organolayers on metal oxides is mainly determined by the covalent bonds between silane molecules with the underlying metal and cross-links between neighboring silane molecules (Si-O-Si lateral bonds)[194]. The exact state of bonding responsible for the stability of organolayers on metal oxides is still a matter of debate. A. Y. Fadeev *et al*. explored the thermal and oxidative stability of the organosilane layers on titanium, zirconium and hafnium dioxides by thermogravimetric analysis (TGA). The organosilane layers showed good thermal and oxidative stability below 200 °C in air because of the cross-linked layers between the silane molecules[195], [196]. However, C. M. Agrawal *et al*. proposed that the excellent stability of dodecyltrichlorosilane (DDTS) layers on TiO_2 under physiological conditions is mainly attributed to the strong Si-O-Ti covalent bonds, and that the Si-O-Si cross-linking formed in the monolayer system was negligible. The hydrogen bonds within the monolayer and the van der Waals interactions between the alkyl chains may also have contributed to the stability of silanes[67].

1.3.1.3 Ortho-dihydroxyaryl (catechols) compounds

1.3.1.3.1 Catechols presentation

Recently ortho-dihydroxyaryl compounds (catechols) (Figure 1.10) have been used for surface functionalization. Although the use of ortho-dihydroxyaryl compounds is not specific for metallic oxide functionalization, it has the advantage of allowing to obtain stable layers without the need of harsh conditions[197], [198]. The binding mechanism is complex due to the fact that the film formation is composed of the attachment of the catechol to the oxide surface and to the oxidation-polymerization/crosslinking reaction of the bound catechol with the ones in the solution. The resulting polymeric film (e.g. polydopamine) has strong interfacial adhesion with the surfaces. The polymerization of catechol can be controlled by the introduction of electron-withdrawing groups, limiting oxidant media and controlling the pH values of solvents[73], [199]. Here we will not discuss much about the polydopamine film formation. We will just discuss the attachment of catechol-based monolayers on metal oxide.

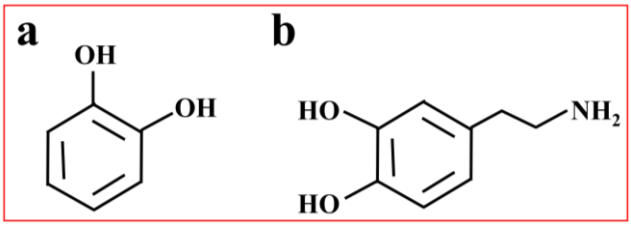

Figure 1.10 Two examples of catechol compounds (a) Simplest catechol, (b) dopamine.

The formation of mono and bidendate complexes require the replacement of the surface hydroxyl by the deprotonated aromatic hydroxyl in a variety of binding modes, which has been shown to be operative for titanium, aluminum and iron oxides. However, the exact

chemistry behind is not fully understood so far. The mechanism of catechol bonding has actually been studied for several years and different interaction forms of catechol groups with surfaces have been proposed[54], [197], [200]. The proposed mechanisms of catechol grafted on oxides surfaces is shown in Figure 1.11.

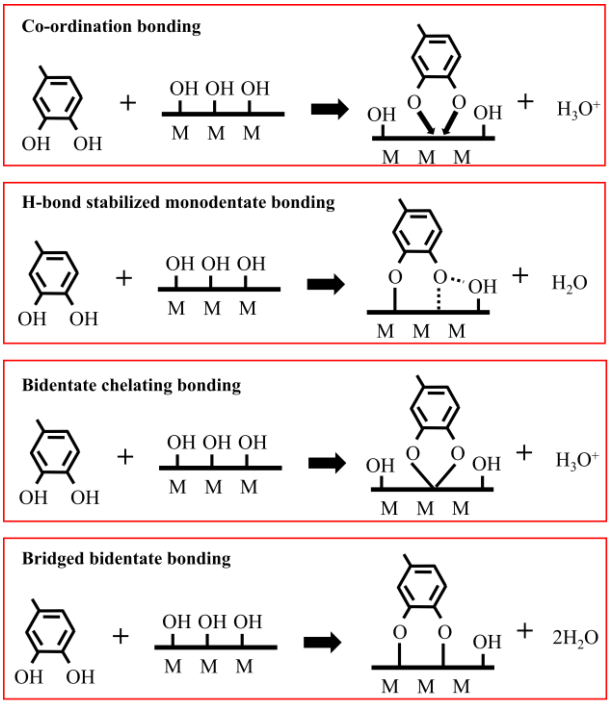

Figure 1.11 The proposed mechanism of catechol molecules binding to metal oxides surfaces.

The real interaction might be a mixture of these different interaction modes and is probably substrate dependent. Different analysis methods such as nuclear magnetic resonance (NMR) spectroscopy, Raman spectroscopy, X-ray photoelectron spectroscopy (XPS) and Scanning Tunneling Microscope (STM), were used to better understand the binding modes (Table 1.5).

Methods	Discussion
Binding mode	On titania, N1s XPS spectra indicate that catechol derivatives results in two possible configurations: H-bond stabilized mononuclear monodentate and binuclear bidentate configurations bonds[73]. Using STM, it was proposed that monodentate or mixed monodentate-bidentate can easily convert from one into the other via proton exchange between the surface and the adsorbed catechol[78], [201].
Orientation	Raman spectroscopy indicates that DOPA adsorbs on TiO_2 surface forming two species depending on the pH values and surface coverages: (1) standing up orthogonal and (2) lying down parallel to the surface[75].

Table 1.5 Different analysis methods of binding modes.

1.3.1.3.2 Protocols for catechol layer formation

Surface functionalization with catechol is performed exclusively from solution. As mentioned above, catechol can oxidize and self-polymerize under alkaline conditions (typically pH 8.5) with oxygen as the oxidant[202]. Indeed, dopamine is liable to oxidation into polydopamine, especially at elevated pH. In order to form dopamine or catechol derivatives monolayers, formation of the monolayer has to be performed in non-alkaline solvents and under inert atmosphere. Solvents used for catechol functionalization include: pure water[73], organic solvents mixed with ultrapure water (water/ethanol 3:2, water/2-propanol 2:1)[203] and acidic buffer buffers[199]. The substrates are immersed in the solution containing catechol (0.2-1 mg/ml) at room temperature with modification times of several minutes to 48 hours under inert atmosphere[72], [73].

1.3.1.3.3 Catechol layers stability

Different binding configurations of catechol derivatives give raise to different bond strength and can thus lead to different stabilities. Dopamine-modified TiO_2 colloids exhibit very stable optical properties when exposed to thousands of 10mJ laser pulses and at daylight even for two to three years[204]. M. Textor *et al*. have tested the chemical stability of catechol-functionalized poly(L-lysine)-graft-poly(ethylene glycol) copolymer: PLL-g-(DHPAA; PEG) layer coated TiO_2 substrate in saturated sodium chloride solution for 17 hours at room temperature[205]. Some reductions in film thickness in high ionic salt solutions was found, possibly due to the loss of some loosely bound polymers. In addition, the stability performance of this copolymer was drastically altered by the presence of DHPAA ligands. Similarly, B. Xu *et al*. showed that dopamine-based anchor on iron oxide surface exhibited exceptional stability after being boiled in Tris buffer for 20 min[206]. E. Reimhult et al. reported PEG-dopamine modified iron oxide nanoparticles exhibited good stability after diluting them in water for at least 4 months without nanoparticle agglomeration[207].

1.3.2 Gold

The study of gold functionalization represents a much lesser part of the work developed during this PhD, we will not go in such a great detail of the literature as we have done concerning oxides functionalization. Nonetheless, let us briefly present those aspects of gold functionalization, namely the choice of the binding group and standard protocols.

1.3.2.1 Alkanethiol

The grafting of a molecule on gold involves reaction with atoms from column 16 in the Mendeleev table mainly sulfur and selenium. The literature is mainly documented on organomercaptan (alkanethiol) gold functionalization. The reaction of organomercaptan give rise to gold–sulfur (Au-S) bonds via anchoring thiols [6], which is shown in Figure 1.12.

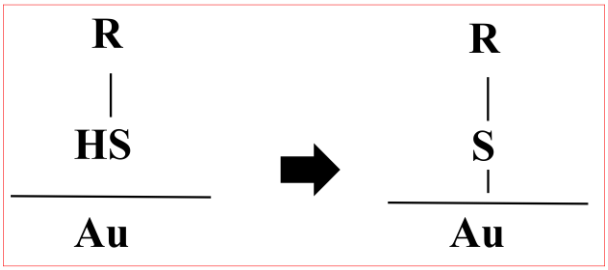

Figure 1.12 Simplified reaction scheme for alkanethiols functionalization on gold surfaces.

Alkanethiols are firstly physisorbed through Van der Waals interactions (between the alkyl chains/gold and and thiol/gold) on the substrate even at very low concentrations in a metastable state, with energies are in the order of 40-100 kJ/mol[208]. Physisorption energy is on the order of 6.1 kJ/mol per CH_2 group, and the order of 33 kJ/mol for a thiol group. Then, the so-formed thiolate is covalently bound onto gold surface, (80-200 kJ/mol)[6], [208]–[210]. At last, the adjacent alkyl chains organize themselves in an ordered and close-packing via Van der Waals forces (4-8 kJ/mol per methyl unit)[211]. Other chemical groups are reported to bind onto a gold surface (Figure 1.13).

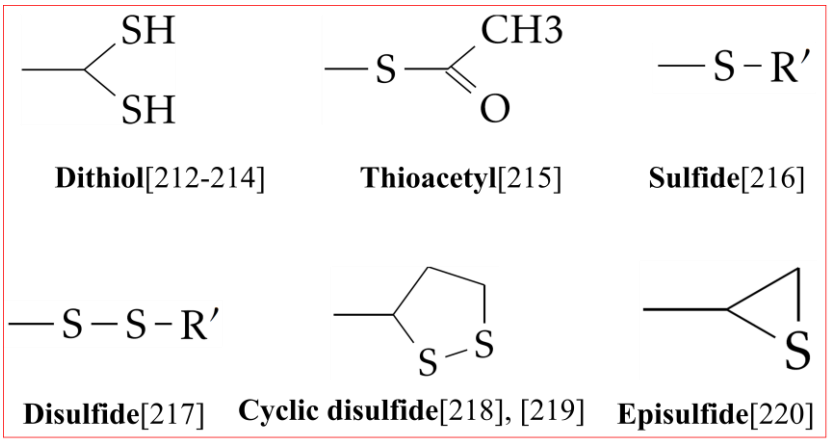

Figure 1.13 Different chemical groups to bind an organic molecule onto a gold surface.

1.3.2.2 Formation of the alkanethiol layers: experimental parameters

An easy way to form thiolate layers on gold surfaces is to immerse the sample in a solvent containing the desired thiols at room temperature. The solvents used to build these thiolate layers are pure ethanol, water/ethanol mixture[219], [221], THF[222], [223], acetonitrile[219], [223], [224], ethyl acetate[224], diethyl ether[224], chloroform[224], hexadecane[223], carbon tetrachloride (CCl_4)[219], [223], dichloromethane (DCM)[224], and toluene[223]. Ethanol is the most common solvent for building thiolate layers. A survey of the publications shows that most protocols use concentrations of 1-10mM with functionalization times of 3-24 hours[225]–[232]. These thiols usually have an alkyl or alkyl-PEG spacer with common lengths of around 3-16 methylene units and 3-6 Ethylene Glycol (EG) units in the case of alkyl-PEGs. Thiolate layers can also be formed by adsorption from a gas phase in ultrahigh

vacuum[233], [234]. Adsorption from a gas phase has been mainly used to obtain fundamental information about the SAM formation mechanisms and kinetics, especially at the early stages.

1.3.3 Characterizations

There are many tools to characterize the chemical state of organolayers at a solid surface. Here we will not give extensive details about these techniques but rather a comparison of their specifications and the complementary information that can be obtained from them (Table 1.6). The values given in this table are only indicative, as variations are possible depending on the parameters and conditions of use. All the following tools will be explained in more detail in the Annex A. In the following paragraphs we will review the state of the art of orthogonal surface functionalization with organolayers.

Characterization	Information	Depth of analysis	Spatial resolution
Contact angle*	Surface energy	0.3-2nm	1mm
Ellipsometry	thickness, dielectric constant	10nm	10-100µm
Electrochemistry	Electric properties	0.1nm	-
XPS imaging	Chemical, elemental	2-5nm	10-50um
XPS*	Chemical, elemental	2-5 nm	mm
ToF-SIMS*	Chemical	1nm	100nm
IR spectroscopy*	Chemical	1-5µm	10µm
PM-IRRAS*	Chemical	1-5 µm	mm
Raman	Chemical	100nm	1µm
AES	Elemental, Chemical	1-2nm	50nm
AFM*	Topography, elasticity, friction	0.2-0.3nm	0.1nm
STM	Elemental	0.1nm	0.1nm
TERS	Chemical	0.2-0.3nm	10nm

Table 1.6 Summary of different surface chemistry characterization tools. "" indicates characterization tools that are used in the present PhD thesis experimental work.*

1.4 Orthogonal chemical functionalization of heterogeneous surface

1.4.1 Introduction to orthogonal chemical functionalization

If a substrate is composed of different materials, orthogonal chemical functionalization can then take advantage of the affinity of different substrate binding head groups for these materials in order to obtain different organolayers on these materials.

1.4.2 State of the art of orthogonal functionalization

Orthogonal functionalization on patterned substrates concerns generally the functionalization of a substrate featuring metallic and oxide areas. In the literature, reported orthogonal functionalization concern mainly dual material substrates composed of a metal and an oxide. The most reported ones are: gold/silica, gold/metal oxide, silica/metal oxide and gold/metal oxide/silica, as shown in Table 1.7. The oxides can be metal oxide such as TiO_2, SiO_2, glass or ITO. Material bearing a native oxide such as silicon, silicon nitride are considered as oxide as their reactivity to substrate binding head groups is similar as to the one of oxides. Considering the gold/oxide dual substrate, one can take advantage of the thiol head groups as a specific reactant for gold modification. Silane, organo-phosphonic acids, carboxylate or amine can be exploited for oxide modification. Several examples of thiol/silane, thiol/phosphonic acids or thiol/carboxylates can be found in the literature. The scheme of the combination of orthogonal functionalization is shown in Figure 1.14.

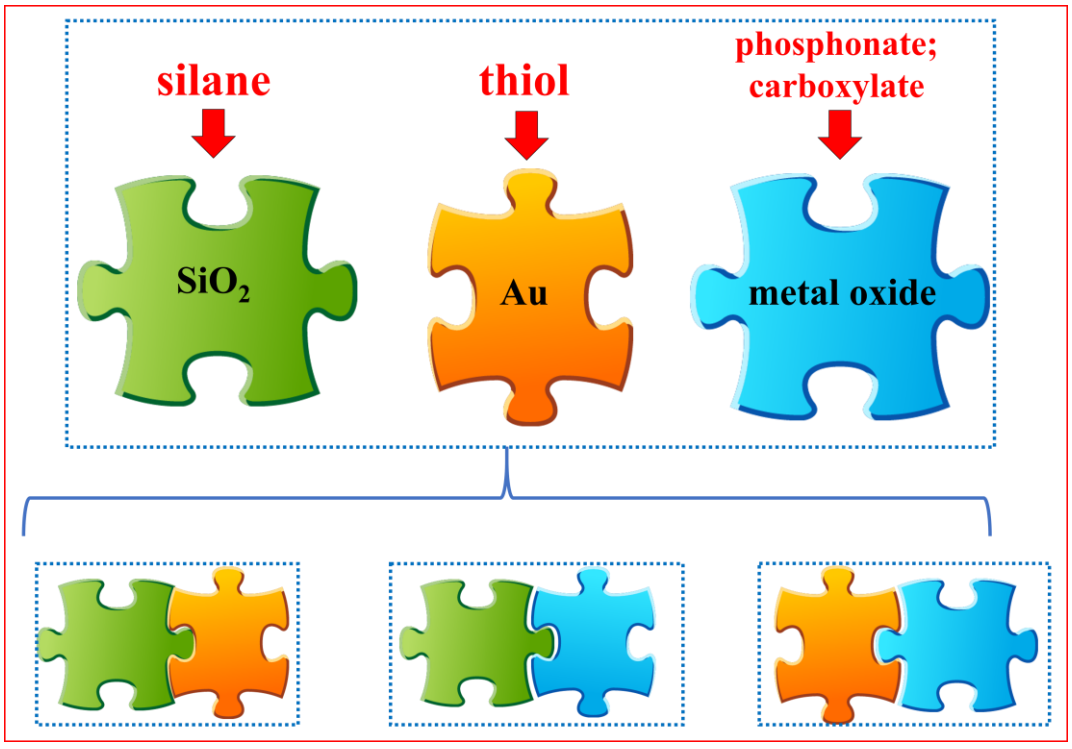

Figure 1.14 Schematic representation of the combination of orthogonal functionalization.

Substrate	Coupling reaction and Conditions	Steps	Discussion	Ref
Au/SiO_2	a mixture of 2.5 all **silane** (PEG-silane), 1.25 mL toluene and 1µL concentrated HCl/**thiol** 5 mM (SH-PEG-NH_2) or 0.6 µM (HS-nucleic acid) in ethanol	2	Orthogonal functionalization have been achieved that combinations of silanes and thiols were grafted on gold/SiO_2 patterned surfaces selectively.	[50], [235]
	1 mM **thiol** (ODT, MUD, MHA, AUT) in ethanol/1 mM **silane** ($Cl_3Si(C_2H_2O)_{6-9}CH_3$) in toluene	2		[47]
	thiol/**silane** 9 mM/1 mM (MUA/F-silane) or 14 mM/1 mM (F-thiol/PEG-silane) or 5 mM/ 1 mM (MU-Biot/PEG-silane) in dichloromethane	1		[51]
	2% **silane** (APTES) in a mixture of acetone and water (95/5), annealing at 110 °C for 2 h/1 mM **thiol** (thiol-OEG) in ethanol	2		[179]
	1 mM **thiol** (HS-C11-EG_6-Biotin) in ethanol/13 µM **silane** (mPEG-silane) in toluene with acetic acid	2		[236], [237]
	1 mM **thiol** (thiol-PEG or thiol-PEG-biotin) in ethanol/10 µg/ml **amine** (PLL-g-PEG or PLL-g-PEG-biotin) in HEPES	2	Thiols were grafted on gold selectively, while amine (PLL-g-PEG) has the affinity on SiO_2.	[238]
Au/glass	2 mM **thiol** (11-mercaptoundecanoic acid in isopropanol/215 µL **silane** (PolyEthylene-Glycol) in 50ml DCM	2	Alkylthiols have a stronger affinity with metals than glass.	[239]
Au/SiN	1mg/ml **amine** (PLL-g-PEG) in HEPES buffer/1mg/ml **streptavidin** in HEPES buffer	2	The PLL-g-PEG was displaced by streptavidin on Au while has no effect on SiN, as streptavidin has a higher affinity to Au than PLL-g-PEG.	[240]
Au/TiO_2	0.3mg/mL **thiol** (SH-PEG/SH-PEG-biotin) in HEPES buffer/0.01 mg/mL **amine** (PLL-g-PEG) in HEPES buffer	2	The protocol developed allowed to graft thiol only on the Au. The remaining TiO_2 was backfilled with amine (PLL-g-PEG).	[49]
SiO_2/TiO_2	0.5mM **phosphonate** (ammonium dodecyl phosphate) in purity water/1mg/mL **amine** (PLL-g-PEG) in HEPES buffer	2	The protocol developed allowed to graft phosphonate only on the TiO_2. The SiO_2 was backfilled by amine (PLL-g-PEG).	[46], [241]

Table 1.7 Summary of orthogonal chemical functionalization on bi-material substrates.

There are only very few examples in the literature of the successful modifications of tri-material bearing substrates, which are summarized in Table 1.8.

Substrates	Chemicals	Discussion
Au/TiO_2/SiO_2 [242], [243]	Thiol/nitrodopamine-biotine/Amine (PLL-g-PEG)	The protocol developed allowed to graft nitrodopamine-biotine only on TiO_2 and thiol only on the Au. The remaining SiO2 surface was backfilled with amine (PLL-g-PEG).
Au/Al_2O_3/Si_3N_4 [45]	Thiol/carboxylate	The selectivity of the thiols for Au and the carboxylic or phosphonic acids for Al_2O_3 was determined by the selective assembly of these reagents on the Au and Al_2O_3 while Si_3N_4 remains unmodified.
Au/ITO/Si_3N_4 [244]	Thiol/carboxylic acid or phosphonic acid	The selectivity of the thiols for Au and the carboxylic or phosphonic acids for ITO was determined by the selective assembly of these reagents on the Au and ITO while Si_3N_4 remains unmodified.

Table 1.8 Summary of orthogonal chemical functionalization on gold/metal oxide/silicon substrates.

1.4.3 Conclusions and perspectives of orthogonal chemical functionalization

Orthogonal chemical functionalization of patterned substrates has already been undertaken by several groups throughout the world. They showed that orthogonal functionalization can be used either for the precise placement of colloids or the enhancement of LSPR-based biosensor with selective capture of target on sensitive areas. Here, we could find some important points worth noting.

Various substrate binding head groups were used: combination of thiol/silane or thiol/phosphonic acid for the modification of gold/oxide substrate. Polylysine was also used for the modification of oxides. However, in this case, it is compulsory to firstly functionalize the gold substrate with a thiol. Indeed, amines are also known to adsorb on gold, whereas thiols do not react with oxide. In other words, if one of the reactant to be used is less selective, it should be used at last to ensure the orthogonality.

In the case of TiO_2/SiO_2 templates, phosphonates were used because phosphonates react selectively on TiO_2 and weakly with SiO_2. Indeed, it has been reported that stable phosphonates layers grafted on SiO_2 need an annealing step to be performed. In fact the T-BAG procedure was developed with the aim to form stable phosphonic acid layers on SiO_2[62]. R. Michel et al. take advantage of the limited stability of SiO_2-phosphonate bond to selectively functionalize TiO_2 within a matrix of SiO_2[241].

However, most of the examples lack direct chemical characterizations of the orthogonal chemical functionalization. Indeed, the successful orthogonality was addressed indirectly using colloids trapping or SPR experiments. Besides, the stability of the formed organolayers

is often not addressed. Finally, most of the reported orthogonal functionalization involves two steps: functionalization of one material after washing, followed by functionalization of the second material. However, if functionalization is truly orthogonal, there is no reason why both functionalizations could not be operated simultaneously. Of course, for the initial research, different independent molecules grafting on the different surfaces step by step could help us to test and understand the orthogonality. And the choice of solvent is also critical, if two molecules are not soluble in one solvent, it is necessary to modify each material step by step.

1.5 Conclusions and presentation of the following work

1.5.1 Titanium tungsten (TiW)

In order to open access to new markets for semi-conductor industries and associated photonics and electronics industrial platforms (industrial analysis, molecular diagnostics, environmental analysis...), the fabrication of chemical sensors and biosensors needs to be fully compatible with industrial production line. The architecture of the sensors' transducers (e.g.: micro or nanophotonic devices such as ring resonators, LSPR devices, nanoelectronic devices such as field effect transistors) are expected to potentially provide better performances than the state of the art (sensitivity, lifetime, reliability) and offer the possibility to be embedded in finalized sensor chips[245], [246]. Exploring the performances of such nanosensors implies to be able to efficiently functionalize the surface of the sensing zones. This consequently implies to study the behavior and the surfaces of materials classically used in industrial production of nanodevices. Silicon dioxide, silicon nitride, titanium oxide, titanium tungsten provide examples of materials that are classically used in such devices. Among these materials, titanium tungsten (TiW) is a material very well mastered in nanoelectronics industrial production lines, and that can be produced with stable properties and behavior. It is used as a diffusion barrier and promoter of adhesion between metal and dielectric[247]–[249]. TiW barrier layers have for instance been investigated extensively for Al and Cu interconnects as well as for silver or gold metallization[250]–[253]. TiW barrier layers applications for different metallization or metallic interconnections in silicon or SiO_2 are listed in Table 1.9.

Systems	Thickness	Stability
Pt/TiW/SiO_2[249]	5nm	600 °C in vacuum, 400 °C in air(12h)
Ag/TiW/Si[254], [255]	170nm / 200nm	600 °C(1h) / 650 °C in vacuum(30min)
Au/TiW(N)/Si[256]	45nm	600 °C in air (2h)
Al /TiW/$CoSi_2$[257]	40nm	550 °C in N_2 (20min)
Al /TiW/Si[250]	80nm	500 °C in air (2h)

Table 1.9 Summary of TiW barrier layers application for metallization or metallic interconnections.

STMicroelectronics' engineer Stéphane Monfray proposed to provide our group with a TiW wafer, in order to study in depth TiW abilities to be functionalized either for attaching molecular probes or to be efficiently passivated and disable molecular adsorption.

1.5.2 Aim of the present thesis

As explained in the general introduction, the aim of the following work was to investigate the orthogonal chemical functionalization of TiW based substrates featuring Au and SiO_2 patterns. To achieve this aim, we have

(1) Studied three different means for the formation of organolayers on TiW. To the best of our knowledge, chemical functionalization of TiW has never been reported before. The three layers were characterized and the stability of the formed layers was also addressed,

(2) Developed and ascertained the orthogonal chemical functionalization of patterned Au/TiW and Au/SiO_2/TiW patterned substrates. To the best of our knowledge, orthogonal functionalization of Au/TiW has never been reported. Furthermore, orthogonal functionalization of triple material substrate is only scarcely reported. We have studied the functionalization of Au/SiO_2/TiW substrate.

(3) Capturing of nanoparticles by electrostatic interaction at specific location on Au/TiW patterned substrate was successfully implemented to prove the interest of such method for colloids trapping.

1.5.3 Substrates and patterns

Different substrates (plain TiW substrates, patterned Au/TiW substrates and patterned Au/SiO_2/TiW substrates) were used during this work, which we can separated into the following categories, as shown in Figure 1.15.

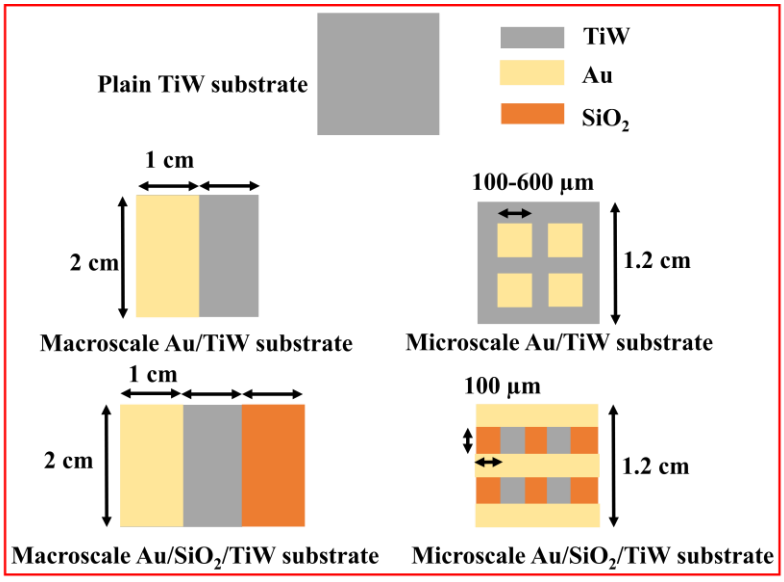

Figure 1.15 Schematic representation of sample dimensions (not to scale).

Plain TiW substrates (200 nm thickness on silicon) were provided by STMicroelectronics. They allow an easy monitoring of different functionalization by methods such as IR, ToF-SIMS (Collaboration with Pr. Didier Léonard, ISA) or XPS. They were used to investigate different organolayers formation.

Macropatterned Au/TiW substrates correspond to TiW substrates with half of the surface covered by gold. They were made by masking half of the substrate during Au e-beam evaporation. Macropatterned Au/SiO_2/TiW substrates correspond to TiW substrates with one third of the surface covered by Au and the other one third of the surface covered by SiO_2. They were made by masking the substrate during Au e-beam evaporation and silica sputtering.

Micropatterned Au/TiW substrates corresponds to TiW substrate with Au structures ranging from 100 µm×100 µm to 600 µm× 600 µm. They were made by UV lithography process. Micropatterned Au/SiO_2/TiW substrates corresponds to TiW substrate with Au lines and silica squares. They were made by a two-step UV lithography process. Patterned substrates were prepared by myself and co-workers. Annex B describe the fabrication of the substrates.

1.5.4 Functionalization

Three molecules were chosen to functionalize TiW with the goal of studying the stability of the formed organolayers on TiW. These molecules were: 3-aminopropylphosphonic acid (APPA), 3-ethoxydimethylsilylpropylamine (APDMES), dopamine (DA) (Figure 1.16). They have same amino headgroup and similar length. They differ only by substrate binding group. The choice of amino terminated molecules was driven by the fact that nitrogen could be used as a reporter.

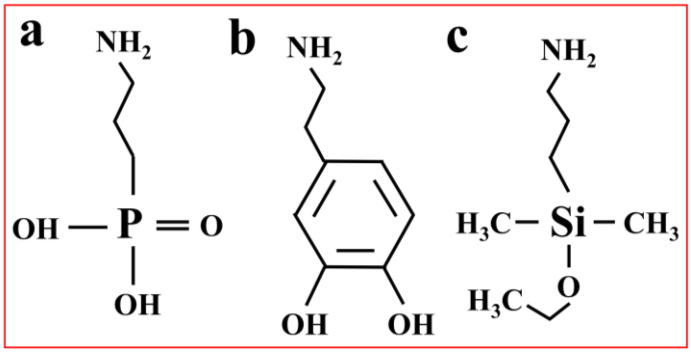

Figure 1.16 Schematic representation of APPA (a)), APDMES (b) and DA (c).

Eventually, perfluorinated thiol (1H,1H,2H,2H-Perfluorodecanethiol), perfluorinated phosphonic acid (1H, 1H,2H,2H-Perfluorooctanephosphonic acid), perfluorinated silane (1H,1H,2H,2H-Perfluorodecyldimethyl-chlorosilane) were used for orthogonal functionalization characterization (XPS, IR and ToF-SIMS imaging). Fluorine enriched molecules have obvious signal for the demonstration of the orthogonality. 11-Mercaptoundecanoic acid (MUAM) was chosen to functionalize gold region of patterned Au/TiW substrates. At natural pH environment, MUAM functionalized surface is negative

charged, which have the possibility for trapping the positive charged nanoparticles or biomolecules.

1.5.5 Characterizations

In the course of this PhD, for the studies of surface chemical functionalization of the organolayers on TiW, Au/TiW and Au/SiO_2/TiW substrates, AFM and XRD were used for information on the roughness and crystallinity. XPS, ToF-SIMS and IR were used to characterize and analyze the composition and stability of different layers. For the studies of orthogonal functionalization on Au/TiW and Au/SiO_2/TiW substrates, XPS and IR were used to characterize the orthogonality of macropatterned substrates. ToF-SIMS imaging was used to characterize the orthogonality of micropatterned substrates. SEM was used to visualize the captured nanoparticles.

1.6 Reference

[1] X. Zhou, F. Boey, F. Huo, L. Huang, H. Zhang, Chemically functionalized surface patterning. *Small*, **2011**, *7*, 2273–2289.

[2] Y. Liang, K. L. Kiick. Heparin-functionalized polymeric biomaterials in tissue engineering and drug delivery applications. *Acta Biomater.*, **2014**, *10*, 1588–1600.

[3] J. Liu, Y. Lu. Adenosine-dependent assembly of aptazyme-functionalized gold nanoparticles and its application as a colorimetric biosensor. *Anal. Chem.*, **2004**, *76*, 1627–1632.

[4] F. Palazon, P. Rojo-Romeo, C. Chevalier, T. Géhin, A. Belarouci, A. Cornillon, F. Zuttion, M. Phaner-Goutorbe, É. Souteyrand, Y. Chevolot, J. P. Cloarec. Nanoparticles selectively immobilized onto large arrays of gold micro and nanostructures through surface chemical functionalizations. *J. Colloid Interface Sci.*, **2015**, *447*, 152–158.

[5] I. Jerman, A. Š. Vuk, M. Koželj, B. Orel, J. Kovač. A structural and corrosion study of triethoxysilyl functionalized POSS coatings on AA 2024 Alloy. *Langmuir*, **2008**, *24*, 5029–5037.

[6] J. C. Love, L. A. Estroff, J. K. Kriebel, R. G. Nuzzo, G. M. Whitesides. Self-assembled monolayers of thiolates on metals as a form of nanotechnology. *Chem. Rev.*, **2005**, *105*, 1103–1170.

[7] L. Strong, G. M. Whitesides. Structures of self-assembled monolayer films of organosulfur compounds adsorbed on gold single crystals: electron diffraction studies. *Langmuir*, **1988**, *4*, 546–558.

[8] Y. Wang, M. Lieberman. Growth of ultrasmooth octadecyltrichlorosilane self-assembled monolayers on SiO_2. *Langmuir*, **2003**, *19*, 1159–1167.

[9] C. P. Tripp, M. L. Hair. Reaction of methylsilanols with hydrated silica surfaces: the hydrolysis of trichloro-, dichloro-, and monochloromethylsilanes and the effects of curing. *Langmuir*, **1995**, *11*, 149–155.

[10] G. Zhang, T. Tanii, T. Zako, T. Hosaka. T. Miyake, Y. Kanari, T. Funatsu, I. Ohdomari. Nanoscale patterning of protein using electron beam lithography of organosilane self-assembled monolayers. *Small*, **2005**, *1*, 833–837.

[11] W. Senaratne, P. Sengupta, C. Harnett, H. Craighead, B. Baird, C. K. Ober. Molecular templates for bio-specific recognition by low-energy electron beam lithography. *NanoBiotechnology*, **2005**, *1*, 23–33.

[12] G. Zhang, T. Tanii, T. Funatsu, I. Ohdomari, Patterning of DNA nanostructures on silicon surface by electron beam lithography of self-assembled monolayer. *Chem. Commun.*, **2004**, *0*, 786–787.

[13] P. M. S. John, H. G. Craighead. Monolayers of fluorinated silanes as electron-beam resists. *J. Vac. Sci. Technol. B Microelectron. Nanometer Struct. Process. Meas. Phenom.*, **1996**, *14*, 69–74.

[14] M. J. Lercel, H. G. Craighead, A. N. Parikh, K. Seshadri, D. L. Allara. Sub-10nm lithography with self-assembled monolayers. *Appl. Phys. Lett.*, **1996**, *68*, 1504–1506.

[15] C. K. Harnett, K. M. Satyalakshmi, H. G. Craighead. Bioactive templates fabricated by low-energy electron beam lithography of self-assembled monolayers. *Langmuir*, **2001**, *17*, 178–182.

[16] J. Rundqvist, J. H. Hoh, D. B. Haviland. Directed immobilization of protein-coated nanospheres to nanometer-scale patterns fabricated by electron beam lithography of poly(ethylene glycol) self-assembled monolayers. *Langmuir*, **2006**, *22*, 5100–5107.

[17] W. Geyer, V. Stadler, W. Eck, A. Gölzhäuser, M. Grunze. Electron induced chemical nanolithography with self-assembled monolayers. *J. Vac. Sci. Technol. B Microelectron. Nanometer Struct. Process. Meas. Phenom.*, **2001**, *19*, 2732–2735.

[18] A. Gölzhäuser, W. Eck, W. Geyer, V. Stadler, T. Weimann, P. Hinze, M. Grunze. Chemical nanolithography with electron beams. *Adv. Mater*., **2001**, *13*, 803–806.

[19] A. Turchanin, A. Tinazli, M. El-Desawy, H. Großmann, M. Schnietz, H. H. Solak, R. Tampé, A. Gölzhäuser. Molecular self-assembly, chemical lithography, and biochemical tweezers: a path for the fabrication of functional nanometer-scale protein arrays. *Adv. Mater*., **2008**, *20*, 471–477.

[20] A. Turchanin, M. Schnietz, M. El-Desawy, H. H. Solak, C. David, A. Gölzhäuser. Fabrication of molecular nanotemplates in self-assembled monolayers by extreme-ultraviolet-induced chemical lithography. *Small*, **2007**, *3*, 2114–2119.

[21] A. Kumar, G. M. Whitesides. Features of gold having micrometer to centimeter dimensions can be formed through a combination of stamping with an elastomeric stamp and an alkanethiol “ink” followed by chemical etching. *Appl. Phys. Lett.*, **1993**, *63*, 2002–2004.

[22] M. Mrksich, G. M. Whitesides. Patterning self-assembled monolayers using microcontact printing: a new technology for biosensors. *Trends Biotechnol.*, **1995**, *13*, 228–235.

[23] J. L. Wilbur, A. Kumar, H. A. Biebuyck, E. Kim, G. M. Whitesides. Microcontact printing of self-assembled monolayers: applications in microfabrication. *Nanotechnology*, **1996**, *7*, 452–457.

[24] Y. Jie, J. R. Niskala, A. C. Johnston-Peck, P. J. Krommenhoek, J. B. Tracy, H. Fan, W, You. Laterally patterned magnetic nanoparticles. *J. Mater. Chem.*, **2012**, *22*, 1962–1968.

[25] J. Robert J. Barsotti, F. Stellacci. Chemically directed assembly of monolayer protected gold nanoparticles on lithographically generated patterns. *J. Mater. Chem.*, **2006**, *16*, 962–965.

[26] Y. Xia, M. Mrksich, E. Kim, G. M. Whitesides. Microcontact printing of octadecylsiloxane on the surface of silicon dioxide and its application in microfabrication. *J. Am. Chem. Soc.*, **199**5, *117*, 9576–9577.

[27] J. Tan, J. Tien, C. Chen. Microcontact printing of proteins on mixed self-assembled monolayers. *Langmuir*, **2002**, *18*, 1067–1070.

[28] A. Bernard, J. P. Renault, B. Michel, H. R. Bosshard, E. Delamarche. Microcontact printing of proteins. *Adv. Mater.*, **2000**, *12*, 471–477.

[29] G. Csucs, R. Michel, J. W. Lussi, M. Textor, G. Danuser. Microcontact printing of novel co-polymers in combination with proteins for cell-biological applications. *Biomaterials*, **2003**, *24*, 1713–1720.

[30] N. L. Jeon, I. S. Choi, G. M. Whitesides. Patterned polymer growth on silicon surfaces using microcontact printing and surface-initiated polymerization. *Appl. Phys. Lett.*, **1999**, *75*, 4201–4203.

[31] M. Ozmen, B. Ertekin, M. Ersoz, V. N. Paunov. Fabrication of albumin-micropatterned surfaces by colloidal microcontact printing technique. *RSC Adv.*, **2013**, *3*, 10420–10426.

[32] G. Binnig, C. F. Quate, C. Gerber. Atomic Force Microscope. *Phys. Rev. Lett.*, **1986**, *56*, 930–933.

[33] S. Hong, C. A. Mirkin. A nanoplotter with both parallel and serial writing capabilities. *Science*, **2000**, *288*, 1808–1811.

[34] S. Hong, J. Zhu, C. A. Mirkin. Multiple ink nanolithography: toward a multiple-pen nano-plotter. *Science*, **1999**, *286*, 523–525.

[35] S. Hong, J. Zhu, C. A. Mirkin. A new tool for studying the in situ growth processes for self-assembled monolayers under ambient conditions. *Langmuir*, **1999**, *15*, 7897–7900.

[36] A. Ivanisevic, C. A. Mirkin. 'Dip-pen' nanolithography on semiconductor surfaces. *J. Am. Chem. Soc.*, **2001**, *123*, 7887–7889.

[37] J. H. Lim, D. S. Ginger, K. B. Lee, J. Heo, J. M. Nam, C. A. Mirkin. Direct-write dip-pen nanolithography of proteins on modified silicon oxide surfaces. *Angew. Chem. Int. Ed.*, **2003**, *42*, 2309–2312.

[38] K. B. Lee, S. J. Park, C. A. Mirkin, J. C. Smith, M. Mrksich. Protein nanoarrays generated by dip-pen nanolithography. *Science*, **2002**, *295*, 1702–1705.

[39] K. B. Lee, J. H. Lim, C. A. Mirkin. Protein nanostructures formed via direct-write dip-pen nanolithography. *J. Am. Chem. Soc.*, **2003**, *125*, 5588–5589.

[40] S. Xu, S. Miller, P. E. Laibinis, G. Liu. Fabrication of nanometer scale patterns within self-assembled monolayers by nanografting. *Langmuir*, **1999**, *15*, 7244–7251.

[41] S. Xu, G. Liu. Nanometer-scale fabrication by simultaneous nanoshaving and molecular self-assembly. *Langmuir*, **1997**, *13*, 127–129.

[42] N. A. Amro, S. Xu, G. Liu. Patterning surfaces using tip-directed displacement and self-assembly. *Langmuir*, **2000**, *16*, 3006–3009.

[43] S. Sun, G. J. Leggett. Matching the resolution of electron beam lithography by scanning near-field photolithography. *Nano Lett.*, **2004**, *4*, 1381–1384.

[44] S. Sun, K. S. L. Chong, G. J. Leggett. Nanoscale molecular patterns fabricated by using scanning near-field optical lithography. *J. Am. Chem. Soc.*, **2002**, *124*, 2414–2415.

[45] P. E. Laibinis, J. J. Hickman, M. S. Wrighton, G. M. Whitesides. Orthogonal self-assembled monolayers: alkanethiols on gold and alkane carboxylic acids on alumina. *Science*, **1989**, *245*, 845–847.

[46] R. Michel, I. Reviakine, D. Sutherland, C. Fokas, G. Csucs, G. Danuser, N. D. Spencer, M. Textor. A novel approach to produce biologically relevant chemical patterns at the nanometer scale: selective molecular assembly patterning combined with colloidal lithography. *Langmuir*, **2002**, *18*, 8580–8586.

[47] M. Bergkvist, N. Niamsiri, A. D. Strickland, C. A. Batt. Substrate selective patterning on lithography defined gold on silica: effect of end-group functionality on intermolecular layer formation. *Surf. Sci*, **2008**, *602*, 2121–2127.

[48] P. H. Mutin, V. Lafond, A. F. Popa, M. Granier, L. Markey, A. Dereux. Selective surface modification of SiO_2−TiO_2 supports with phosphonic acids. *Chem. Mater.*, **2004**, *16*, 5670–5675.

[49] L. Feuz, P. Jönsson, M. P. Jonsson, F. Höök. Improving the limit of detection of nanoscale sensors by directed binding to high-sensitivity areas. *ACS Nano*, **201**0, *4*, 2167–2177.

[50] P. Anstaett, Y. Zheng, T. Thai, A. M. Funston, U. Bach, G. Gasser. Synthesis of stable peptide nucleic acid-modified gold nanoparticles and their assembly onto gold surfaces. *Angew. Chem. Int. Ed.*, **2013**, *52*, 4217–4220.

[51] F. Palazon, D. Léonard, T. L. Mogne, F. Zuttion, C. Chevalier, M. Phaner-Goutorbe, É. Souteyrand, Y. Chevolot, J. P. Cloarec. Orthogonal chemical functionalization of patterned gold on silica surfaces. *Beilstein J Nanotechnol.*, **2015**, *6*, 2272–2277.

[52] J. Haaheim, O. A. Nafday. Dip pen nanolithography®: a 'desktop nanofab™' approach using high-throughput flexible nanopatterning. *Scanning*, **2008**, *30*, 137–150.

[53] C. R. K. Marrian, D. M. Tennant. Nanofabrication. *J. Vac. Sci. Technol. A*, **2003**, *21*, 207–215.

[54] S. P. Pujari, L. Scheres, A. T. M. Marcelis, H. Zuilhof. Covalent surface modification of oxide surfaces. *Angew. Chem. Int. Ed.*, **2014**, *53*, 6322–6356.

[55] C. Haensch, S. Hoeppener, U. S. Schubert. Chemical modification of self-assembled silane based monolayers by surface reactions. *Chem. Soc. Rev.*, **2010**, *39*, 2323–2334.

[56] J. J. Cras, C. A. Rowe-Taitt, D. A. Nivens, F. S. Ligler. Comparison of chemical cleaning methods of glass in preparation for silanization. *Biosens. Bioelectron.*, **1999**, *14*, 683–688.

[57] M. E. McGovern, K. M. R. Kallury, M. Thompson. Role of solvent on the silanization of glass with octadecyltrichlorosilane. *Langmuir*, **1994**, *10*, 3607–3614.

[58] K. Wen, R. Maoz, H. Cohen, J. Sagiv, A. Gibaud, A. Desert, B. M. Ocko. Postassembly chemical modification of a highly ordered organosilane multilayer: new insights into the structure, bonding, and dynamics of self-assembling silane monolayers. *ACS Nano*, **2008**, *2*, 579–599.

[59] H. Han, J. Wu, C. W. Avery, M. Mizutani, X. Jiang, M. Kamigaito, Z. Chen, C. Xi, K. Kuroda. Immobilization of amphiphilic polycations by catechol functionality for antimicrobial coatings. *Langmuir*, **2011**, *27*, 4010–4019.

[60] N. Herzer, S. Hoeppener, U. S. Schubert. Fabrication of patterned silane based self-assembled monolayers by photolithography and surface reactions on silicon - oxide substrates. *Chem. Commun.*, **2010**, *46*, 5634–5652.

[61] A. Glaser, J. Foisner, H. Hoffmann, G. Friedbacher. Investigation of the role of the interplay between water and temperature on the growth of alkylsiloxane submonolayers on silicon. *Langmuir*, **2004**, *20*, 5599–5604.

[62] E. L. Hanson, J. Schwartz, B. Nickel, N. Koch, M. F. Danisman. Bonding self-assembled, compact organophosphonate monolayers to the native oxide surface of silicon. *J. Am. Chem. Soc*., **2003**, *125*, 16074–16080.

[63] A. Vega, P. Thissen, Y. J. Chabal. Environment-controlled tethering by aggregation and growth of phosphonic acid monolayers on silicon oxide. *Langmuir*, **2012**, *28*, 8046–8051.

[64] H. Lee, K. D. Lee, K. B. Pyo, S. Y. Park, H. Lee. Catechol-grafted poly(ethylene glycol) for PEGylation on versatile substrates. *Langmuir*, **2010**, *26*, 3790–3793.

[65] H. J. Martin, K. H. Schulz, J. D. Bumgardner, K. B. Walters. XPS study on the use of 3-aminopropyltriethoxysilane to bond chitosan to a titanium surface. *Langmuir*, **2007**, *23*, 6645–6651.

[66] G. Zorn, J. E. Baio, T. Weidner, V. Migonney, D. G. Castner. Characterization of poly(sodium styrene sulfonate) thin films grafted from functionalized titanium surfaces. *Langmuir*, **2011**, *27*, 13104–13112.

[67] G. Mani, D. M. Johnson, D. Marton, V. L. Dougherty, M. D. Feldman, D. Patel, A. A. Ayon, C. M. Agrawal. Stability of self-assembled monolayers on titanium and gold. *Langmuir*, **2008**, *24*, 6774–6784.

[68] M. Iijima, M. Kobayakawa, H. Kamiya. Tuning the stability of TiO_2 nanoparticles in various solvents by mixed silane alkoxides. *J. Colloid Interface Sci.*, **2009**, *337*, 61–65.

[69] N. Griep-Raming, M. Karger, H. Menzel. Using benzophenone-functionalized phosphonic acid to attach thin polymer films to titanium surfaces. *Langmuir*, **2004**, *20*, 11811–11814.

[70] A. Kanta, R. Sedev, J. Ralston. The formation and stability of self-assembled monolayers of octadecylphosphonic acid on titania. *Colloids Surf. Physicochem. Eng. Asp.*, **2006**, *291*, 51–58.

[71] R. Luschtinetz, J. Frenzel, T. Milek, G. Seifert. Adsorption of phosphonic acid at the TiO_2 anatase (101) and rutile (110) surfaces. *J. Phys. Chem. C*, **2009**, *113*, 5730–5740.

[72] B. Malisova, S. Tosatti, M. Textor, K. Gademann, S. Zürcher. Poly(ethylene glycol) adlayers immobilized to metal oxide substrates through catechol derivatives: influence of assembly conditions on formation and stability. *Langmuir*, **2010**, *26*, 4018–4026.

[73] M. Rodenstein, S. Zürcher, S. G. P. Tosatti, N. D. Spencer. Fabricating chemical gradients on oxide surfaces by means of fluorinated, catechol-based, self-assembled monolayers. *Langmuir*, **2010**, *26*, 16211–16220.

[74] T. H. Anderson, J. Yu, A. Estrada, M. U. Hammer, J. H. Waite, J. N. Israelachvili. The contribution of DOPA to substrate–peptide adhesion and internal cohesion of mussel-Inspired synthetic peptide films. *Adv. Funct. Mater.*, **2010**, *20*, 4196–4205.

[75] N. Lee, D. R. Hummer, D. A. Sverjensky, T. Rajh, R. M. Hazen, A. Steele, G. D. Cody. Speciation of L-DOPA on nanorutile as a function of pH and surface coverage using surface-enhanced Raman Sspectroscopy (SERS). *Langmuir*, **2012**, *28*, 17322–17330.

[76] J. L. Dalsin, L. Lin, S. Tosatti, J. Vörös, M. Textor, P. B. Messersmith. Protein resistance of titanium oxide surfaces modified by biologically inspired mPEG−DOPA. *Langmuir*, **2005**, *21*, 640–646.

[77] R. Rodríguez, M. A. Blesa, A. E. Regazzoni. Surface complexation at the TiO_2 (anatase)/ squeous solution interface: chemisorption of catechol. *J. Colloid Interface Sci.*, **1996**, *177*, 122–131.

[78] S. C. Li, L. N. Chu, X. Q. Gong, U. Diebold. Hydrogen bonding controls the dynamics of catechol adsorbed on a TiO_2 (110) surface. *Science*, **2010**, *328*, 882–884.

[79] R. Wehlauch, J. Hoecker, K. Gademann. Nitrocatechols as tractable surface release systems. *ChemPlusChem*, **2012**, *77*, 1071–1074.

[80] F. Li, J. D. Fabbri, R. I. Yurchenko, A. N. Mileshkin, J. N. Hohman, H. Yan, H. Yuan, I. C. Tran, T. M. Willey, M. Bagge-Hansen, J. E. P. Dahl, R. M. K. Carlson, A. A. Fokin, P. R. Schreiner, Z. Shen, N. A. Melosh. Covalent attachment of diamondoid phosphonic acid dichlorides to tungsten oxide surfaces. *Langmuir*, **2013**, *29*, 9790–9797.

[81] A. M. M. Jani, I. M. Kempson, D. Losic, N. H. Voelcker. Dressing in layers: layering surface functionalities in nanoporous aluminum oxide membranes. *Angew. Chem. Int. Ed.*, **2010**, *49*, 7933–7937.

[82] L. N. Mitchon, J. M. White. Growth and analysis of octadecylsiloxane monolayers on Al_2O_3 (0001). *Langmuir*, **2006**, *22*, 6549–6554.

[83] L. T. Truong, Å. Larsen, B. Holme, S. Diplas, F. K. Hansen, J. Roots, S. Jørgensen. Dispersibility of silane-functionalized alumina nanoparticles in syndiotactic polypropylene. *Surf. Interface Anal.*, **2010**, *42*, 1046–1049.

[84] I. Lee, R. P. Wool. Controlling amine receptor group density on aluminum oxide surfaces by mixed silane self assembly. *Thin Solid Films*, **2000**, *379*, 94–100.

[85] I. Levine, S. M. Weber, Y. Feldman, T. Bendikov, H. Cohen, D. Cahen, A. Vilan. Molecular length, monolayer density, and charge transport: lessons from Al–AlOx/Alkyl–phosphonate/Hg iunctions. *Langmuir*, **2012**, *28*, 404–415.

[86] P. Thissen, M. Valtiner, G. Grundmeier. Stability of phosphonic acid self-assembled monolayers on amorphous and single-crystalline aluminum oxide surfaces in aqueous solution. *Langmuir*, **2010**, *26*, 156–164.

[87] M. Giza, P. Thissen, G. Grundmeier. Adsorption kinetics of organophosphonic acids on plasma-modified oxide-covered aluminum surfaces. *Langmuir*, **2008**, *24*, 8688–8694.

[88] S. Sun, G. J. Leggett. Micrometer and nanometer scale photopatterning of self-assembled monolayers of phosphonic acids on aluminum oxide. *Nano Lett.*, **2007**, *7*, 3753–3758.

[89] W. O. Yah, H. Xu, H. Soejima, W. Ma, Y. Lvov, A. Takahara. Biomimetic dopamine derivative for selective polymer modification of halloysite nanotube lumen. *J. Am. Chem. Soc.*, **2012**, *134*, 12134–12137.

[90] G. S. Tulevski, Q. Miao, M. Fukuto, R. Abram, B. Ocko, R. Pindak, M. L. Steigerwald, C. R. Kagan, C. Nuckolls. Attaching organic semiconductors to gate oxides: in situ assembly of monolayer field effect transistors. *J. Am. Chem. Soc.*, **2004**, *126*, 15048–15050.

[91] D. Costenaro, F. Carniato, G. Gatti, C. Bisio, L. Marchese. On the physico-chemical properties of ZnO nanosheets modified with luminescent CdTe Nanocrystals. *J. Phys. Chem. C*, **2011**, *115*, 25257–25265.

[92] R. Turgeman, O. Gershevitz, O. Palchik, M. Deutsch, B. M. Ocko, A. Gedanken, C. N. Sukenik. Oriented growth of ZnO crystals on self-assembled monolayers of functionalized alkyl silanes. *Cryst. Growth Des.*, **2004**, *4*, 169–175.

[93] H. Shi, W. Li, L. Sun, Y. Liu, H. Xiao, S. Fu. Synthesis of silane surface modified ZnO quantum dots with ultrastable, strong and tunable luminescence. *Chem. Commun.*, **2011**, *47*, 11921–11923.

[94] J. W. Soares, J. E. Whitten, D. W. Oblas, D. M. Steeves. Novel photoluminescence properties of surface-modified nanocrystalline zinc oxide: toward a reactive scaffold. *Langmuir*, **2008**, *24*, 371–374.

[95] J. Chen, R. E. Ruther, Y. Tan, L. M. Bishop, R. J. Hamers. Molecular adsorption on ZnO (1010) single-crystal surfaces: morphology and charge transfer. *Langmuir*, **2012**, *28*, 10437–10445.

[96] P. J. Hotchkiss, M. Malicki, A. J. Giordano, N. R. Armstrong, S. R. Marder. Characterization of phosphonic acid binding to zinc oxide. *J. Mater. Chem.*, **2011**, *21*, 3107–3112.

[97] C. L. Perkins. Molecular anchors for self-assembled monolayers on ZnO: a direct comparison of the thiol and phsphonic acid moieties. *J. Phys. Chem. C*, **2009**, *113*, 18276–18286.

[98] I. Lange, S. Reiter, M. Pätzel, A. Zykov, A. Nefedov, J. Hildebrandt, S. Hecht, S. Kowarik, C. Wöll, G. Heimel, D. Neher. Tuning the work function of polar zinc oxide surfaces using modified phosphonic acid self-assembled monolayers. *Adv. Funct. Mater.*, **2014**, *24*, 7014–7024.

[99] M. Manesse, R. Sanjines, V. Stambouli, C. Jorel, B. Pelissier, M. Pisarek, R. Boukherroub, S. Szunerits. Preparation and characterization of silver substrates coated with antimony-doped SnO_2 thin films for surface plasmon resonance studies. *Langmuir*, **2009**, *25*, 8036–8041.

[100] Y. Cheng, K. Chen, N. L. Meyer, J. Yuan, L. S. Hirst, P. B. Chase, P. Xiong. Functionalized SnO_2 nanobelt field-effect transistor sensors for label-free detection of cardiac troponin. *Biosens. Bioelectron.*, **2011**, *26*, 4538–4544.

[101] V. Stambouli, M. Labeau, I. Matko, B. Chenevier, O. Renault, C. Guiducci, P. Chaudouët, H. Roussel, D. Nibkin, E. Dupuis. Development and functionalisation of Sb doped SnO_2 thin films for DNA biochip applications. *Sens. Actuators B Chem.*, **2006**, *113*, 1025–1033.

[102] N. R. Armstrong, V. R. Shepard. Differential-capacitance studies of silane-modified tin oxide (SnO_2) electrodes at low modulation frequencies. *J. Phys. Chem.*, **1981**, *85*, 2965–2970.

[103] C. K. Luscombe, H. Li, W. T. S. Huck, A. B. Holmes. Fluorinated silane self-assembled monolayers as resists for patterning indium tin oxide. *Langmuir*, **2003**, *19*, 5273–5278.

[104] J. Das, C. H. Huh, K. Kwon, S. Park, S. Jon, K. Kim, H. Yang. Comparison of the nonspecific binding of DNA-conjugated gold nanoparticles between polymeric and monomeric self-assembled monolayers. *Langmuir*, **2009**, *25*, 235–241.

[105] V. M. Bermudez, A. D. Berry, H. Kim, A. Piqué. Functionalization of indium tin oxide. *Langmuir*, **2006**, *22*, 11113–11125.

[106] R. A. Hatton, S. R. Day, M. A. Chesters, M. R. Willis. Organic electroluminescent devices: enhanced carrier injection using an organosilane self assembled monolayer (SAM) derivatized ITO electrode. *Thin Solid Films*, **2001**, *394*, 291–296.

[107] P. J. Hotchkiss, S. C. Jones, S. A. Paniagua, A. Sharma, B. Kippelen, N. R. Armstrong, S. R. Marder. The modification of indium tin oxide with phosphonic acids: mechanism of binding, tuning of surface properties, and potential for use in organic electronic applications. *Acc. Chem. Res.*, **2012**, *45*, 337–346.

[108] M. Chockalingam, N. Darwish, G. Le Saux, J. J. Gooding. Importance of the indium tin oxide substrate on the quality of self-assembled monolayers formed from organophosphonic acids. *Langmuir*, **2011**, *27*, 2545–2552.

[109] M. Gliboff, H. Li, K. M. Knesting, A. J. Giordano, D. Nordlund, G. T. Seidler, J. L. Brédas, S. R. Marder, D. S. Ginger. Competing effects of fluorination on the orientation of aromatic and aliphatic phosphonic acid monolayers on indium tin oxide. *J. Phys. Chem. C*, **2013**, *117*, 15139–15147.

[110] K. Jo, H. Yu, H. Yang. Formation kinetics and stability of phosphonate self-assembled monolayers on indium–tin oxide. *Electrochim. Acta*, **2011**, *56*, 4828–4833.

[111] C. E. J. Cordonier, A. Nakamura, K. Shimada, A. Fujishima. Photoacid generating ligands for development of positive-tone directly photopatternable metal complexes. *Langmuir*, **2011**, *27*, 3157–3165.

[112] S. P. Pujari, Y. Li, R. Regeling, H. Zuilhof. Tribology and stability of organic monolayers on CrN: a comparison among silane, phosphonate, alkene, and alkyne chemistries. *Langmuir*, **2013**, *29*, 10405–10415.

[113] J. P. Matinlinna, K. Laajalehto, T. Laiho, I. Kangasniemi, L. V. J. Lassila, P. K. Vallittu. Surface analysis of Co–Cr–Mo alloy and Ti substrates silanized with trialkoxysilanes and silane mixtures. *Surf. Interface Anal.*, **2004**, *36*, 246–253.

[114] D. A. Puleo. Retention of enzymatic activity immobilized on silanized Co-Cr-Mo and Ti-6Al-4V. *J. Biomed. Mater. Res.*, **1997**, *37*, 222–228.

[115] W. Guo, J. Zhu, Z. Cheng, Z. Zhang, X. Zhu. Anticoagulant surface of 316L stainless steel modified by surface-initiated atom transfer radical polymerization. *ACS Appl. Mater. Interfaces*, **2011**, *3*, 1675–1680.

[116] A. Raman, M. Dubey, I. Gouzman, E. S. Gawalt. Formation of self-assembled monolayers of alkylphosphonic acid on the native oxide surface of SS316L. *Langmuir*, **2006**, *22*, 6469–6472.

[117] R. Bhure, T. M. Abdel-Fattah, C. Bonner, F. Hall, A. Mahapatro. Stability of phosphonic self assembled monolayers (SAMs) on cobalt chromium (Co–Cr) alloy under oxidative conditions. *Appl. Surf. Sci.*, **2011**, *257*, 5605–5612.

[118] R. Bhure, A. Mahapatro, C. Bonner, T. M. Abdel-Fattah. In vitro stability study of organophosphonic self assembled monolayers (SAMs) on cobalt chromium (Co–Cr) alloy. *Mater. Sci. Eng. C*, **2013**, *33*, 2050–2058.

[119] E. Faure, E. Halusiak, F. Farina, N. Giamblanco, C. Motte, M. Poelman, C. Archambeau, C. V. D. Weerdt, J. Martial, C. Jérôme, A. S. Duwez, C. Detrembleur. Clay and DOPA containing polyelectrolyte multilayer film for imparting anticorrosion properties to galvanized steel. *Langmuir*, **2012**, *28*, 2971–2978.

[120] H. E. Ries, H. D. Cook. Monomolecular films of mixtures: I. Stearic acid with isostearic acid and with tri-p-cresyl phosphate. Comparison of components with

octadecylphosphonic acid and with tri-o-xenyl phosphate. *J. Colloid Sci.*, **1954**, *9*, 535–546.

[121] C. Queffélec, M. Petit, P. Janvier, D. A. Knight, B. Bujoli. Surface modification using phosphonic acids and esters. *Chem. Rev.*, **2012**, *112*, 3777–3807.

[122] M. B. Mitchell, V. N. Sheinker, E. A. Mintz. Adsorption and decomposition of dimethyl methylphosphonate on metal oxides. *J. Phys. Chem. B*, **1997**, *101*, 11192–11203.

[123] G. Guerrero, P. H. Mutin, A. Vioux. Anchoring of phosphonate and phosphinate coupling molecules on titania particles. *Chem. Mater.*, **2001**, *13*, 4367–4373.

[124] P. H. Mutin, G. Guerrero, A. Vioux. Hybrid materials from organophosphorus coupling molecules. *J. Mater. Chem.*, **2005**, *15*, 3761–3768.

[125] N. Adden, L. J. Gamble, D. G. Castner, A. Hoffmann, G. Gross, H. Menzel. Phosphonic acid monolayers for binding of bioactive molecules to titanium surfaces. *Langmuir*, **2006**, *22*, 8197–8204.

[126] F. Brodard-Severac, G. Guerrero, J. Maquet, P. Florian, C. Gervais, P. H. Mutin. High-field ^{17}O MAS NMR investigation of phosphonic acid monolayers on titania. Chem. Mater., **2008**, *20*, 5191–5196.

[127] S. A. Paniagua, P. J. Hotchkiss, S. C. Jones, S. R. Marder, A. Mudalige, F. S. Marrikar, J. E. Pemberton, N. R. Armstrong. Phosphonic acid modification of indium−tin oxide electrodes: combined XPS/UPS/Contact Angle Studies. *J. Phys. Chem. C*, **2008**, *112*, 7809–7817.

[128] M. Gliboff, L. Sang, K. M. Knesting, M. C. Schalnat, A. Mudalige, E. L. Ratcliff, H. Li, A. K. Sigdel, A. J. Giordano, J. J. Berry, D. Nordlund, G. T. Seidler, J. L. Brédas, S. R. Marder, J. E. Pemberton, D. S. Ginger. Orientation of phenylphosphonic acid self-assembled monolayers on a transparent conductive oxide: a combined NEXAFS, PM-IRRAS, and DFT Study. *Langmuir*, **2013**, *29*, 2166–2174.

[129] E. Smecca, A. Motta, M. E. Fragalà, Y. Aleeva, G. G. Condorelli. Spectroscopic and theoretical study of the grafting modes of phosphonic acids on ZnO Nanorods. *J. Phys. Chem. C*, **2013**, *117*, 5364–5372.

[130] S. Pawsey, M. McCormick, S. D. Paul, R. Graf, Y. S. Lee, L. Reven, H. W. Spiess. ^{1}H fast MAS NMR studies of hydrogen-bonding interactions in self-assembled monolayers. *J. Am. Chem. Soc.*, **2003**, *125*, 4174–4184.

[131] S. Gupta, H. Gleskova. Dry growth of n-octylphosphonic acid monolayer for low-voltage organic thin-film transistors. *Org. Electron.*, **2013**, *14*, 354–361.

[132] N. Tsud, M. Yoshitake. Vacuum vapour deposition of phenylphosphonic acid on amorphous alumina. *Surf. Sci.*, **2007**, *601*, 3060–3066.

[133] T. Hauffman, O. Blajiev, J. Snauwaert, C. van Haesendonck, A. Hubin, H. Terryn. Study of the self-assembling of n-Octylphosphonic acid layers on aluminum oxide. *Langmuir*, **2008**, *24*, 13450–13456.

[134] K. Wapner, M. Stratmann, G. Grundmeier. Structure and stability of adhesion promoting aminopropyl phosphonate layers at polymer/aluminium oxide interfaces. *Int. J. Adhes. Adhes.*, **2008**, *28*, 59–70.

[135] B. Zhang, T. Kong, W. Xu, R. Su, Y. Gao, G. Cheng. Surface functionalization of zinc oxide by carboxyalkylphosphonic acid self-assembled monolayers. *Langmuir*, **2010**, *26*, 4514–4522.

[136] X. Chen, E. Luais, N. Darwish, S. Ciampi, P. Thordarson, J. J. Gooding. Studies on the effect of solvents on self-assembled monolayers formed from organophosphonic acids on indium tin oxide. *Langmuir*, **2012**, *28*, 9487–9495.

[137] P. Thissen, A. Vega, T. Peixoto, Y. J. Chabal. Controlled, low-coverage metal oxide activation of silicon for organic functionalization: unraveling the phosphonate bond. *Langmuir*, **2012**, *28*, 17494–17505.

[138] H. Y. Nie, M. J. Walzak, N. S. McIntyre. Bilayer and odd-numbered multilayers of octadecylphosphonic acid formed on a Si substrate studied by atomic force microscopy. *Langmuir*, **2002**, *18*, 2955–2958.

[139] L. Sang, A. Mudalige, A. K. Sigdel, A. J. Giordano, S. R. Marder, J. J. Berry, J. E. Pemberton. PM-IRRAS determination of molecular orientation of phosphonic acid self-assembled monolayers on indium zinc oxide. *Langmuir*, **2015**, *31*, 5603–5613.

[140] H. Nie, M. J. Walzak, N. S. McIntyre. Delivering octadecylphosphonic acid self-assembled monolayers on a Si wafer and other oxide surfaces. *J. Phys. Chem. B*, **2006**, *110*, 21101–21108.

[141] L. Sang, K. M. Knesting, A. Bulusu, A. K. Sigdel, A. J. Giordano, S. R. Marder, J. J. Berry, S. Graham, D. S. Ginger, J. E. Pemberton. Effect of time and deposition method on quality of phosphonic acid modifier self-assembled monolayers on indium zinc oxide. *Appl. Surf. Sci.*, **2016**, *389*, 190-198.

[142] K. M. Knesting, P. J. Hotchkiss, B. A. MacLeod, S. R. Marder, D. S. Ginger. Spatially modulating interfacial properties of transparent conductive oxides: patterning work function with phosphonic acid self-assembled monolayers. *Adv. Mater.*, **2012**, *24*, 642–646.

[143] S. Marcinko, A. Y. Fadeev. Hydrolytic stability of organic monolayers supported on TiO_2 and ZrO_2. *Langmuir*, **2004**, *20*, 2270–2273.

[144] K. Jo, H. Yang. Comparative study of stability of phosphonate self-assembled monolayers on indium–tin oxide electrodes prepared using different methods. *J. Electroanal. Chem.*, **2014**, *712*, 8–13.

[145] E. P. Plueddemann. Silane adhesion promoters in coatings. *Prog. Org. Coat.*, **1983**, *11*, 297–308.

[146] E. P. Plueddemann. Chemistry of Silane Coupling Agents. *Silane Coupling Agents, Springer US*, **1991**, 31–54.

[147] S. K. Vashist, E. Lam, S. Hrapovic, K. B. Male, J. H. T. Luong. Immobilization of antibodies and enzymes on 3-aminopropyltriethoxysilane-functionalized bioanalytical platforms for biosensors and diagnostics. *Chem. Rev*., **2014**, *114*, 11083–11130.

[148] E. F. Vansant, P. V. D. Voort, K. C. Vrancken. Characterization and chemical modification of the silica surface. *Elsevier*, **1995**.

[149] M. P. Q. Argañaraz, J. M. Ramallo-López, G. Benítez, A. Rubert, E. D. Prieto, L. M. Gassa, R. C. Salvarezzaa, M. E. Vela. Optimization of the surface properties of nanostructured Ni–W alloys on steel by a mixed silane layer. *Phys. Chem. Chem. Phys.*, **2015**, *17*, 14201–14207.

[150] C. G. Núñez, M. Sachsenhauser, B. Blashcke, A. G. Marín, J. A. Garrido, J. L. Pau. Effects of hydroxylation and silanization on the surface properties of ZnO nanowires. *ACS Appl. Mater. Interfaces*, **2015**, *7*, 5331–5337.

[151] I. Anac, T. J. McCarthy. Chemical modification of chromium oxide surfaces using organosilanes. *J. Colloid Interface Sci.*, **2009**, *331*, 138–142.

[152] G. Mani, M. D. Feldman, S. Oh, C. M. Agrawal. Surface modification of cobalt-chromium-tungsten-nickel alloy using octadecyltrichlorosilanes. *Appl. Surf. Sci.*, **2009**, *255*, 5961–5970.

[153] W. Gu, C. P. Tripp. Reaction of silanes in supercritical CO_2 with TiO_2 and Al_2O_3, *Langmuir*, **2006**, *22*, 5748–5752.

[154] Y. Lin, L. Wang, J. W. Krumpfer, J. J. Watkins, T. J. McCarthy. Hydrophobization of inorganic oxide surfaces using dimethylsilanediol. *Langmuir*, **2013**, *29*, 1329–1332.

[155] K. D. Lork, K. K. Unger, J. N. Kinkel. Role of the functional group in n-octydimethylsilanes in the synthesis of C8 reversed-phase silica packings for high-performance liquid chromatography. *J. Chromatogr. A*, **1986**, *352*, 199–211.

[156] C. P. Tripp, M. L. Hair. Chemical attachment of chlorosilanes to silica: a two-step amine-promoted reaction. *J. Phys. Chem.*, **1993**, *97*, 5693–5698.

[157] M. R. Alexander, R. D. Short, F. R. Jones, W. Michaeli, C. J. Blomfield. A study of HMDSO/O_2 plasma deposits using a high-sensitivity and energy resolution XPS instrument: curve fitting of the Si2p core level. *Appl. Surf. Sci.*, **1999**, *137*, 179–183.

[158] Z. Yang, Y. Chevolot, T. Géhin, V. Dugas, N. Xanthopoulos, V. Laporte, T. Delair, Y. Ataman-Önal, G. Choquet-Kastylevsky, É. Souteyrand, E. Laurencea. Characterization of three amino-functionalized surfaces and evaluation of antibody immobilization for the multiplex detection of tumor markers involved in colorectal cancer. *Langmuir*, **2013**, *29*, 1498–1509.

[159] J. C. Shearer, M. J. Fisher, D. Hoogeland, E. R. Fisher. Composite SiO_2/TiO_2 and amine polymer/TiO_2 nanoparticles produced using plasma-enhanced chemical vapor deposition. *Appl. Surf. Sci.*, **2010**, *256*, 2081–2091.

[160] R. A. Shircliff, I. T. Martin, J. W. Pankow, J. Fennell, P. Stradins, M. L. Ghirardi, S. W. Cowley, H. M. Branz. High-resolution X-ray photoelectron spectroscopy of mixed silane monolayers for DNA attachment. *ACS Appl. Mater. Interfaces*, **2011**, *3*, 3285–3292.

[161] J. Zhang, D. S. Wavhal, E. R. Fisher. Mechanisms of SiO_2 film deposition from tetramethylcyclotetrasiloxane, dimethyldimethoxysilane, and trimethylsilane plasmas. *J. Vac. Sci. Technol. A*, **2004**, *22*, 201–213.

[162] A. Bellel, S. Sahli, P. Raynaud, Y. Segui, Z. Ziari, D. Eschaich, G. Dennler. Improvement of the polyimide surface wettability using SiO_x films deposited in a DECR reactor from HMDSO/O_2 mixtures. *Plasma Processes Polym.*, **2005**, *2*, 586–594.

[163] A. Grüniger, A. Bieder, A. Sonnenfeld, P. R. von Rohr, U. Müller, R. Hauert. Influence of film structure and composition on diffusion barrier performance of SiO_x thin films deposited by PECVD. *Surf. Coat. Technol.*, **2006**, *200*, 4564–4571.

[164] L. A. O'Hare, B. Parbhoo, S. R. Leadley. Development of a methodology for XPS curve-fitting of the Si2p core level of siloxane materials. *Surf. Interface Anal.*, **2004**, *36*, 1427–1434.

[165] C. P. Tripp, M. L. Hair. Reaction of chloromethylsilanes with silica: a low-frequency infrared study. *Langmuir*, **1991**, *7*, 923–927.

[166] C. P. Tripp, M. L. Hair. Reaction of alkylchlorosilanes with silica at the solid/gas and solid/liquid interface. *Langmuir*, **1992**, *8*, 1961–1967.

[167] R. Tian, O. Seitz, M. Li, W. Hu, Y. J. Chabal, J. Gao. Infrared characterization of interfacial Si−O bond formation on silanized flat SiO_2/Si surfaces. *Langmuir*, **2010**, *26*, 4563–4566.

[168] R. M. Pasternack, S. R. Amy, Y. J. Chabal. Attachment of 3-(aminopropyl)triethoxysilane on silicon oxide surfaces: dependence on solution temperature. *Langmuir*, **2008**, *24*, 12963–12971.

[169] N. Aissaoui, L. Bergaoui, J. Landoulsi, J. F. Lambert, S. Boujday. Silane layers on silicon surfaces: mechanism of interaction, stability, and influence on protein adsorption. *Langmuir*, **2012**, *28*, 656–665.

[170] M. A. Ramin, G. L. Bourdon, K. Heuzé, M. Degueil, C. Belin, T. Buffeteau, B. Bennetau, L. Vellutini. Functionalized hydrogen-bonding self-assembled monolayers grafted onto SiO_2 Substrates. *Langmuir*, **2012**, *28*, 17672–17680.

[171] Y. Mousli, L. Rouvière, I. Traboulsi, J. Hunel, T. Buffeteau, K. Heuzé, L. Vellutini, E. Genin. Hydrosilylation of azide-containing olefins as a convenient access to azidoorganotrialkoxysilanes for self-assembled monolayer elaboration onto silica by spin coating. *ChemistrySelect*, **2018**, *3*, 7333–7339.

[172] M. Meillan, T. Buffeteau, G. L. Bourdon, L. Thomas, M. Degueil. K. Heuzé, B. Bennetau, L. Vellutini. Mixed self-assembled monolayers with internal urea group on silica surface. *ChemistrySelect*, **2017**, *2*, 11868–11874.

[173] H. Rahma, T. Buffeteau, C. Belin, G. L. Bourdon, M. Degueil, B. Bennetau, L. Vellutini, K. Heuzé. Resolving the chemical nature of nanodesigned silica surface obtained via a bottom-up approach. *ACS Appl. Mater. Interfaces*, **2013**, *5*, 6843–6849.

[174] D. H. Dinh, L. Vellutini, B. Bennetau, C. Dejous, D. Rebière, É. Pascal, D. Moynet, C. Belin, B. Desbat, C. Labrugère, J. P. Pillot. Route to smooth silica-based surfaces decorated with novel self-assembled monolayers (SAMs) containing glycidyl-terminated very long hydrocarbon chains. *Langmuir*, **2009**, *25*, 5526–5535.

[175] J. Sagiv. Organized monolayers by adsorption. 1. Formation and structure of oleophobic mixed monolayers on solid surfaces. *J. Am. Chem. Soc.*, **1980**, *102*, 92–98.

[176] D. L. Angst, G. W. Simmons. Moisture absorption characteristics of organosiloxane self-assembled monolayers. *Langmuir*, **1991**, *7*, 2236–2242.

[177] Y. Zheng, T. Thai, P. Reineck, L. Qiu, Y. Guo, U. Bach. DNA-directed self-assembly of core-satellite plasmonic nanostructures: a highly sensitive and reproducible near-IR SERS Sensor. *Adv. Funct. Mater.*, **2013**, *23*, 1519–1526.

[178] Z. Guo, R. A. Guilfoyle, A. J. Thiel, R. Wang, L. M. Smith. Direct fluorescence analysis of genetic polymorphisms by hybridization with oligonucleotide arrays on glass supports. *Nucleic Acids Res.*, **1994**, *22*, 5456–5465.

[179] E. Briand, V. Humblot, J. Landoulsi, S. Petronis, C. M. Pradier, B. Kasemo, S. Svedhem. Chemical modifications of Au/SiO_2 template substrates for patterned biofunctional surfaces. *Langmuir*, **2011**, *27*, 678–685.

[180] P. J. Rodríguez-Cantó, M. Martínez-Marco, F. J. Rodríguez-Fortuño, B. Tomás-Navarro, R. Ortuño, S. Peransí-Llopis, A. Martínez. Demonstration of near infrared gas sensing using gold nanodisks on functionalized silicon. *Opt. Express*, **2011**, *19*, 7664–7672.

[181] G. Chen, S. Chen, Y. Chen, Y. Hsu. Site-selective electroless metallization on porous organosilica films by multisurface modification of alkyl monolayer and vacuum plasma. *Langmuir*, **2013**, *29*, 511–518.

[182] J. Duchet, B. Chabert, J. P. Chapel, J. F. Gérard, J. M. Chovelon, N. Jaffrezic-Renault. Influence of the deposition process on the structure of grafted alkylsilane layers. *Langmuir*, **1997**, *13*, 2271–2278.

[183] V. Dugas, C. Demesmay, Y. Chevolot, É. Souteyrand. *Use of organosilanes in biosensors*. *Nova Science Pub Inc; UK ed. edition*, **2010**, 978-1616680299.

[184] K. Shabtai, S. R. Cohen, H. Cohen, I. Rubinstein. A composite gold silicon oxide surface for mesoscopic patterning. *J. Phys. Chem. B*, **2003**, *107*, 5540–5546.

[185] J. Gun, J. Sagiv. On the formation and structure of self-assembling monolayers: III. Time of formation, solvent retention, and release. *J. Colloid Interface Sci.*, **1986**, *112*, 457–472.

[186] R. Maoz, H. Cohen, J. Sagiv. Specific nonthermal chemical structural transformation induced by microwaves in a single amphiphilic bilayer self-assembled on silicon. *Langmuir*, **1998**, *14*, 5988–5993.

[187] N. Rozlosnik, M. C. Gerstenberg, N. B. Larsen. Effect of solvents and concentration on the formation of a self-assembled monolayer of octadecylsiloxane on silicon (001). *Langmuir*, **2003**, *19*, 1182–1188.

[188] J. Kim, G. J. Holinga, G. A. Somorjai. Curing induced structural reorganization and enhanced reactivity of amino-terminated organic thin films on solid substrates: observations of two types of chemically and structurally unique amino groups on the surface. *Langmuir*, **2011**, *27*, 5171–5175.

[189] K. M. R. Kallury, M. Thompson, C. P. Tripp, M. L. Hair. Interaction of silicon surfaces silanized with octadecylchlorosilanes with octadecanoic acid and octadecanamine studied by ellipsometry, X-ray photoelectron spectroscopy and reflectance Fourier transform infrared spectroscopy. *Langmuir*, **1992**, *8*, 947–954.

[190] D. Hausmann, J. Becker, S. Wang, R. G. Gordon. Rapid vapor deposition of highly conformal silica nanolaminates. *Science*, **2002**, *298*, 402–406.

[191] F. Zhang, K. Sautter, A. M. Larsen, D. A. Findley, R. C. Davis, H. Samha, M. R. Linford. Chemical vapor deposition of three aminosilanes on silicon dioxide: surface characterization, stability, effects of silane concentration, and cyanine dye adsorption. *Langmuir*, **2010**, *26*, 14648–14654.

[192] A. Hozumi, K. Ushiyama, H. Sugimura, O. Takai. Fluoroalkylsilane monolayers formed by chemical vapor surface modification on hydroxylated oxide surfaces. *Langmuir*, **1999**, *15*, 7600–7604.

[193] R. D. Lowe, M. A. Pellow, T. D. P. Stack, C. E. D. Chidsey. Deposition of dense siloxane monolayers from water and trimethoxyorganosilane vapor. *Langmuir*, **2011**, 27, 9928–9935.

[194] A. Ulman. Formation and structure of self-assembled monolayers. *Chem. Rev.*, **1996**, *96*, 1533–1554.

[195] R. Helmy, A. Y. Fadeev. Self-assembled monolayers supported on TiO_2: comparison of $C_{18}H_{37}SiX_3$ (X = H, Cl, OCH_3), $C_{18}H_{37}Si(CH_3)_2Cl$, and $C_{18}H_{37}PO(OH)_2$. *Langmuir*, **2002**, *18*, 8924–8928.

[196] A. Y. Fadeev, R. Helmy, S. Marcinko. Self-assembled monolayers of organosilicon hydrides supported on titanium, zirconium, and hafnium dioxides. *Langmuir*, **2002**, *18*, 7521–7529.

[197] Q. Ye, F. Zhou, W. Liu. Bioinspired catecholic chemistry for surface modification. *Chem. Soc. Rev.*, **2011**, *40*, 4244–4258.

[198] Y. Liu, K. Ai, L. Lu. Polydopamine and its derivative materials: synthesis and promising applications in energy, environmental, and biomedical fields. *Chem. Rev.*, **2014**, *114*, 5057–5115.

[199] Y. Liu, B. Yu, J. Hao, F. Zhou. Amination of surfaces via self-assembly of dopamine. *J. Colloid Interface Sci.*, **2011**, *362*, 127–134.

[200] L. Petrone. Molecular surface chemistry in marine bioadhesion. *Adv. Colloid Interface Sci.*, **2013**, *195–196*, 1-18.

[201] S. Li, J. Wang, P. Jacobson, X. Gong, A. Selloni, U. Diebold. Correlation between bonding geometry and band gap states at organic−inorganic interfaces: catechol on rutile TiO_2 (110). *J. Am. Chem. Soc.*, **2009**, *131*, 980–984.

[202] H. Lee, S. M. Dellatore, W. M. Miller, P. B. Messersmith. Mussel-inspired surface chemistry for multifunctional coatings. *Science*, **2007**, *318*, 426–430.

[203] Q. Ye, H. Wang, B. Yu, F. Zhou. Self-assembly of catecholic ferrocene and electrochemical behavior of its monolayer. *RSC Adv.*, **2015**, *5*, 60090–60095.

[204] T. Rajh, O. Poluektov, A. A. Dubinski, G. Wiederrecht, M. C. Thurnauer, A. D. Trifunac. Spin polarization mechanisms in early stages of photoinduced charge separation in surface-modified TiO_2 nanoparticles. *Chem. Phys. Lett.*, **2001**, *344*, 31–39.

[205] S. Saxer, C. Portmann, S. Tosatti, K. Gademann, S. Zürcher, M. Textor. Surface assembly of catechol-functionalized poly(l-lysine)-graft-poly(ethylene glycol) copolymer on titanium exploiting combined electrostatically driven self-organization and biomimetic strong adhesion. *Macromolecules*, **2010**, *43*, 1050–1060.

[206] H. Gu, K. Xu, Z. Yang, C. K. Chang, B. Xu. Synthesis and cellular uptake of porphyrin decorated iron oxide nanoparticles—a potential candidate for bimodal anticancer therapy. *Chem. Commun.*, **2005**, *0*, 4270–4272.

[207] E. Amstad, T. Gillich, I. Bilecka, M. Textor, E. Reimhult. Ultrastable iron oxide nanoparticle colloidal suspensions using dispersants with catechol-derived anchor groups. *Nano Lett.*, **2009**, *9*, 4042–4048.

[208] D. J. Lavrich, S. M. Wetterer, S. L. Bernasek, G. Scoles. Physisorption and chemisorption of alkanethiols and alkyl sulfides on Au (111). *J. Phys. Chem. B*, **1998**, *102*, 3456–3465.

[209] R. G. Nuzzo, B. R. Zegarski, L. H. Dubois. Fundamental studies of the chemisorption of organosulfur compounds on gold (111). Implications for molecular self-assembly on gold surfaces. *J. Am. Chem. Soc.*, **1987**, *109*, 733–740.

[210] J. B. Schlenoff, M. Li, H. Ly. Stability and self-exchange in alkanethiol monolayers. *J. Am. Chem. Soc.*, **1995**, *117*, 12528–12536.

[211] L. Salem. Attractive forces between long saturated chains at short distances. *J. Chem. Phys.*, **1962**, *37*, 2100–2113.

[212] Y. S. Shon, S. M. Gross, B. Dawson, M. Porter, R. W. Murray. Alkanethiolate-protected gold clusters generated from sodium S-dodecylthiosulfate (Bunte Salts). *Langmuir*, **2000**, *16*, 6555–6561.

[213] Y. S. Shon, T. R. Lee. Desorption and exchange of self-assembled monolayers (SAMs) on gold generated from chelating alkanedithiols. *J. Phys. Chem. B*, **2000**, *104*, 8192–8200.

[214] R. Colorado, R. J. Villazana, T. R. Lee. Self-assembled monolayers on gold generated from aliphatic dithiocarboxylic acids. *Langmuir*, **1998**, *14*, 6337–6340.

[215] J. M. Tour, L. J. II, D. L. Pearson, J. J. S. Lamba, T. P. Burgin, G. M. Whitesides, D. L. Allara, A. N. Parikh, S. Atre. Self-assembled monolayers and multilayers of conjugated

thiols, α,ω-dithiols, and thioacetyl-containing adsorbates. Understanding attachments between potential molecular wires and gold surfaces. *J. Am. Chem. Soc.*, **1995**, *117*, 9529–9534.

[216] E. B. Troughton, C. D. Bain, G. M. Whitesides, R. G. Nuzzo, D. L. Allara, M. D. Porter. Monolayer films prepared by the spontaneous self-assembly of symmetrical and unsymmetrical dialkyl sulfides from solution onto gold substrates: structure, properties, and reactivity of constituent functional groups. *Langmuir*, **1988**, *4*, 365–385.

[217] R. G. Nuzzo, D. L. Allara. Adsorption of bifunctional organic disulfides on gold surfaces. *J. Am. Chem. Soc.*, **1983**, *105*, 4481–4483.

[218] T. M. Willey, A. L. Vance, C. Bostedt, T. Buuren, R. W. Meulenberg, L. J. Terminello, C. S. Fadley. Surface structure and chemical switching of thioctic acid adsorbed on Au (111) as observed using near-edge X-ray absorption fine structure. *Langmuir*, **2004**, *20*, 4939–4944.

[219] Z. Li, T. Niu, Z. Zhang, G. Feng, S. Bi. Studies on the effect of solvents on self-assembly of thioctic acid and Mercaptohexanol on gold. *Thin Solid Films*, **2011**, *519*, 4225–4233.

[220] M. Suzuki. Study on chemical reaction of methylthiirane on gold colloid by surface-enhanced Raman scattering. *Langmuir*, **1999**, *15*, 7409–7410.

[221] L. Li, S. Chen, J. Zheng, B. D. Ratner, S. Jiang. Protein adsorption on oligo (ethylene glycol)-terminated alkanethiolate self-assembled monolayers: the molecular basis for nonfouling behavior. *J. Phys. Chem. B*, **2005**, *109*, 2934–2941.

[222] R. Schweiss, D. Pleul, F. Simon, A. Janke, P. B. Welzel, B. Voit, W. Knoll, Carsten Werner. Electrokinetic potentials of binary self-assembled monolayers on gold: acid−base reactions and double layer structure. *J. Phys. Chem. B*, **2004**, *108*, 2910–2917.

[223] C. D. Bain, E. B. Troughton, Y. T. Tao, J. Evall, G. M. Whitesides, R. G. Nuzzo. Formation of monolayer films by the spontaneous assembly of organic thiols from solution onto gold. *J. Am. Chem. Soc.*, **1989**, *111*, 321–335.

[224] H. Bayat, D. Tranchida, B. Song, W. Walczyk, E. Sperotto, H. Schönherr. Binary self-assembled monolayers of alkanethiols on gold: deposition from solution versus microcontact printing and the study of surface nanobubbles. *Langmuir*, **2011**, *27*, 1353–1358.

[225] N. Afara, S. Omanovic, M. Asghari-Khiavi. Functionalization of a gold surface with fibronectin (FN) covalently bound to mixed alkanethiol self-assembled monolayers (SAMs): The influence of SAM composition on its physicochemical properties and FN surface secondary structure. *Thin Solid Films*, **2012**, *522*, 381–389.

[226] N. Battaglini, Z. Qin, P. Campiglio, V. Repain, C. Chacon, S. Rousset, P. Lang. Directed growth of mixed self-assembled monolayers on a nanostructured template: a step toward the patterning of functional molecular domains. *Langmuir*, **2012**, *28*, 15095–15105.

[227] J. Houplin, L. Amiaud, V. Humblot, I. Martin, E. Matar, R. Azria, C. M. Pradier, A. Lafosse. Selective terminal function modification of SAMs driven by low-energy electrons (0–15 eV). *Phys. Chem. Chem. Phys.*, **2013**, *15*, 7220–7227.

[228] V. Lebec, J. Landoulsi, S. Boujday, C. Poleunis, C. M. Pradier, A. Delcorte. Probing the orientation of β-Lactoglobulin on gold surfaces modified by alkyl thiol self-assembled monolayers. *J. Phys. Chem. C*, **2013**, *117*, 11569–11577.

[229] A. Scholten, B. Menges, M. Juebner, M. A. Rothschild, K. Bender. A mixed alkanethiol based immunosensor for surface plasmon field-enhanced fluorescence spectroscopy in serum. *Analyst*, **2013**, *138*, 1705–1712.

[230] J. N. Ngunjiri, D. J. Stark, T. Tian, K. A. Briggman, J. C. Garno. Immobilization of proteins on carboxylic acid functionalized nanopatterns. *Anal. Bioanal. Chem.*, **2013**, *405*, 1985–1993.

[231] A. Vallée, V. Humblot, R. Al Housseiny, S. Boujday, C. M. Pradier. BSA adsorption on aliphatic and aromatic acid SAMs: Investigating the effect of residual surface charge and sublayer nature. *Colloids Surf. B Biointerfaces*, **2013**, *109*, 136–142.

[232] D. Mercier, C. Mercader, S. Quere, L. Hairault, C. Méthivier, C. M. Pradier. Specific interactions of functionalised gold surfaces with ammonium perchlorate or starch; towards a chemical cartography of their mixture. *Appl. Surf. Sci.*, **2012**, *258*, 9518–9525.

[233] G. E. Poirier. Characterization of organosulfur molecular monolayers on Au (111) using scanning tunneling microscopy. *Chem. Rev.*, **1997**, *97*, 1117–1128.

[234] F. Schreiber. Structure and growth of self-assembling monolayers. *Prog. Surf. Sci.*, **2000**, *65*, 151–257.

[235] Y. Zheng, C. H. Lalander, T. Thai, S. Dhuey, S. Cabrini, U. Bach. Gutenberg-style printing of self-assembled nanoparticle arrays: electrostatic nanoparticle immobilization and DNA-mediated transfer. *Angew. Chem. Int. Ed.*, **2011**, *50*, 4398–4402.

[236] M. Palma, J. J. Abramson, A. A. Gorodetsky, E. Penzo, R. L. Gonzalez Jr., M. P. Sheetz, C. Nuckolls, J. Hone, S. J. Wind. Selective biomolecular nanoarrays for parallel single-molecule investigations. *J. Am. Chem. Soc.*, **2011**, *133*, 7656–7659.

[237] H. Cai, S. J. Wind. Improved glass surface passivation for single-molecule nanoarrays. *Langmuir*, **2016**, *32*, 10034–10041.

[238] R. Marie, A. B. Dahlin, J. O. Tegenfeldt, F. Höök. Generic surface modification strategy for sensing applications based on Au/SiO_2 nanostructures. *Biointerphases*, **2007**, *2*, 49–55.

[239] M. Trevisan, Y. Chevolot, V. Monnier, J. P. Cloarec, É. Souteyrand, A. Duval, J. Moreau, M. Canva. Elaboration and grafting of magnetic bead-chains for detection of anisotropy with polarimetric surface plasmon resonance imaging system. *Int. J. Nanosci.*, **2012**, *11*, 1240012 1–5.

[240] K. Kumar, A. B. Dahlin, T. Sannomiya, S. Kaufmann, L. Isa, E. Reimhult. Embedded plasmonic nanomenhirs as location-specific biosensors. *Nano Lett.*, **2013**, *13*, 6122–6129.

[241] R. Michel, J. W. Lussi, G. Csucs, I. Reviakine, G. Danuser, B. Ketterer, J. A. Hubbell, M. Textor, N. D. Spencer. Selective molecular assembly patterning: a new approach to micro- and nanochemical patterning of surfaces for biological applications. *Langmuir*, **2002**, *18*, 3281–3287.

[242] N. Zhang, Y. Liu, J. Yang, X. Su, J. Deng, C. C. Chum, M. Hong, J. Teng. High sensitivity molecule detection by plasmonic nanoantennas with selective binding at electromagnetic hotspots. *Nanoscale*, **2014**, *6*, 1416–1422.

[243] L. Feuz, M. P. Jonsson, F. Höök. Material-selective surface chemistry for nanoplasmonic sensors: optimizing sensitivity and controlling binding to local hot spots. *Nano Lett.*, **201**2, *12*, 873–879.

[244] T. J. Gardner, C. D. Frisbie, M. S. Wrighton. Systems for orthogonal self-assembly of electroactive monolayers on Au and ITO: an approach to molecular electronics. *J. Am. Chem. Soc.*, **1995**, *117*, 6927–6933.

[245] G. T. Ayele, S. Monfray, F. Boeuf, J. P. Cloarec, S. Ecoffey, D. Drouin, E. Puyoo, A. Souifi. Development of ultrasensitive extended-gate Ion-sensitive-field-effect-transistor based on industrial UTBB FDSOI transistor. *47th European Solid-State Device Research Conference (ESSDERC)*, **2017**, 264–267.

[246] L. Rahhal, G. T. Ayele, S. Monfray, J. P. Cloarec, B. Fornacciari, E. Pardoux, C. Chevalier, S. Ecoffey, D. Drouin, P. Morin, P. Garnier, F. Boeuf, A. Souifi. High sensitivity pH sensing on the BEOL of industrial FDSOI transistors. *Solid-State Electron.*, **2017**, *134*, 22–29.

[247] H. Akazawa. Highly adhesive Pt-electrode films directly deposited on SiO_2 by electron-cyclotron-resonance plasma sputtering. *Surf. Coat. Technol.*, **2010**, *204*, 1836–1841.

[248] O. Valet, P. Doppelt, P. K. Baumann, M. Schumacher, E. Balnois, F. Bonnet, H. Guillon. Study of platinum thin films deposited by MOCVD as electrodes for oxide applications. *Microelectron. Eng.*, **2002**, *64*, 457–463.

[249] P. Simon, J. Nazon, B. Domenichini, S. Bourgeois. Comparative study of air and vacuum annealing atmosphere towards Pt/Ti–W/SiO_2 stability. *Thin Solid Films*, **2013**, *548*, 138–142.

[250] S. S. Cohen, M. J. Kim, B. Gorowitz, R. Saia, T. F. McNelly, G. Todd. Direct W–Ti contacts to silicon. *Appl. Phys. Lett.*, **1984**, *45*, 414–416.

[251] S. E. Babcock, K. N. Tu. Titanium-tungsten contacts to silicon. II. Stability against aluminum penetration. *J. Appl. Phys.*, **1986**, *59*, 1599–1605.

[252] S. Wang, S. Suthar, C. Hoeflich, B. J. Burrow. Diffusion barrier properties of TiW between Si and Cu. *J. Appl. Phys.*, **1993**, *73*, 2301–2320.

[253] D. B. Bergstrom, I. Petrov, J. E. Greene. Al/Ti_xW_{1-x} metal/diffusion-barrier bilayers: interfacial reaction pathways and kinetics during annealing. *J. Appl. Phys.*, **1997**, *82*, 2312–2322.

[254] S. K. Bhagat, N. D. Theodore, T. L. Alford. Thermal stability of tungsten–titanium diffusion barriers for silver metallization. *Thin Solid Films*, **2008**, *516*, 7451–7457.

[255] T. L. Alford, L. Chen, K. S. Gadre. Stability of silver thin films on various underlying layers at elevated temperatures. *Thin Solid Films*, **2003**, *429*, 248–254.

[256] M. Liehr, J. P. Delrue, R. Caudano. Comparative study of Nb and TiW barrier layers between Au and a-SiO_2. *J. Vac. Sci. Technol. A*, **1984**, *2*, 288–291.

[257] F. Yang, M. Chen. Evaluation of in situ formed W–Ti and $MoSi_2$ as a diffusion barrier to Al for $CoSi_2$ silicided contact. *J. Vac. Sci. Technol. B Microelectron. Nanometer Struct. Process. Meas. Phenom.*, **1993**, *11*, 744–751.

Chapter 2

Surface chemical functionalization of titanium tungsten substrate with silane, phosphonic acid or ortho-dihydroxyaryl based organolayers

2 Surface chemical functionalization of titanium tungsten substrate with silane, phosphonic acid or ortho-dihydroxyaryl based organolayers

2.1 Introduction

Surface chemical functionalization of inorganic materials has been developed for various applications, such as surface patterning fabrication[1], tissue engineering[2], biosensors[3] and corrosion inhibition[4]. Surface chemical functionalization can be achieved either using polymeric material deposition or by the attachment of low molecular weight functional molecules bearing a chemical group that can react with the surface of the materials (substrate-binding head group) to form an organolayer. For example, the most reported reactions are the ones of thiols on gold surfaces and of silanes on silica surfaces though the formation of Au-S and Si-O bond, respectively[5]–[8]. Surface functionalization of metallic oxides, semiconductor oxides or material without oxygen in the bulk but bearing surface bound hydroxyl groups can be achieved using a variety of substrate-binding head groups such as organosilane, alkyl iodides, alkyne, alkene, amine, carboxylic acids, hydroxamic acids[9]. In the following, we will focus on the use of organosilanes, organo phosphonic acids and *ortho*-dihydroxyaryl compounds for metal oxide derivatization. Herein, metal oxide does not necessarily refer to the bulk of the material but to the top layer.

Silanization of a wide variety of oxides have been reported including metallic oxides or their native oxide layer such as aluminum oxide, titanium oxide, steel and nickel alloy[10]–[13]. Silane monolayers formation on metal oxide is attributed to either one step reaction or two step reaction mechanisms. In the one step mechanism, the direct condensation of pendant hydroxyls from the surface of the oxide with the silane occurs at an appreciable rate for temperature above 300-400°C with chlorosilanes and above 100-200°C with alkoxy silanes[14], [15]. The two step mechanism involved first, the hydrolysis of the leaving group (chloro, alkoxy or hydride) of the organosilane leading to an organo-silanol. Then, dehydration of the resulting silanol with pendant hydroxyl groups from the substrate lead to the formation of a Si-O-M bond. Furthermore, in the case of multifunctional silane, lateral crosslinking between organo-silanols, can take place. However, under uncontrolled experimental conditions cross linking reactions can lead to 3D polysiloxane network. The temperature, the solvent and the surface water content are critical parameters for the formation of reproducible organosilane layers[16]–[18]. Furthermore, the density of grafted organosilane is governed by the surface silanol density when 3D polymerization does not occur. Surface grafting densities are ranking between 0.14 to 3.5 µmol/m² on silica based

substrates. The stability of the Si-O-M bond ranks from good to poor as follow: Si-O-Si > Si-O-Al > Si-O-Cu > Si-O-Fe > Si-O-Ni > Si-O-Zn > Si-O-Pb > Si-O-Sn > Si-O-C[19].

Alternatively, phosphonic acids and their phosphonate ester derivatives have been used for surface functionalization of metal oxides, such as aluminum oxide, titanium oxide, tungsten oxide and iron oxide [10], [20]–[23]. The reaction mechanism is complex and leads to a multitude of binding modes that depend on the metal oxide in particular its Lewis acidity, temperature, pH value, concentration and solvent[24]. On silica, hetero-condensation of phosphonic acids with pending silanols requires annealing temperature in the 120-140°C while it seems not compulsory with other oxides in particular titania[25], [26]. In addition, it was proposed that the P-O-W bonds is twice as strong as S-Au bonds, which may provide a more robust attachment of some molecules to certain metal oxide surface[10], [27]. For example, the stability of an organo phosphonate layer has been demonstrated to be higher on CrN than the one observed with organosilane[28].

Although the use of *ortho*-dihydroxyaryl compounds such as catechols is not specific for metallic oxide functionalization, it has the advantage of allowing to obtain stable layers without the need of harsh conditions[29], [30]. However, the binding mechanism is complex due to the fact that the film formation is composed of the attachment of the catechol to the oxide surface and to the oxidation-polymerization/crosslinking reaction of the bound catechol with the ones in solution. The resulting polymeric film has strong interfacial adhesion with a wide range of surfaces. The cross-link is favored under alkaline and oxidative conditions. The binding of catechol to oxide surfaces seems to involve the formation of monodendate and bidendate complexes and requires the replacement of the surface hydroxyl by the deprotonated aromatic hydroxyl. The oxidation/polymerization of catechols could be successfully controlled by the introduction of electron-withdrawing groups, limiting oxidant media and controlling the pH values[31], [32].

In order to open access to semiconductor industries and photonics industrial platforms such as molecular diagnostics and environmental analysis, the fabrication of transduction devices needs to be fully compatible with industrial production. The architecture of the transducers should also potentially provide better performances and offer the possibility to be embedded in a finalized sensor chip. TiW used as a barrier layer material has already been reported in some electronic structure[33]–[41]. Although, surface modification of titanium oxide has been widely described, the functionalization of tungsten oxide have only been reported with organophosphonic acid, to the best of our knowledge, surface functionalization of TiW has never been reported[23], [42].

In this context, this study provides for the first time functionalization studies on TiW layers deposited on silicon substrates. Since titanium and tungsten are prone to form oxide layers, we first assessed that a surface oxide layer is indeed present after plasma oxygen cleaning.

Next we compared the formation of organolayers on TiW using organosilane, phosphonic acid and *ortho*-dihydroxyaryl compounds. Three molecules: 3-aminopropylphosphonic acid (APPA), 3-ethoxydimethylsilylpropylamine (APDMES), dopamine (DA) were used to functionalize the TiW surface with the goal of studying the stability of the formed organolayers. X-ray photoelectron spectroscopy (XPS), Time-of-flight secondary Ion mass spectrometry (ToF-SIMS) and Fourier transform infrared spectroscopy (FTIR) were used to characterize and analyze the different layers. APDMES, APPA and DA are primary amine molecules. The amino-functionalized surfaces are expected to provide a foundation and prospect for further applications.

2.2 Experimental section

2.2.1 Materials

200 nm thickness TiW on Si substrate was prepared by STMicroelectronics. Chemicals are of reagent or higher grade commercially available. Dopamine hydrochloride 97% (DA) and 3-aminopropylphosphonic acid (APPA) 97% were purchased from Sigma-Aldrich. (3-aminopropyl)-dimethylethoxysilane (APDMES) 99.9% was purchased from abcr GmbH. Dichloromethane (DCM) 99.9% was purchased from Sigma-Aldrich and dried over molecular sieves before use. The ultrapure water (18.2 MΩ) used for all the experiments was obtained by VEOLIA water system.

2.2.2 Chemical functionalization

The substrates were cleaned by oxygen plasma treatment (Anatech) at 400 sccm of oxygen, 350 W of forward power (10W reflected power) for 5 min to remove any organic contamination and to obtain a hydroxyl-terminated surface. After being activated, organolayers were formed by immersing the TiW substrates in the solutions of the three different molecules.

TiW was functionalized with APDMES using the following protocol: substrates were immersed in 25 ml dried DCM containing 10µl APDMES (3 mM) for 48 hours. The samples were then rinsed with fresh DCM for 5 min under ultrasound (Branson, 42 kHz, 100 W) followed by a stream of ultrapure water and dried with nitrogen flow.

TiW was functionalized with APPA using the following protocol: substrates were immersed in 10 mM APPA aqueous solution for 24 hours. The samples were then rinsed with ultrapure water for 5 min under sonication followed by a stream of ultrapure water before drying with nitrogen flow.

TiW was functionalized with DA using the following protocol: substrates were immersed in 0.5 mg/mL degassed ultrapure water of dopamine (2.5 mM) for 24 hours under nitrogen

atmosphere. The samples were then rinsed with ultrapure water for 5 min under sonication followed by a stream of ultrapure water before drying with nitrogen flow.

Herein TiW functionalized by APDMED, APPA and DA organolayers were named by APDMES-TiW, APPA-TiW and DA-TiW, respectively.

2.2.3 Organolayers stability

APDMES-TiW, APPA-TiW and DA-TiW were immersed in ultrapure water and incubated at 70 °C for up to 1 hour. After removal from the water, the samples were rinsed in ultrapure water. All samples were dried with nitrogen flow.

2.2.4 Characterization

X-Ray Diffraction (XRD). The crystal structure of TiW was characterized by XRD. A Rigaku Smartlab diffractometer with a rotating anode (power 9 kW) was used. The source emitted CuK radiation that was monochromatized by a double Ge (220) crystal to select the CuKα 1 ray (λ = 0.15406nm). The detector is a point scintillation counter.

Atomic Force Microscopy (AFM). Surface topography of TiW was monitored using a SMENA B (NT-MDT) AFM microscope in tapping modulation (AM) mode with Mikromash XSC11 with Al backside tips (resonance frequency 80 kHz). Data analysis was performed by Gwyddion Software.

Attenuated total reflectance Fourier transform infrared (ATR-FTIR). ATR-FTIR was analyzed using a Thermo Nicolet 6700 spectrometer with MCT detector (Electron Corporation, USA) by a germanium crystal from 800 cm^{-1} to 4000 cm^{-1}. Results were obtained from averages of 256 scans at a resolution of 4 cm^{-1}.

Time-of-flight secondary ion mass spectrometry (ToF-SIMS). ToF-SIMS measurements were performed with a Physical Electronics TRIFT III instrument (Physical Electronics, Chanhassen, MN) operated with a pulsed Au ion gun (ion current of 2 nA) over a 300 μm × 300 μm area. The ion dose was kept below the static conditions limits. Data were analyzed using WinCadence software. Mass calibration was performed on hydrocarbon secondary ions.

X-ray Photoelectron Spectroscopy (XPS). XPS measurements were performed with a VSW spectrometer using a monochromatized X-ray source (Al Kα 1486.6 eV). Spectrum acquisitions were performed under ultrahigh vacuum conditions (UHV, 10^{-9} Torr). Take-off angle was 90° relative to the substrate surface. The pass energies were 100 eV and 20 eV for wide-scan and high-resolution elemental scans, respectively. The data reduction (atomic concentration, shift, curve fitting, etc.) was performed with CasaXPS software. The C-C contribution in C1s core level was fixed at 284.6 eV. Full width at half maximum (FWHM) for the component peaks of Si2p, P2p, N1s, and O1s were constrained to be 1.7 eV, 1.9 eV, 1.7 eV, and 1.4 eV, respectively.

2.3 Results and discussions

2.3.1 Roughness and crystallinity of TiW

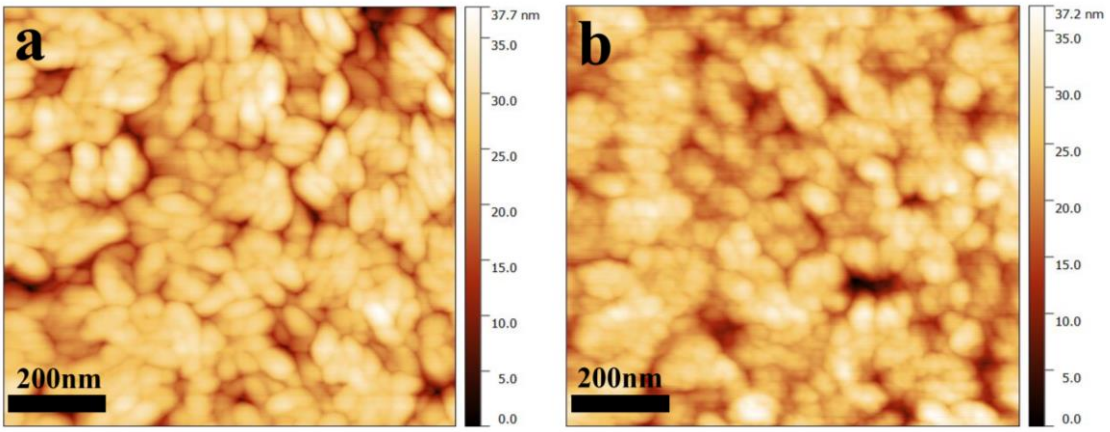

Figure 2.1 AFM image of TiW surface before (a) and after (b) O_2 plasma.

The AFM images show that the surface topography of TiW before and after oxygen plasma cleaning (Figure 2.1). It is formed of small islands having a width of ca. 100 nm and heights of ca. 35-40 nm. The Root Mean Square (RMS) was found to be around 3.9 ± 0.5 nm. This rugosity does not seem to be altered by oxygen plasma cleaning. This surface topography suggests that it would be difficult to obtain information on organolayers built on such surfaces through topography as the organolayers are expected to be on the order of 1nm thick.

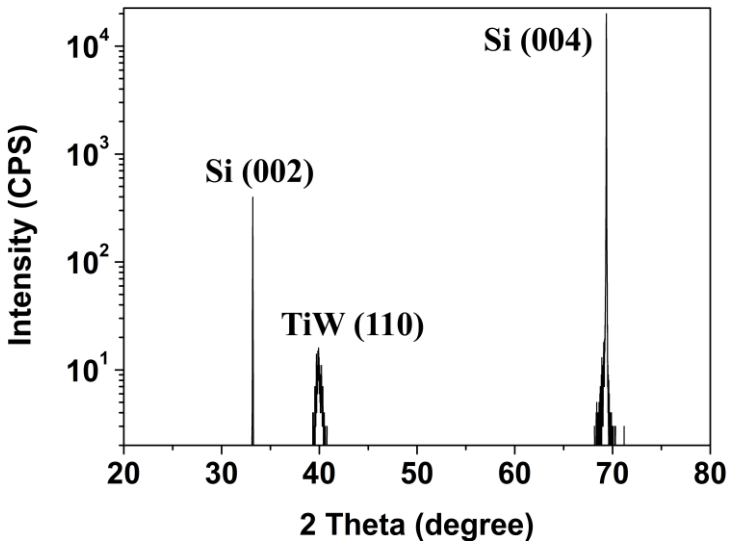

Figure 2.2 XRD pattern of TiW surface.

Figure 2.2 shows the XRD spectra of oxygen plasma cleaned TiW measured in a range of 2θ from 20° to 80°, which reveals the (110) diffraction peak of TiW at 2θ=39.9°[33], [34], [40]. The other two peaks result from the silicon substrate. The XRD diffraction spectrum of TiW is consistent with a body centre cubic (bcc) phase[38], [40]. According to the Bragg's law and standard formula for cubic system[43], [44], as shown in the functions below:

$$2d\,\mathrm{Sin}\theta = \lambda$$

$$\frac{1}{d^2} = \frac{h^2 + l^2 + k^2}{a^2}$$

λ is the wavelength of the incident wave (1.54059 Å), θ is the scattering angle (39.9364°), d is the lattice spacing, (h, k, l) is the (110) plane, the lattice constant (a) of TiW deduced from the XRD pattern is 3.186 Å. According to the XPS results in Table 2.1, the atom ratio of W/Ti is 2.444. After the normalization, the stoichiometric composition of TiW was suggested to be $Ti_{0.29}W_{0.71}$[38], [40].

2.3.2 TiW surface functionalization with organolayers

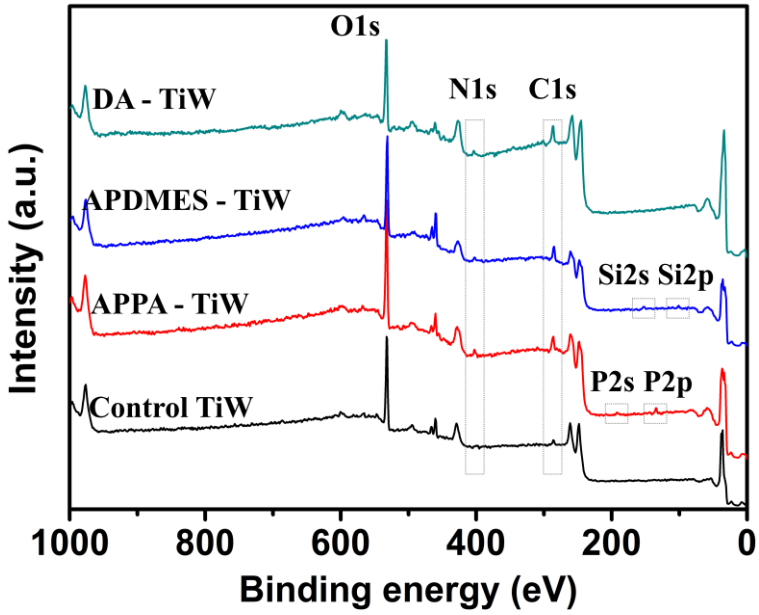

Figure 2.3 XPS survey scans of control TiW, APPA-TiW, APDMES-TiW and DA-TiW.

XPS survey scan spectra of control TiW surface after plasma cleaning and the three organolayers functionalized TiW are shown in Figure 2.3. From the three organolayers coated TiW XPS spectra, APPA-TiW showed distinct N1s (401.0 eV), P2s (190.3 eV) and P2p (133.2 eV) peaks, APDMES-TiW showed distinct N1s (401.0 eV), Si2s (153.3 eV) and Si2p (101.3 eV) peaks, and DA-TiW showed distinct N1s (401.0 eV) in addition to W and Ti core levels. Also, the carbon atomic percentages of three organolayers coated TiW specimens were significantly higher than the control TiW: they are attributed to the successful grafting of DA, APPA and APDMES molecules on TiW. On the control TiW, no P, Si or N were detected. The ratio W/Ti was 2.42 and the oxygen atomic percentage was 65% which is expected considering the stoichiometry of the two oxides and the respective atomic percentage of titanium and tungsten. After surface functionalization, the decrease of Ti, W and O atomic percentages was observed as expected for core levels from a substrate covered by an overlayer. As the ratio W4f/Ti2p remains stable but the O1s/Ti2p increases, part of the oxygen may originate from the organic contamination. This is comforted by the correlated

increase of the C1s atomic percentage. On all functionalized surfaces, a similar N atomic percentage was observed (3-4%). 3.3% of P and 3.6% of Si were measured on APPA-TiW and APDMES-TiW, respectively. The N/P and N/Si ratios (nearly 1) are in good agreement with the chemical structures of two molecules. The chemical compositions of different elements are listed in Table 2.1. For each functionalization type, XPS spectra were measured on two different substrates. One region was analyzed on the first substrate, and two regions were analyzed on the second substrate. After XPS fitting and analysis, the three measurements values were averaged. In this table, uncertainty values for each line indicate the calculated standard deviation for the three regions of the functionalized TiW.

	C1s	O1s	Ti2p	W4f	N1s	P2p	Si2p
	Control and organolayers functionalized TiW						
Control	**9.6 ± 0.8**	**65.6 ± 1.1**	**7.2 ± 0.8**	**17.6 ± 0.8**	**-**	**-**	**-**
APPA-TiW	**33.3 ± 1.0**	**53.2 ± 0.9**	**2.0 ± 0.6**	**4.6 ± 0.6**	**3.6 ± 0.3**	**3.3 ± 0.3**	**-**
APDMES-TiW	**29.8 ± 0.9**	**55.8 ± 0.5**	**2.4 ± 0.7**	**4.8 ± 0.6**	**3.5 ± 0.4**	**-**	**3.6 ± 0.5**
DA-TiW	**38.7 ± 0.5**	**49.9 ± 1.0**	**2.7 ± 0.5**	**5.3 ± 0.6**	**3.3 ± 0.3**	**-**	**-**
	Organolayers functionalized TiW after immersion in 70 °C H_2O for 60 mins						
APPA-TiW	**30.6 ± 0.7**	**57.5 ± 0.6**	**2.5 ± 0.4**	**4.5 ± 0.5**	**2.5 ± 0.2**	**2.4 ± 0.3**	**-**
APDMES-TiW	**22.7 ± 0.6**	**61.1 ± 0.5**	**5.0 ± 0.6**	**10.5 ± 0.7**	**0.3 ± 0.1**	**-**	**0.4 ± 0.1**
DA-TiW	**29.2 ± 0.8**	**58.8 ± 0.9**	**2.8 ± 0.5**	**7.6 ± 0.4**	**1.6 ± 0.2**	**-**	**-**

Table 2.1 XPS determined atomic concentrations (%) of Control and three organolayers functionalized TiW before and after immersion in H_2O at 70 °C.

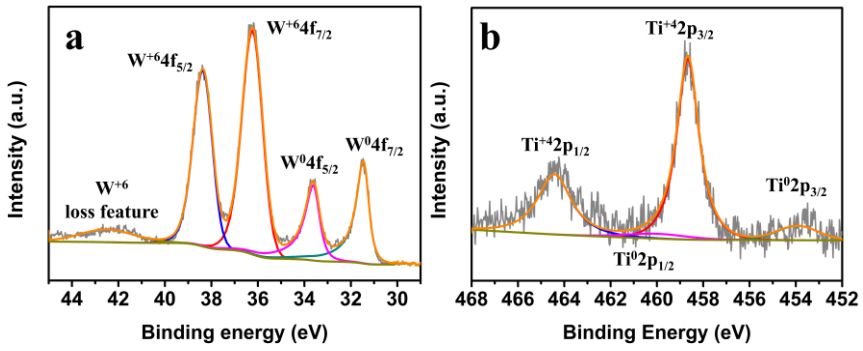

Figure 2.4 High-resolution XPS W4f peak (a) and Ti2p peak (b) of control TiW.

On the control TiW (Figure 2.4a), doublet peaks of $W4f_{7/2}$ and $W4f_{5/2}$ appeared at 31.6 eV and 33.7 eV corresponding to the metallic W state in the high-resolution XPS W4f spectrum. Two well-defined peaks located at 36.1 eV and 38.2 eV were consistent with those of the W^{6+} state

in oxides[45], [46]. In Figure 2.4b, $Ti2p_{3/2}$ and $Ti2p_{1/2}$ with binding energy of 458.6 eV and 464.4 eV correspond to Ti^{4+} state in oxides while two other peaks were merely observed peaks at 453.7 eV and 459.7 eV and corresponded to metallic Ti[47], [48]. Therefore, XPS W4f and Ti2p high resolution spectra revealed that Ti and W oxides are present on the surface of TiW, opening the possibility of using organosilane, organophosphonic acid and ortho-dihydroxyaryl compound for its surface functionalization.

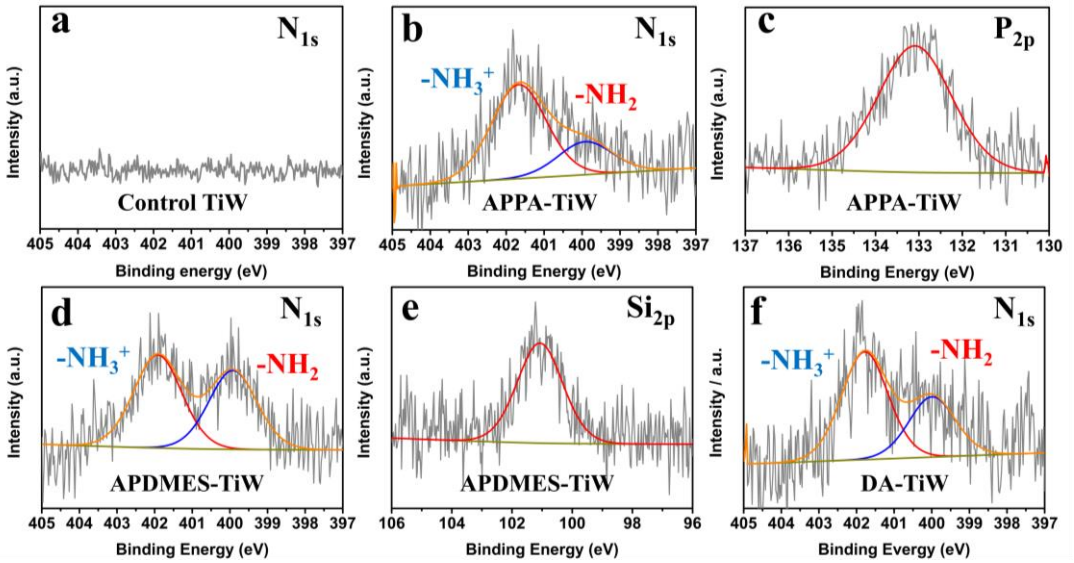

Figure 2.5 (a) High-resolution XPS N1s peak of control TiW. (b) High-resolution XPS N1s peak and (c) P2p peak of APPA-TiW. (d) High-resolution XPS N 1s peak and (e) Si2p peak of APDMES-TiW. (f) High-resolution XPS N1s peak of DA-TiW.

Figure 2.5a showed no N1s peak appeared on the control TiW, P2p and Si2p being not detected. Figure 2.5b and Figure 2.4c showed the high-resolution XPS peaks of N1s and P2p of APPA-TiW surface. Due to the dissymmetry of the N1s, two contributions seem to be present on the high-resolution N1s spectra of APPA-TiW, which were associated with a free amine $-NH_2$ group at 399.8 eV and protonated amine $-NH_3^+$ group at 401.7 eV, respectively[49], [50].

High-resolution XPS spectra of the P2p confirmed phosphonic acid functionalization, the binding energy is considered as a good indicator of the covalent attachment of the phosphonic acid group with TiW moiety. Indeed, in the literatures, it has been reported the evolution of the binding energy of the P2p band is a reliable indicator to evaluate the grafting process of the acids. The P2p peak is centered at 134.1 ± 0.5 eV as expected for the non-deprotonated $–PO_3H_2$ acid[51]–[53]. It is generally accepted that the P2p binding energy of the phosphonic head groups $[PO_n(OH)_m]^x$ depends on the number of O atoms bonded to the P atom and on the n/m ratio. Here, n is the "free" O ligands (as shown in the blue circle) while m is the covalent bound OH ligands (as shown in the red circle). The shift of P2p peak is associated with the deprotonation of the terminal P-OH, which increases the n/m ratio leading to a decrease in the binding energy. In our work, after grafting on TiW, the P2p band is shifted at 133.2 eV. The

shift to a lower binding energy seems to be due to a full or partial deprotonation of terminal P-OH groups upon coordination with the TiW surface and the corresponding formation of a negative charge on the phosphate headgroup. In other words, this shift seems to indicate the presence of the deprotonation, which leads to the occurrence of P-O-TiW bonds. The observed P2p shift of 0.9 eV here is in agreement with typical shifts reported for phosphonic acids on metal oxide surfaces[51]–[53]. The scheme of chemical shift of P2p peak and covalent bonding of APPA on TiW is shown in Figure 2.6.

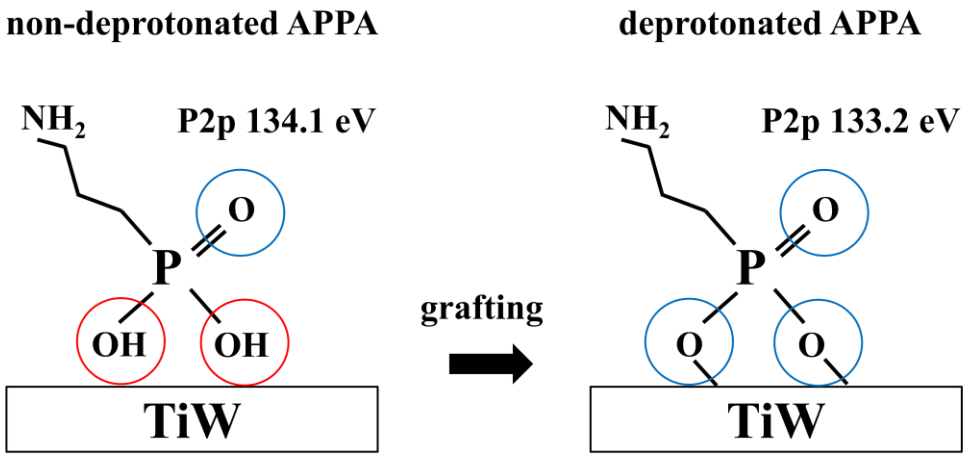

Figure 2.6 The scheme of chemical shift of P2p peak and covalent bonding of APPA on TiW.

From high-resolution N1s spectra of APDMES-TiW, two peaks are observed at 399.7 eV and 401.7 eV (Figure 2.5d). These contributions were again assigned to $-NH_2$ and $-NH_3^+$ groups[49], [50]. From high-resolution Si2p spectra of APDMES-TiW (Figure 2.5e), a Si2p peak was observed at 101.3 eV and assigned to the Si-O linkage of APDMES to the TiW surface. The covalent attachment of a monofunctional organosilane is the result of a single condensation reaction to metal oxide surface. Therefore, the silicon atom of the organosilane is linked with a single oxygen atom and therefore the binding energy is lower than the one measured on silica or multifunctional silanes[49], [54], [55]. The high-resolution N1s XPS spectra of DA-TiW displayed two peaks at a binding energy of about 399.7 eV and 401.7 eV (Figure 2.5f), which are also attributed to the NH_2 and $-NH_3^+$ groups.

It has been reported that the bonding between an amine and a surface bound hydroxyl is much weaker than any other bonding, and rinsing with the solvent easily removes physisorbed molecules[9], [56]. Here we therefore tend to neglect the interaction of the molecule with TiW via the amine with TiW. However, we did not directly verify this possibility. Facing this issue, amine molecules without phosphonic acid, silane or catechol groups could be used such as propylamine ($CH_3CH_2CH_2NH_2$) or 3,3,3-trifluoropropylamine ($CF_3CH_2CH_2NH_2$). CH_3 and CF_3 groups are not active, which would help to verify the interaction between the amine and TiW.

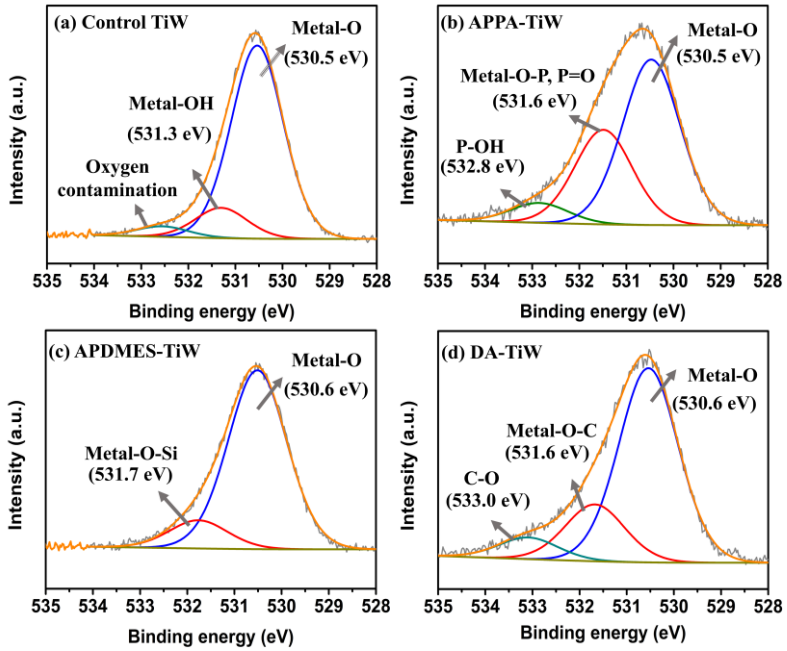

Figure 2.7 High-resolution XPS of O1s components of (a) control TiW, (b) APPA-TiW, (c) APDMES-TiW and (d) DA-TiW.

The high-resolution O1s spectrum of different organolayers coated on metal oxide surface have been reported before. The binding energy of the components depends on the type of organolayers grafted on the surface[10], [32]. Figure 2.7a shows the high-resolution O1s XPS component of the control TiW. The FWHM of the oxygen contribution was set to 1.4 eV due to the metal-O contribution. Such a FWHM imposes at least three O1s peaks for correct fitting (R^2 above 0.969). Ti and W are very different elements, so two contributions are expected for the O1s. However, we decided to deconvolute the O1s with only one contribution. The peak at 530.5 eV was assigned to lattice oxygen from the metal oxides. The peak at 531.3 eV was assigned to the chemisorbed oxygen caused by surface hydroxyl, respectively. The other weak peak at higher binding energy represents the surface oxygen contamination. In addition, it could be seen that the metal-O bonding oxygen was observed for all surfaces after functionalization also. However, in Figure 2.7b, the peak at 531.6 eV was assigned to P-O-metal and P=O. The peaks located at 532.8 eV is ascribed to P-OH species. In our case, the ratio of P=O oxygen contribution over the one of P-OH should be 0.5 for the pure APPA powder. However, after grafting on TiW, the ratio between these two components is increased to 4.8, which results from the transformation of the P-OH bonds into P-O-metal bonds. Thus, we propose that the molecule bonds on the surface via the two deprotonated OH groups while the P=O is not directly bonded to the surface[10], [57], [58]. The O1s XPS spectrum of APDMES-TiW was resolved into only two components (Figure 2.7c). Besides the metal-O bonding oxygen, the peak at 531.7 eV was attributed to oxygen atoms in surface hydroxyl or Si-O-metal species, which is agreement with the other studies[10], [59], [60]. As expected, no O1s peak assigned from Si-O-Si at higher binding energy were observed as we

have used a monovalent silane. In Figure 2.7d, the peak at 531.6 eV was assigned to metal-O-C. The peak located at higher binding energy (533.0 eV) is ascribed to oxygen bonded to aromatic carbon[32], [61]. A variety of binding mode between the catechol molecules and oxide surface have been studied before. Although bidentate mode of attachment was referred to as the stable structure, we proposed that monodentate and bidentate complexes co-exist on the surface because of the free catechol -OH, which a monodentate mode means that only one of catechol-OH moiety is involved to metal atom[62].

ToF-SIMS analysis was also used to characterize three organolayers functionalized TiW with the aim of confirming XPS results thanks to the molecular information brought by the mass detection. However, please note that new samples were specifically prepared, which could explain some lack of consistency between the two sets of surface analysis results. Negative mode spectra (Figure 2.8a-d) indicate first an increase in relative intensity of the nitrogen content for the APPA, APDMES and DA modified TiW compared to the TiW (as displayed by the CN^- peak detected at m/z 26.00, this peak being for the most part related to $C_2H_2^-$ at m/z 26.02 for the control sample).

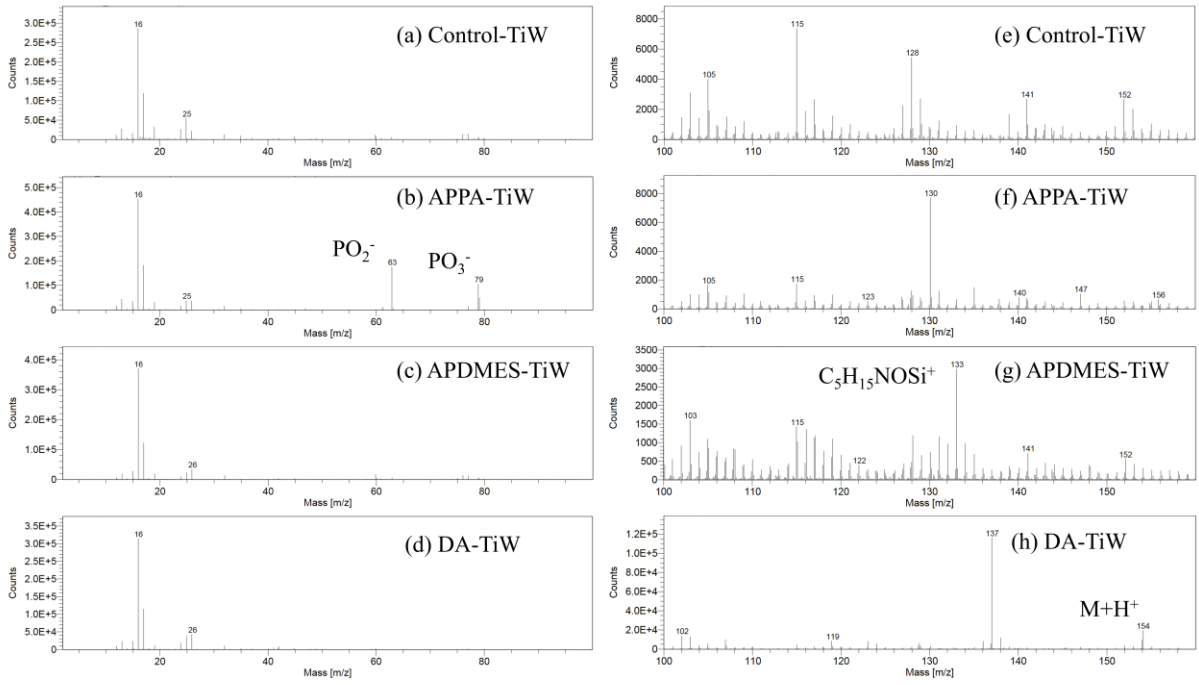

Figure 2.8 Negative mode (a-d) and positive mode (e-h) ToF-SIMS spectra of control TiW, APPA-TiW, APDMES-TiW and DA-TiW in the ranges of m/z 0-100 (negative mode) and m/z 100-160 (positive mode).

A strong relative intensity for the phosphonic acid group characteristic peaks (PO_2^- m/z 62.97 and PO_3^- m/z 78.97) is specifically detected for the APPA-TiW[63]. Positive mode spectra display a strong relative intensity of peaks related to Ti such as peaks at m/z 47.95 and m/z 63.94 for Ti^+ and TiO^+, respectively but also W related peaks (data not displayed). ToF-SIMS is sensitive to the top layers, which indicates that TiW substrate is significantly detected and

thus not fully covered with the intended surface modification. An increase in the relative intensity of the peak at m/z 30 (CH_4N^+) is noticeable (data not shown here). Contamination is also detected such as aromatic peaks at m/z 77.04, 91.05, 105.07, 115.05 etc. corresponding to $C_6H_5^+$, $C_7H_7^+$, $C_8H_9^+$, $C_9H_7^+$, respectively (Figure 2.8e-h). Nitrogen-based contamination has been also detected at the surface of the APPA-TiW sample at m/z 130.15. APDMES and DA molecules information related to the functionalization was more clearly detected in the positive mode. At the surface of APDMES-TiW, peaks were detected at m/z 116.09 ($C_5H_{14}NSi^+$), 133.08 ($C_5H_{15}NOSi^+$). At the surface of DA-TiW, a peak is detected at m/z 154.08 that corresponds to $M+H^+$. Please note that a peak was also detected in the negative mode at m/z 152.06 that corresponds to $M-H^-$ (data not displayed).

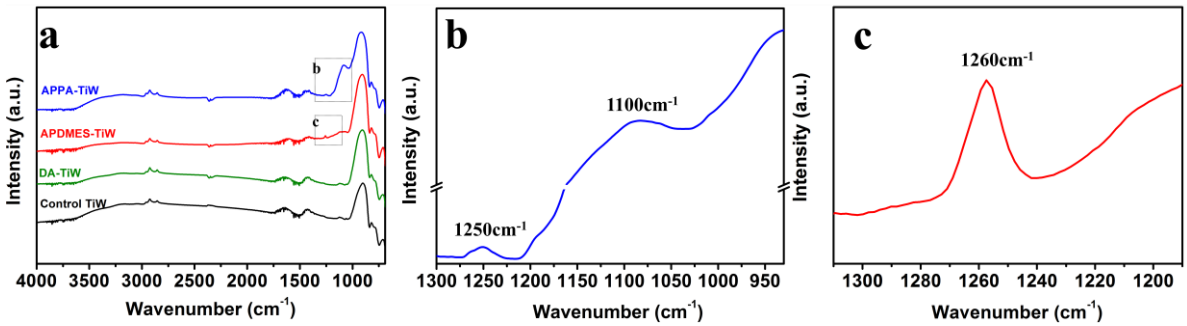

Figure 2.9 (a) ATR-FTIR spectra of control and three organolayers functionalized TiW surface. (c) Enlarged spectrum of the APPA-TiW substrate from 950 cm^{-1} to 1300 cm^{-1}. (c) Enlarged spectrum of the APDMES-TiW substrate from 1300 cm^{-1} to 1200 cm^{-1}.

ATR-FTIR spectra of APDMES-TiW, DA-TiW and APPA-TiW surfaces are presented in Figure 2.9a. It shows intense peaks at 1000 cm^{-1} resulted from the metal oxide stretching vibration mode. For the APPA-TiW substrate, the absorbance peaks at around 1100 cm^{-1} developed which can be assigned to symmetric valence bands of salts of alkylphosphonic groups. The presence of the stretching in the spectrum indicates the deprotonation of the phosphonic acid group. A broad band at 1250 cm^{-1} is assigned to the P=O stretching mode from the free P=O groups of molecules. It also indicated that APPA bonding to TiW surface occurred via the two deprotonated OH groups while the P=O does not directly bond to the surface, which is agreement with other studies reporting that the bonding mode of phosphonate to the metal oxide surfaces occurs via a bidentate bonding (Figure 2.9b)[64], [65]. The intense peak of APDMES-TiW around 1260 cm^{-1} (Figure 2.9c) was attributed to the Si-CH_3 bend from the monovalent molecule and confirmed the presence of APDMES on TiW[66].

It has been reported that dopamine can be oxidized and that it can self-polymerize spontaneously under alkaline conditions (pH > 7.5) with oxygen as the oxidant. To achieve a polydopamine film on substrates, the concentration of dopamine should be higher than 2 mg/ml. When dopamine is added into an alkaline solution, the polymerization of dopamine

immediately occurs, causing a color change from colorless to light brown, and finally turning to deep brown with the reaction time[29], [30]. TiW substrate was also functionalized by polydopamine under the same conditions. Dopamine was dissolved in a Tris-HCl buffer solution (10 mM, pH 8.5) to prepare the dopamine solution (2mg/ml) prior to further functionalization. TiW substrate was immersed in the solution for 24 hours. The surface of the substrate turned deep brown. Then the substrate was rinsed under ultrasound in DI H_2O for 5min, and dried with N_2 flow. The polydopamine modified TiW substrate was measured by XPS and ATR-FTIR, as shown in Figure 2.10.

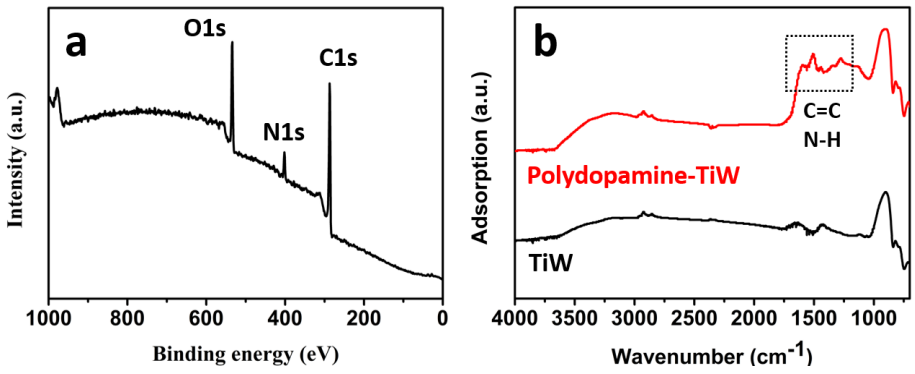

Figure 2.10 (a) XPS survey scan of polydopamine-TiW. (b) ATR-FTIR spectra of control TiW and polydopamine-TiW.

It can be seen that C1s peak increased and N1s peak appeared obviously. However, no Ti and W element peaks can be measured. It seems to indicate that the polydopamine formed a thick film on the TiW substrates. From ATR-FTIR spectra of polydopamine modified TiW substrate the broad absorption bands from 1600 cm^{-1} to 1510 cm^{-1} were attributed to the overlap of the C=C resonance vibration and N-H bending vibration in aromatic rings, which indicated the existence of polydopamine on the TiW surface due to the polymerization. Our goal was to avoid DA polymerization on TiW substrates. The reaction was made under nitrogen atmosphere and the solvent is degassed ultrapure water (pH < 7). The oxidation and polymerization of dopamine could be successfully avoided by limiting the oxidant media and controlling the pH values[31], [32]. From the XPS, IR and ToF-SIMS results, the polydopamine signals were not detected on DA-TiW surface.

2.3.3 Stability of three organolayers

The XPS and ToF-SIMS analysis demonstrated the successful attachment of the three molecules to TiW. Next, we wanted to address the stability of the resulting organolayers. To this aim, modified substrates were immersed in 70°C DI water and XPS atomic (at. %) were determined as a function of immersion time. The change of different elements concentration is also listed in Table 2.1. The ratios of N1s at. % to (Ti2p at. % +W4f at. %) were calculated based on the changes in the elemental concentrations, as shown in the Figure 2.11a. The N1s at. % / (Ti2p at. %+W4f at. %) ratio of APPA-TiW decreased from 0.55 to 0.38 in the first 15

min and then it remained constant for the next 45 min. It also showed that the N1s at. % / (Ti2p at. %+W4f at. %) ratio of DA-TiW decreased continuously from 0.42 to 0.19 up to 60 min. However, the changes in the N1s at. % / (Ti2p at. %+W4f at. %) ratio of APDMES-TiW from 0.47 to 0.02 and then it remained constant for at least of 60 min, which a rapid and significant decrease was observed after 15 min. In Table 2.1, it can be noted that the contributions of the substrate (W at. % and Ti at. %) increased after 60 min immersion from 2.5 to 5 % for Ti at. % and from 5 to 10 % for W at. % suggesting that the contribution of the substrate increased. According to the N1s atomic percentage (at. %), we proposed that approximately 95 % of the APDMES layer is removed after immersion of the sample (reference: APDMES-TiW without immersion). A maximum of 30 % of the APPA layer and 50 % of the DA layer were desorbed as well. (Figure 2.11b). The Si2p at. % / (Ti2p at. % +W4f at. %) ratio for APDMES-TiW and the P2p at. % / (Ti2p at. % +W4f at. %) ratio for APPA-TiW decreased after immersion similarly to the N1s at. % / (Ti2p at. %+W4f at. %) ratio. (Figure 2.11c, d). These observations suggest that the rate and amount of molecules desorbed for APDMES-TiW is the highest. DA-TiW seems slightly less stable than APPA-TiW although the atomic percentage of Ti and W is similar for the two modifications after 60 min immersion.

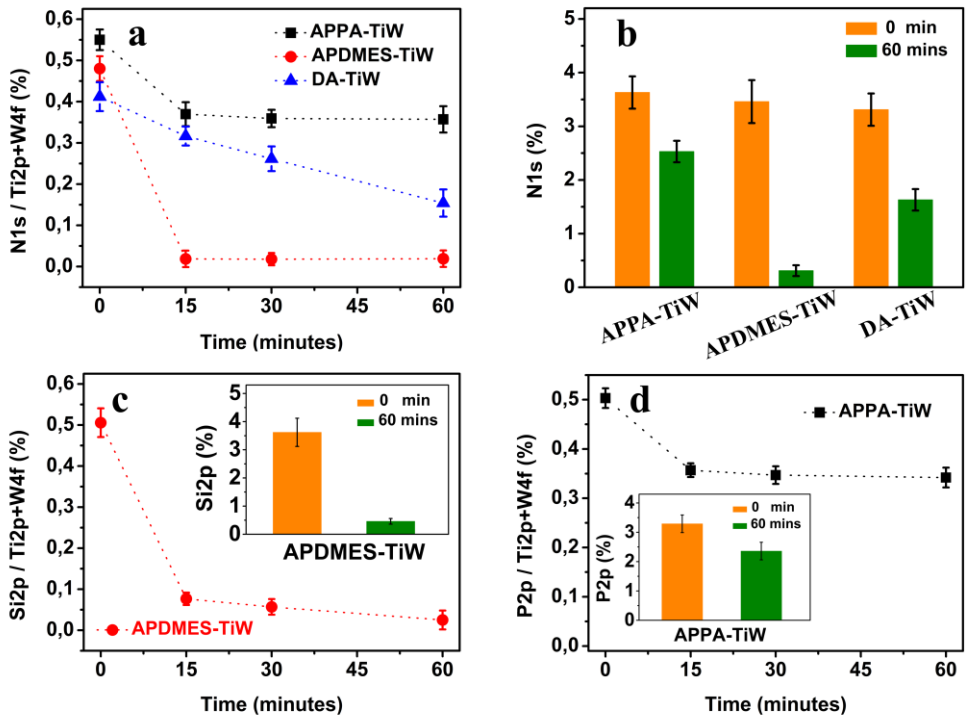

Figure 2.11 (a) N1s at. %/(Ti2p at. %+ W4f at. %) ratio for the APPA- TiW, APDMES-TiW and DA-TiW as a function of immersion time in water at 70°C. (b) N1s atomic percentage (at. %) of APPA-TiW, APDMES-TiW and DA-TiW before and after 60 min immersion in H_2O at 70°C. (c) Si2p at. % / (Ti2p at. % +W4f at. %) ratio of APDMES-TiW in H_2O at 70°C as a function of immersion time. The inset shows the Si2p concentration change. (d) P2p at. % / (Ti2p at. % + W4f at. %) ratio of APPA-TiW DI H_2O at 70°C as a function of immersion time. The inset shows the P2p concentration change.

In some comparative published studies, the stability of different organolayers on metal oxide have been reported. The exact state of bonding responsible for the stability of organolayers on metal oxides is still a matter of debate. It has been claimed that Si-O-Ti is more stable than P-O-Ti[10], [67]. However, M. J. Stevens suggested that the stability was rather in fact due to the lateral crosslinking of multifunctional organosilane[68]. In our case, lateral cross linking was not possible as we have used a monovalent silane. We observed that 95% of the APDMES layer was removed after 15 min of immersion time in 70 °C H_2O suggesting that the Si-O-Ti or Si-O-W bonds are some-how labile and that the stability reported by several authors may rather be due to lateral cross linking. Different phosphonate layers on indium–tin oxide, cobalt chromium alloys and aluminum surfaces were found to be stable and strongly bound[69]–[74]. In addition, it has been showed that tungsten oxide surface can react with phosphonate molecules to form the covalently attach tethered by phosphonate linkers. And the P-O bonds (3.5 eV/bond) on tungsten/tungsten oxide seems to be twice as strong as S-Au attachments (1.7 eV/bond)[27]. Here the rate and amount of molecules desorbed for APPA-TiW are lower compared to the other two layers which maybe resulted from the stronger P-O-Ti and P-O-W covalent bonds. For DA layer, we proposed that monodentate and bidentate complexes of catechol co-exist on the surface. In the literature, the bidentate attachment is considered more stable than the monodendate complex. It may well be that after immersion in 70 °C H_2O, the relatively unstable monodentate complexes may desorbed from the surface continuously[32], [62], [75].

2.4 Conclusions

We developed three different organolayers on TiW, which has been analyzed by XPS, ToF-SIMS and IR. Firstly, XPS, IR and ToF-SIMS spectroscopy seem to sustain the formation of a covalent attachment between APPA and TiW. Similarly, the bonding of APDMES layer seems to occur through the covalent bonds between the monovalent silane and oxide. Our results tend to indicate that DA binding on TiW leads to monodentate and bidentate configurations grafting. Secondly, the stability of three organolayers on TiW was also investigated. Based on XPS, the good stability of APPA layer is mainly attributed to stronger P-O-W and P-O-Ti covalent bonds, stability of DA layer on TiW was inferior to the stability of APPA layer probably because of the instability of monodentate mode. Extensive desorption of APDMES molecules occurred within 15 min of immersion in 70 °C water due to the lack of lateral cross linking in the layer. As a novel functional metal oxide, quite good stability of phosphonic acid organolayer functionalized TiW has important significance in terms of further functionalization and integrated multi-materials patterned substrate devices.

2.5 Reference

[1] X. Zhou, F. Boey, F. Huo, L. Huang, H. Zhang. Chemically functionalized surface patterning. *Small*, **2011**, *7*, 2273–2289.

[2] Y. Liang, K. L. Kiick. Heparin-functionalized polymeric biomaterials in tissue engineering and drug delivery applications. *Acta Biomater.*, **2014**, *10*, 1588–1600.

[3] J. Liu, Y. Lu. Adenosine-dependent assembly of aptazyme-functionalized gold nanoparticles and its application as a colorimetric biosensor. *Anal. Chem.*, **2004**, *76*, 1627–1632.

[4] I. Jerman, A. Š. Vuk, M. Koželj, B. Orel, J. Kovač. A structural and corrosion study of triethoxysilyl functionalized POSS coatings on AA 2024 Alloy. *Langmuir*, **2008**, *24*, 5029–5037.

[5] J. C. Love, L. A. Estroff, J. K. Kriebel, R. G. Nuzzo, G. M. Whitesides. Self-assembled monolayers of thiolates on metals as a form of nanotechnology. *Chem. Rev.*, **2005**, *105*, 1103–1170.

[6] L. Strong, G. M. Whitesides. Structures of self-assembled monolayer films of organosulfur compounds adsorbed on gold single crystals: electron diffraction studies. *Langmuir*, **1988**, *4*, 546–558.

[7] D. F. S. Petri, G. Wenz, P. Schunk, T. Schimmel. An improved method for the assembly of amino-terminated monolayers on SiO_2 and the vapor deposition of gold layers. *Langmuir*, **1999**, *15*, 4520–4523.

[8] Y. Wang, M. Lieberman. Growth of ultrasmooth octadecyltrichlorosilane self-assembled monolayers on SiO_2. *Langmuir*, **2003**, *19*, 1159–1167.

[9] S. P. Pujari, L. Scheres, A. T. M. Marcelis, H. Zuilhof. Covalent surface modification of oxide surfaces. *Angew. Chem. Int. Ed.*, **2014**, *53*, 6322–6356.

[10] G. Mani, D. M. Johnson, D. Marton, V. L. Dougherty, M. D. Feldman, D. Patel, A. A. Ayon, C. M. Agrawal. Stability of self-assembled monolayers on titanium and gold. *Langmuir*, **2008**, *24*, 6774–6784.

[11] M. Pantoja, B. Díaz-Benito, F. Velasco, J. Abenojar, J. C. Real. Analysis of hydrolysis process of γ-methacryloxypropyltrimethoxysilane and its influence on the formation of silane coatings on 6063 aluminum alloy. *Appl. Surf. Sci.*, **2009**, *255*, 6386–6390.

[12] L. Pang, L. Zhong, H. Zhou, X. Wu, X. Chen. Grafting of ionic liquids on stainless steel surface for antibacterial application. *Colloids Surf. B Biointerfaces*, **2015**, *126*, 162–168.

[13] M. P. Q. Argañaraz, J. M. Ramallo-López, G. Benítez, A. Rubert, E. D. Prieto, L. M. Gassa, R. C. Salvarezzaa, M. E. Vela. Optimization of the surface properties of nanostructured Ni–W alloys on steel by a mixed silane layer. *Phys. Chem. Chem. Phys.*, **2015**, *17*, 14201–14207.

[14] C. P. Tripp, M. L. Hair. Reaction of methylsilanols with hydrated silica surfaces: the hydrolysis of trichloro-, dichloro-, and monochloromethylsilanes and the effects of curing. *Langmuir*, **1995**, *11*, 149–155.

[15] K. D. Lork, K. K. Unger, J. N. Kinkel. Role of the functional group in n-octydimethylsilanes in the synthesis of C8 reversed-phase silica packings for high-performance liquid chromatography. *J. Chromatogr. A*, **1986**, *352*, 199–211.

[16] A. Glaser, J. Foisner, H. Hoffmann, G. Friedbacher. Investigation of the role of the interplay between water and temperature on the growth of alkylsiloxane submonolayers on silicon. *Langmuir*, **2004**, *20*, 5599–5604.

[17] M. E. McGovern, K. M. R. Kallury, M. Thompson. Role of solvent on the silanization of glass with octadecyltrichlorosilane. *Langmuir*, **1994**, *10*, 3607–3614.

[18] D. L. Angst, G. W. Simmons. Moisture absorption characteristics of organosiloxane self-assembled monolayers. *Langmuir*, **1991**, *7*, 2236–2242.

[19] V. Dugas, C. Demesmay, Y. Chevolot, É. Souteyrand. *Use of organosilanes in biosensors*. *Nova Science Pub Inc; UK ed. edition*, **2010**, 978-1616680299.

[20] P. G. Mingalyov, G. V. Lisichkin. Chemical modification of oxide surfaces with organophosphorus(V) acids and their esters," *Russ. Chem. Rev.*, 2006, 75, 541–557.

[21] M. Giza, P. Thissen, G. Grundmeier. Adsorption kinetics of organophosphonic acids on plasma-modified oxide-covered aluminum surfaces. *Langmuir*, **2008**, *24*, 8688–8694.

[22] S. Mohapatra, P. Pramanik. Synthesis and stability of functionalized iron oxide nanoparticles using organophosphorus coupling agents. *Colloids Surf. Physicochem. Eng. Asp.*, **2009**, *339*, 35–42.

[23] F. Li, J. D. Fabbri, R. I. Yurchenko, A. N. Mileshkin, J. N. Hohman, H. Yan, H. Yuan, I. C. Tran, T. M. Willey, M. Bagge-Hansen, J. E. P. Dahl, R. M. K. Carlson, A. A. Fokin, P. R. Schreiner, Z. Shen, N. A. Melosh. Covalent attachment of diamondoid phosphonic acid dichlorides to tungsten oxide surfaces. *Langmuir*, **2013**, *29*, 9790–9797.

[24] C. Queffélec, M. Petit, P. Janvier, D. A. Knight, B. Bujoli. Surface modification using phosphonic acids and esters. *Chem. Rev.*, **2012**, *112*, 3777–3807.

[25] E. L. Hanson, J. Schwartz, B. Nickel, N. Koch, M. F. Danisman. Bonding self-assembled, compact organophosphonate monolayers to the native oxide surface of silicon. *J. Am. Chem. Soc.*, **2003**, *125*, 16074–16080.

[26] A. Vega, P. Thissen, Y. J. Chabal. Environment-controlled tethering by aggregation and growth of phosphonic acid monolayers on silicon oxide. *Langmuir*, **2012**, *28*, 8046–8051.

[27] M. Dubey, T. Weidner, L. J. Gamble, D. G. Castner. Structure and order of phosphonic acid-based self-assembled monolayers on Si (100). *Langmuir*, **2010**, *26*, 14747–14754.

[28] S. P. Pujari, Y. Li, R. Regeling, H. Zuilhof. Tribology and stability of organic monolayers on CrN: a comparison among silane, phosphonate, alkene, and alkyne chemistries. *Langmuir*, **2013**, *29*, 10405–10415.

[29] Q. Ye, F. Zhou, W. Liu. Bioinspired catecholic chemistry for surface modification. *Chem. Soc. Rev.*, **2011**, *40*, 4244–4258.

[30] Y. Liu, K. Ai, L. Lu. Polydopamine and its derivative materials: synthesis and promising applications in energy, environmental, and biomedical fields. *Chem. Rev.*, **2014**, *114*, 5057–5115.

[31] Y. Liu, B. Yu, J. Hao, F. Zhou. Amination of surfaces via self-assembly of dopamine. *J. Colloid Interface Sci.*, **2011**, *362*, 127–134.

[32] M. Rodenstein, S. Zürcher, S. G. P. Tosatti, N. D. Spencer. Fabricating chemical gradients on oxide surfaces by means of fluorinated, catechol-based, self-assembled monolayers. *Langmuir*, **2010**, *26*, 16211–16220.

[33] C. K. Wang, S. J. Chang, Y. K. Su, C. S. Chang, Y. Z. Chiou, C. H. Kuo, T. K. Lin, T. K. Ko, J. J. Tang. GaN MSM photodetectors with TiW transparent electrodes. *Mater. Sci. Eng. B*, **2004**, *112*, 25–29.

[34] H. C. Chiua, C. H. Chen, C. W. Yang, H. L. Kao, F. H. Huang, S. W. Peng. Highly thermally stable in situ SiN_X passivation AlGaN/GaN enhancement-mode high electron mobility transistors using TiW refractory gate structure. *J. Vac. Sci. Technol. B*, **2013**, *31*, 051212 1-4.

[35] A. Roshanghias, G. Khatibi, R. Pelzer, J. Steinbrenner. On the effects of thickness on adhesion of TiW diffusion barrier coatings in silicon integrated circuits. *Surf. Coat. Technol.*, **2014**, *259*, 386–392.

[36] F. Battegay, M. Fourel, Barrier material selection for TSV last, flipchip & 3D-UBM & RDL integrations. *ECTC*, **2015**, 1183–1192.

[37] S. K. Bhagat, N. D. Theodore, T. L. Alford. Thermal stability of tungsten–titanium diffusion barriers for silver metallization. *Thin Solid Films*, **2008**, *516*, 7451–7457.

[38] J. L. Alay, H. Bender, G. Brijs, A. Demesmaeker, W. Vandervorst. Quantitative analysis of W(N), TiW and TiW(N) matrices using XPS, AES, RBS, EPMA and XRD. *Surf Interface Anal.*, **1991**, *17*, 373–382.

[39] S. Wang, S. Suthar, C. Hoeflich, B. Burrow. Diffusion barrier properties of TiW between Si and Cu. *J. Appl. Phys.* **1993**, *73*, 2301–2320.

[40] J. C. Chiou, M. C. Chen. Thermal stability of $Cu/CoSi_2$ contacted p^+n shallow junction with and without TiW diffusion barrier. *J. Electrochem. Soc.*, **1994**, *141*, 2804–2810.

[41] J. C. Chiou, K. C. Juang, M. C. Chen. TiW (N) as diffusion barriers between Cu and Si. *J. Electrochem. Soc*., **1995**, *142*, 2326–2331.

[42] L. M. Bishop, J. C. Yeager, X. Chen, J. N. Wheeler, M. D. Torelli, M. C. Benson, S. D. Burke, J. A. Pedersen, R. J. Hamers. A citric acid-derived ligand for modular functionalization of metal oxide surfaces via 'click' chemistry. *Langmuir*, **2012**, *28*, 1322–1329.

[43] B. E. Warren. X-ray Diffraction. *Courier Corporation*, **1990**.

[44] J. A. Nielsen, D. McMorrow. Elements of Modern X-ray Physics. *John Wiley & Sons*, **2011**.

[45] S. Xu, L. Diao. Study of tungsten oxidation in $O_2/H_2/N_2$ downstream plasma. *J. Vac. Sci. Technol. A*, **2008**, *26*, 360–364.

[46] F. Y. Xie, L. Gong, X. Liu, Y. T. Tao, W. H. Zhang, S. H. Chen, H. Meng, J. Chen. XPS studies on surface reduction of tungsten oxide nanowire film by Ar^+ bombardment. *J. Electron Spectrosc. Relat. Phenom.*, **2012**, *185*, 112–118.

[47] U. Vogel, E. Brachmann, S. Oswald, S. Menzel, T. Gemming, J. Eckert. Evaluation of a mobile vacuum transfer system for in vacuo XPS analysis using as-deposited Ti thin-films. *Vacuum*, **2015**, *117*, 81–84.

[48] F. Riboni, L. G. Bettini, D. W. Bahnemann, E. Selli. WO_3–TiO_2 vs. TiO_2 photocatalysts: effect of the W precursor and amount on the photocatalytic activity of mixed oxides. *Catal. Today*, **2013**, *209*, 28–34.

[49] Z. Yang, Y. Chevolot, T. Géhin, V. Dugas, N. Xanthopoulos, V. Laporte, T. Delair, Y. Ataman-Önal, G. Choquet-Kastylevsky, É. Souteyrand, E. Laurencea. Characterization of three amino-functionalized surfaces and evaluation of antibody immobilization for the multiplex detection of tumor markers involved in colorectal cancer. *Langmuir*, **2013**, *29*, 1498–1509.

[50] S. Noel, B. Liberelle, L. Robitaille, G. De Crescenzo. Quantification of primary amine groups available for subsequent biofunctionalization of polymer surfaces. *Bioconjug. Chem.*, **2011**, *22*, 1690–1699.

[51] D. Bonvin, J. a. M. Bastiaansen, M. Stuber, H. Hofmann, M. M. Ebersold. ATP and NADPH coated iron oxide nanoparticles for targeting of highly metabolic tumor cells. *J. Mater. Chem. B*, **2017**, *5*, 8353–8365.

[52] C. Tudisco, V. Oliveri, M. Cantarella, G. Vecchio, G. G. Condorelli. Cyclodextrin anchoring on magnetic Fe_3O_4 nanoparticles modified with phosphonic linkers. *Eur. J. Inorg. Chem.*, **2012**, *2012*, 5323–5331.

[53] M. Textor, L. Ruiz, R. Hofer, A. Rossi, K. Feldman, G. Hähner, N. D. Spencer. Structural chemistry of self-assembled monolayers of octadecylphosphoric acid on tantalum oxide surfaces. *Langmuir*, **2000**, *16*, 3257–3271.

[54] R. Bai, L. Xue, R. Dou, S. Meng, C. Xie, Q. Zhang, T. Guo, T. Meng. Light-triggered release from pickering emulsions stabilized by TiO_2 nanoparticles with tailored wettability. *Langmuir*, **2016**, *32*, 9254–9264.

[55] M. R. Alexander, R. D. Short, F. R. Jones, W. Michaeli, C. J. Blomfield. A study of HMDSO/O_2 plasma deposits using a high-sensitivity and -energy resolution XPS instrument: curve fitting of the Si2p core level. *Appl. Surf. Sci.*, **1999**, *137*, 179–183.

[56] J. J. Benítez, S. Kopta, D. F. Ogletree, M. Salmeron. Preparation and characterization of self-assembled monolayers of octadecylamine on mica using hydrophobic solvents. *Langmuir*, **2002**, *18*, 6096–6100.

[57] N. Adden, L. J. Gamble, D. G. Castner, A. Hoffmann, G. Gross, H. Menzel. Phosphonic acid monolayers for binding of bioactive molecules to titanium surfaces. *Langmuir*, **2006**, *22*, 8197–8204.

[58] G. Zorn, I. Gotman, E. Y. Gutmanas, R. Adadi, G. Salitra, C. N. Sukenik. Surface modification of Ti45Nb alloy with an alkylphosphonic acid self-assembled monolayer. *Chem. Mater.*, **2005**, *17*, 4218–4226.

[59] R. D. Palma, W. Laureyn, F. Frederix, K. Bonroy, J. J. Pireaux, G. Borghs, G. Maes. Formation of dense self-assembled monolayers of (n-Decyl)trichlorosilanes on Ta/Ta_2O_5. *Langmuir*, **2007**, *23*, 443–451.

[60] W. Laureyn, D. Nelis, P. V. Gerwen, K. Baert, L. Hermans, R. Magnée, J. J. Pireaux, G. Maesc. Nanoscaled interdigitated titanium electrodes for impedimetric biosensing. *Sens. Actuators B Chem.*, **2000**, *68*, 360–370.

[61] A. Ganguly, S. Sharma, P. Papakonstantinou, J. Hamilton. Probing the thermal deoxygenation of graphene oxide using high-resolution in situ X-ray-based spectroscopies. *J. Phys. Chem. C*, **2011**, *115*, 17009–17019.

[62] Y. Yang, W. Yan, C. Jing. Dynamic adsorption of catechol at the goethite/aqueous solution interface: a molecular-scale study. *Langmuir*, **2012**, *28*, 14588–14597.

[63] K. Wapner, M. Stratmann, G. Grundmeier. Structure and stability of adhesion promoting aminopropyl phosphonate layers at polymer/aluminium oxide interfaces. *Int. J. Adhes. Adhes.*, **2008**, *28*, 59–70.

[64] L. Sang, K. M. Knesting, A. Bulusu, A. K. Sigdel, A. J. Giordano, S. R. Marder, J. J. Berry, S. Graham, D. S. Ginger, J. E. Pemberton. Effect of time and deposition method on quality of phosphonic acid modifier self-assembled monolayers on indium zinc oxide. *Appl. Surf. Sci.*, **2016**, *389*, 190–198.

[65] R. C. Longo, K. Cho, W. G. Schmidt, Y. J. Chabal, P. Thissen. Monolayer doping via phosphonic acid grafting on silicon: microscopic insight from infrared spectroscopy and density functional theory calculations. *Adv. Funct. Mater.*, **2013**, *23*, 3471–3477.

[66] L. D. White, C. P. Tripp. Reaction of (3-aminopropyl)dimethylethoxysilane with amine catalysts on silica surfaces. *J. Colloid Interface Sci.*, **2000**, *232*, 400–407.

[67] G. Philippin, J. Delhalle, Z. Mekhalif. Comparative study of the monolayers of $CH_3(CH_2)_nSiCl_3$ and $CH_3(CH_2)_nPO(OH)_2$, n=4 and 13, adsorbed on polycrystalline titanium substrates. *Appl. Surf. Sci.*, **2003**, *212–213*, 530–536.

[68] M. J. Stevens. Thoughts on the structure of alkylsilane monolayers. *Langmuir*, **1999**, *15*, 2773–2778.

[69] A. Kanta, R. Sedev, J. Ralston. The formation and stability of self-assembled monolayers of octadecylphosphonic acid on titania. *Colloids Surf. Physicochem. Eng. Asp.*, **2006**, *291*, 51–58.

[70] K. Jo, H. Yang. Comparative study of stability of phosphonate self-assembled monolayers on indium–tin oxide electrodes prepared using different methods. *J Electroanal Chem*, **2014**, *712*, 8–13.

[71] K. Jo, H. Yu, H. Yang. Formation kinetics and stability of phosphonate self-assembled monolayers on indium–tin oxide. *Electrochimica Acta*, **2011**, *56*, 4828–4833.

[72] R. Bhure, A. Mahapatro, C. Bonner, T. M. Abdel-Fattah. In vitro stability study of organophosphonic self assembled monolayers (SAMs) on cobalt chromium (Co–Cr) alloy. *Mater. Sci. Eng. C*, **2013**, *33*, 2050–2058.

[73] R. Bhure, T. M. Abdel-Fattah, C. Bonner, F. Hall, A. Mahapatro. Stability of phosphonic self assembled monolayers (SAMs) on cobalt chromium (Co–Cr) alloy under oxidative conditions. *Appl. Surf. Sci.*, **2011**, *257*, 5605–5612.

[74] P. Thissen, M. Valtiner, G. Grundmeier. Stability of phosphonic acid self-assembled monolayers on amorphous and single-crystalline aluminum oxide surfaces in aqueous solution. *Langmuir*, **2010**, *26*, 156–164.

[75] T. H. Anderson, J. Yu, A. Estrada, M. U. Hammer, J. H. Waite, J. N. Israelachvili. The contribution of DOPA to substrate–peptide adhesion and internal cohesion of mussel-inspired synthetic peptide films. *Adv. Funct. Mater.*, **2010**, *20*, 4196–4205.

Chapter 3

Orthogonal chemical functionalization of patterned Au/TiW substrate for selective immobilization of nanoparticles

3 Orthogonal chemical functionalization of patterned Au/TiW substrate for selective immobilization of nanoparticles

3.1 Introduction

Orthogonal self-assembly of different molecules onto patterned substrates was first proposed in 1989. It offered a versatile method for controlling the interfacial properties of multi-material pattern substrates[1], [2]. Orthogonal chemical functionalization is based on organic molecules bearing different anchoring groups that will react selectively with different materials on the patterned substrates[3]–[5]. If molecules used for orthogonal functionalization are truly selective for each material, it offers the perspective of controlling and modifying the characteristics of each material surfaces and incorporating new functionalities on defined nanofabricated devices. For example, the selective binding of colloids or biomolecules onto an array of predefined regions was achieved by the orthogonal functionalization of each materials of the surface[6]–[14].

Different combinations of chemical compounds and inorganic substrates have been used in such surface functionalization protocols, such as metal oxide/SiO_2[4], [15], Au/metal oxide[1], [16], [17] or Au/SiO_2[5], [10], [18]–[20] templates selectively functionalized with thiols, silanes, phosphonic acids or carboxylic acids.

Among various potential inorganic materials, TiW is well mastered in electronic industry, where it is used as an effective diffusion barrier[21]–[29]. TiW is implemented in nanoelectronic devices on an industrial scale, with a very high control on its characteristics. In this perspective, TiW could be used in chemical sensors or biosensors, either (1) as core material for nanotransducing zone (e.g. in nanoelectronic chemical sensors), or (2) for covering surfaces outside of nanotransducing zone. In the case (1), TiW has to be functionalized with molecular probes. It has already been shown that TiW can be modified with small organic molecules by surface functionalization in chapter 2. The study has for instance demonstrated good stability of phosphonic acid organolayers on TiW. In case (2) TiW could be functionalized with a passivation layer repelling molecules to be detected, as already presented by F. Palazon et al[10]. In this approach, it would be useful to functionalize differently the transducing zone (e.g. Au or SiO_2) and the TiW zone. Orthogonal functionalization of a substrate including TiW and another material should therefore be studied.

In this work, we present orthogonal chemical functionalization of Au patterns on TiW, as a first practical assay involving TiW and another material. Thiol based chemistry and

phosphonic acid based chemistry were used for the selective derivatization of Au and TiW, respectively. Orthogonal chemical functionalization was verified by direct characterization using X-ray photoelectron spectroscopy (XPS), polarization modulation infrared reflection absorption spectroscopy (PM-IRRAS) and time-of-flight secondary ion mass spectrometry (ToF-SIMS) mapping. Then Au/TiW patterned substrates were functionalized with mercapto-undecamine. Thanks to the orthogonality of thiol/Au versus phosphonic acid/TiW reactions, only the gold features were modified leading to amine derivatized surface. It allowed localizing carboxy-functionalized nanoparticles by electrostatic interaction on gold with a selectivity above 10 compared to TiW.

3.2 Experimental section

3.2.1 Materials and patterns

Chemicals are of reagent grade commercially available. 1H,1H,2H,2H-Perfluorodecanethiol (F-thiol) 97% was purchased from Sigma-Aldrich. 1H,1H,2H,2H-(Tridecafluorooct-1-yl)phosphonic acid (F-phosphonic acid) was purchased from SiKÉMIA. Dichloromethane (DCM) 99.9% was purchased from Sigma-Aldrich then degassed and dried over molecular sieves. Isopropanol 99.9% was purchased from Fluka. 11-mercapto-1-undecylamine (MUAM) 99% and ethanol 99.8% were purchased from Sigma-Aldrich. Carboxylatex particles (300 nm diameter, 3% solids, product code: 02131) were purchased from Ademtech. Ultrapure water (18.2 MΩ) used for all the experiments was obtained by VEOLIA water system.

Macroscale patterned Au/TiW substrates S1 and S2 were prepared using the following protocol: the surfaces consisted of a 2 cm^2 TiW substrate onto which half of the surface was covered by gold thin film (5 nm chromium and 200 nm gold).

Microscale patterned Au/TiW substrates S3, S4 and S5 were prepared using UV lithography process to define squares with typical dimensions ranging from 100 µm to 600 µm. Chromium (5 nm) and gold (50 nm) were deposited by electron beam evaporation.

After lift-off, the samples were cleaned by oxygen plasma treatment (HARRICK) at the oxygen flow rate of 14 mL/min, RF power level of 38 W for 5 min to ensure that no residual resist remained on the surface. The patterned substrates pictures are shown in Figure 3.1. The UV lithography process and materials deposition conditions are shown in Annex B.

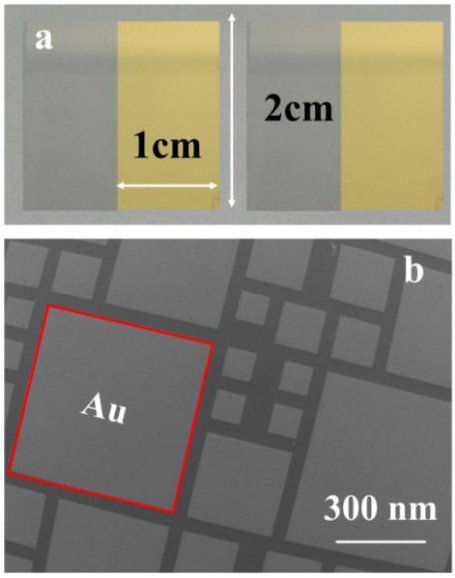

Figure 3.1 Optical photos of macropatterned substrates S1 and S2 (a). SEM image of microscale patterned substrates S3, S4 and S5 (b).

3.2.2 Chemical functionalization

Patterned substrates S1 and S3 were functionalized by F-thiol using the following protocol: substrates were immersed in 25 ml dried DCM containing 100 µl F-thiol (14 mM) for 48 hours. Then the samples were rinsed with DCM for 5 min under ultrasound (Branson, 42 kHz, 100 W) followed by a stream of ultrapure water and dried with nitrogen flow.

Patterned substrates S2 and S4 were functionalized by F-phosphonic acid using the following protocol: substrates were immersed in 20 ml ultrapure water containing 8.5 mg F-phosphonic acid (1 mM) for 16 hours. The substrates were then rinsed with isopropanol for 5 min under ultrasound (Branson, 42 kHz, 100 W) followed by a stream of ultrapure water and dried with nitrogen flow.

Patterned substrates S5 were functionalized by MUAM using the following protocol: substrates were immersed in a previously degassed 1 mM ethanolic solution of MUAM for 4 hours and then rinsed 5 min in ethanol under sonication (Branson, 42 kHz, 100 W) to remove potentially adsorbed multilayers, followed by 5 min rinse in ultrapure water and then dried under nitrogen flow.

Nanoparticles trapping: 20 µL of carboxylate-functionalized nanoparticles solution were dissolved in 2 ml of PBS-1X adjusted to pH 7.4 in a centrifuge tube. The S5 substrates functionalized by MUAM were maintained vertically in the centrifuge tube fully immersed in the nanoparticles solution without agitation at room temperature. No sedimentation of colloidal dispersions was observed overnight. The immobilized S5 samples were rinsed twice with ultrapure water and dried under nitrogen. A control sample without functionalization was

immersed in a solution of carboxylate-functionalized nanoparticles overnight and rinsed in the same way.

3.2.3 Characterization

X-ray Photoelectron Spectroscopy (XPS). XPS measurements on macropatterned substrates S1 and S2 were performed using a focused monochromatized X-ray source (Al Kα 1486.6 eV). Spectrum acquisitions were performed under ultrahigh vacuum conditions (UHV, 10^{-9} Torr). Take-off angle was 90° relative to the substrate surface. The pass energies were 100 eV and 20 eV for wide-scan and high-resolution elemental scans, respectively. The data reduction was performed with CasaXPS software. The dimensions of TiW and Au patterns were largely higher than XPS beam, so that each material of a same substrate could be characterized individually. For each substrate, at least three measurements were performed on different locations of a same material, thus providing triplicate quantitative data for respectively TiW and Au of the same substrate.

Polarization-modulation infrared reflection absorption spectroscopy (PM-IRRAS). PM-IRRAS spectra was recorded on macroscopic substrates S1 and S2 using a Nicolet 6700 FTIR spectrometer from Thermo Scientific coupled to a Hinds Instrument PEM-100 ZnSe photoelastic modulator driven at 50 kHz (polarization switch from p to s at 100 kHz). The acquisition and spectra analysis parameters, as well as theoretical elements about PM-IRRAS have been detailed elsewhere. The dimensions of TiW and Au macropatterns were largely higher than IR beam, so that each material of a same substrate could be characterized individually.

Time-of-flight secondary ion mass spectrometry (ToF-SIMS). ToF-SIMS mapping measurements were performed on micropatterned substrates S3 and S4 with a Physical Electronics TRIFT III instrument (Physical Electronics, Chanhassen, MN) operated with a pulsed Au ion gun (ion current of 2 nA) over a 300 μm × 300 μm area. The ion dose was kept below the static conditions limits. Data were analyzed using WinCadence software. Mass calibration was performed on hydrocarbon secondary ions. For each substrate, at least three measurements were performed on different locations, thus providing triplicate quantitative data and images.

Scanning Electron Microscopy (SEM). SEM images were performed on micropatterned substrates S5 before and after nanoparticles trapping with a Mira3 SEM from TESCAN. It was operated with an acceleration tension of 5 kV, a current beam of 250 μA with a detection of secondary electrons. SEM image analysis with ImageJ software allowed us to compute quantitative data. At least three measurements were performed on different locations, thus providing triplicate quantitative images.

3.3 Results and discussion

3.3.1 Orthogonality of macroscale substrates

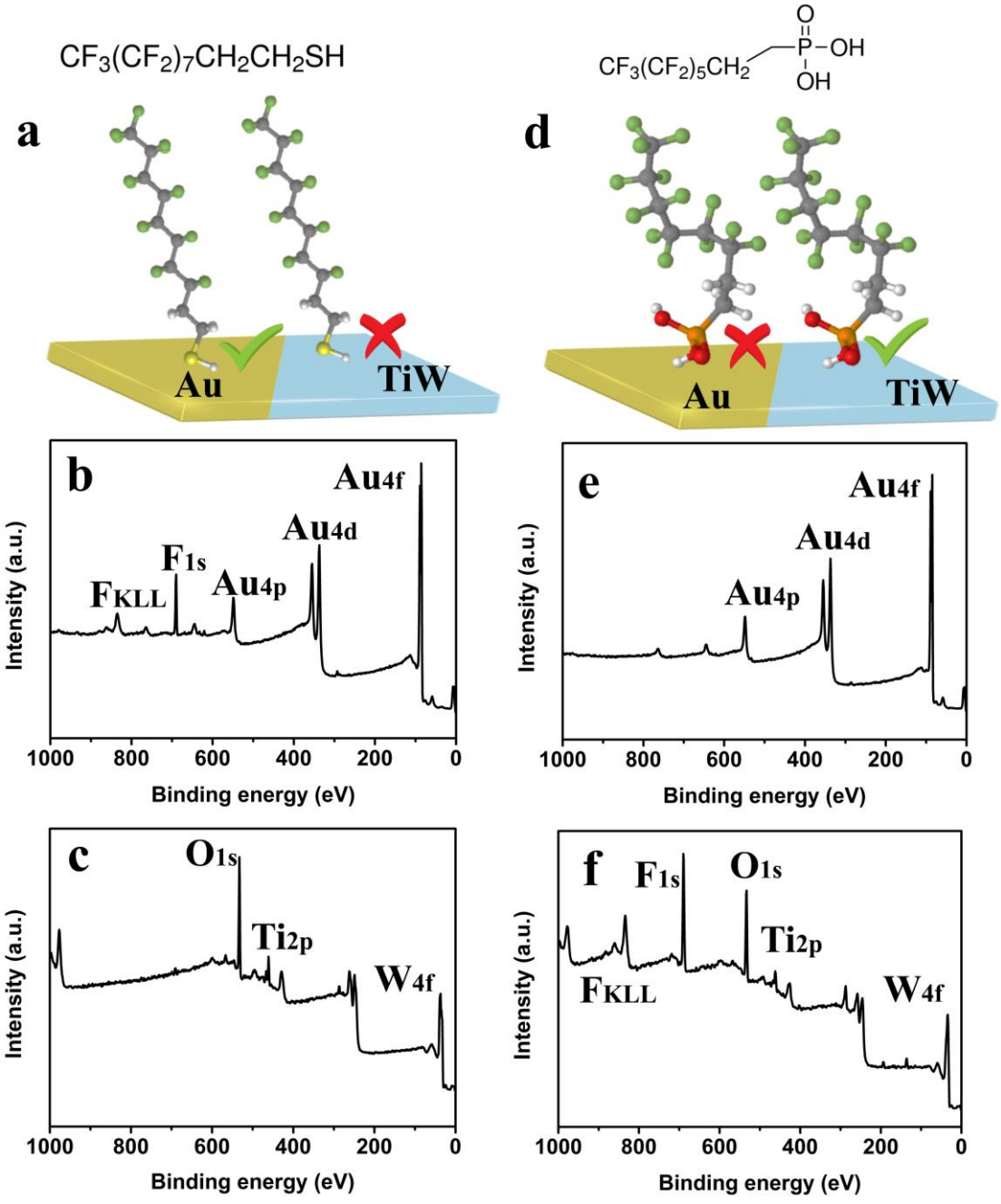

Figure 3.2 (a) Scheme of a macropatterned Au/TiW substrate functionalized with F-thiol. The corresponding XPS survey spectra measured on gold and TiW are displayed in (b) and (c). (d) Scheme of a macropatterned Au/TiW substrate functionalized with F-phosphonic acid. The corresponding XPS survey spectra measured on Au and TiW are displayed in (e) and (f).

The macroscale patterned Au/TiW substrates were functionalized by either 1H,1H,2H,2H-perfluorodecanethiol (F-thiol, Figure 3.2a) or (1H,1H,2H,2H-Tridecafluorooct-1-

yl)phosphonic acid (F-phosphonic acid, Figure 3.2d) and were analyzed using XPS. Survey and high-resolution spectra were recorded for areas corresponding to either Au or TiW. Figure 3.2b and Figure 3.2c show the XPS survey spectra of Au and TiW areas of macroscale substrates after incubation with perfluorinated thiol. On Au, fluorine was clearly evidenced by the F1s and F_{KLL} peaks, showing the presence of the perfluorinated thiol. On the contrary, fluorine could not be observed on TiW. After incubation of the macroscale substrate with F-phosphonic acid, F1s and F_{KLL} peaks were only observed on TiW. Such peaks were not observed on Au (Figure 3.2e, f).

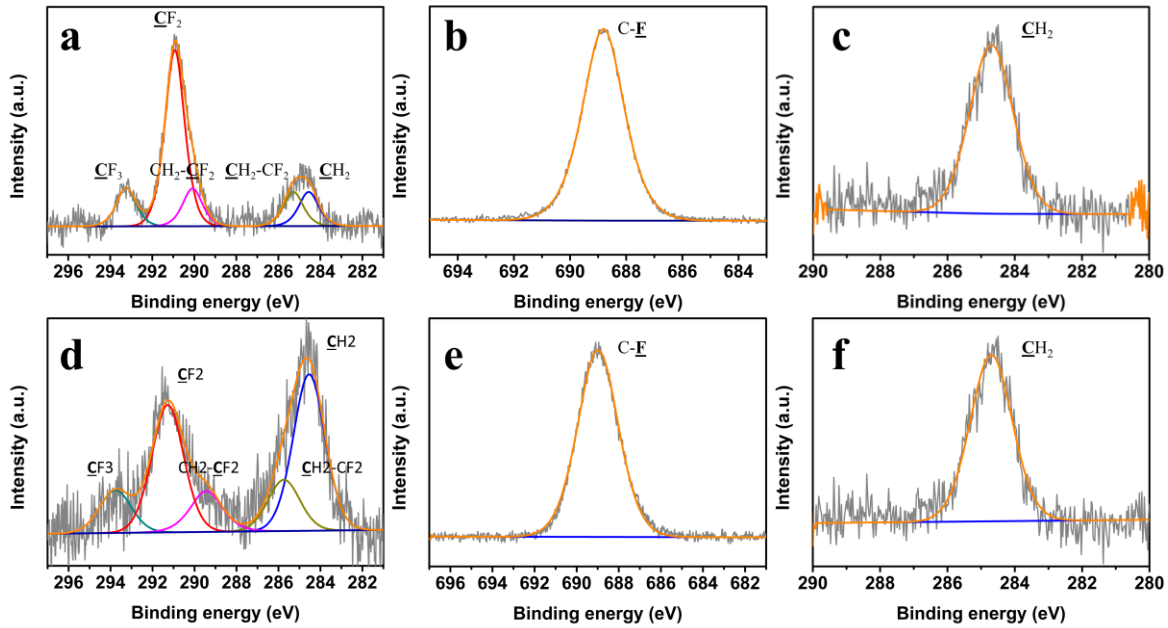

Figure 3.3 High-resolution XPS C1s (a) and F1s (b) spectrum of Au region for F-thiol functionalized patterned substrates. High-resolution XPS C1s (c) spectrum of TiW region for F-thiol functionalized patterned substrates. High-resolution XPS C1s (d) and F1s (e) spectrum of Au region for F-phosphonic acid functionalized patterned substrates. High-resolution XPS C1s (f) spectrum of Au region for F- phosphonic acid functionalized patterned substrates.

High resolution XPS spectrum of F1s and C1s confirmed the presence of F-thiol on Au area only (Figure 3.3a, b). Indeed, after incubation with perfluorinated thiol, the contributions at 293 eV, 291.5 eV and 290 eV were only observed on Au area and can be attributed to CF_3, CF_2-CF_2 and CH_2-CF_2, respectively. On TiW area, only the contribution at 284.6 eV was observed for the C1s and corresponded to hydrocarbon (Figure 3.3c). Similarly, after incubation with F-phosphonic acid, high resolution XPS spectrum of F1s and C1s confirmed that the perfluorinated molecule is only present on TiW area (Figure 3.3d, e). Indeed, the contributions at 293 eV, 291.5 eV and 290 eV attributed to CF_3, CF_2-CF_2 and CH_2-CF_2 were only observed on TiW. On Au, only hydrocarbon contribution (284.6 eV) was observed (Figure 3.3f).

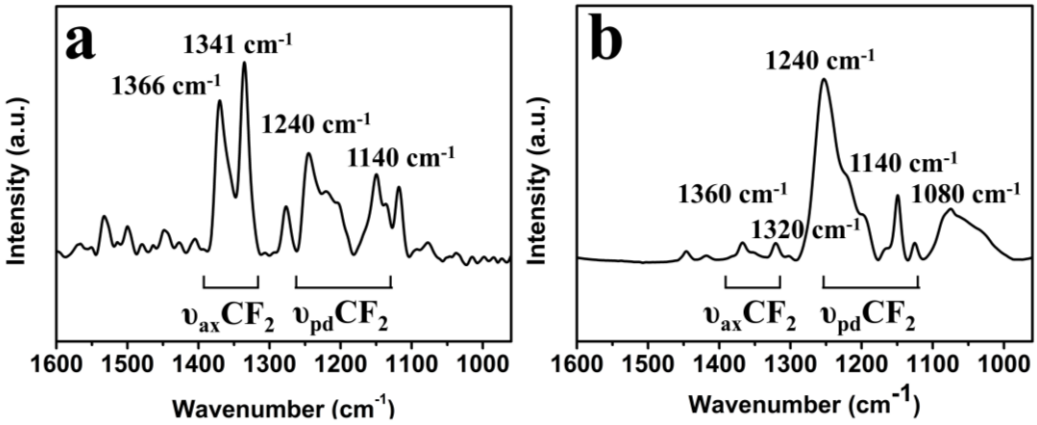

Figure 3.4 (a) PM-IRRAS spectra recorded on Au of patterned substrates functionalized by F-thiol. (b) PM-IRRAS spectra recorded on TiW of patterned substrates functionalized by F-phosphonic acid.

Figure 3.4a displays the PM-IRRAS spectra corresponding to the Au area of macroscale patterned substrate functionalized with F-thiol. It has been found that C-F stretching vibrations region from 1000 cm^{-1} to 1600 cm^{-1} present on Au. Additionally, on TiW no C-F stretching vibrations peaks were observed indicating that F-thiol was below PM-IRRAS detection limit on TiW. PM-IRRAS spectra of the TiW areas following incubation with F-phosphonic acid is displayed in Figure 3.4b. A broad peak at around 1080 cm^{-1} was attributed to the P-O bend[30], [31]. In detail, bands at 1240 cm^{-1} and 1140 cm^{-1} were assigned to asymmetric and symmetric CF_2 stretching vibrations. Peaks at 1320 cm^{-1} and 1366 cm^{-1} were referenced as axial CF_2 stretching vibration bands $\upsilon_{ax}CF_2$[32], [33].

3.3.2 Orthogonality of microscale substrates

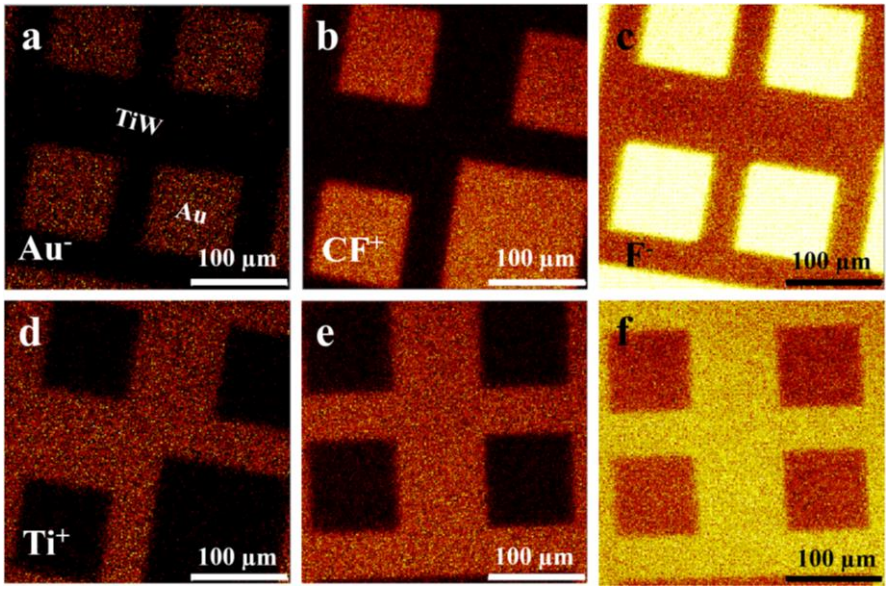

Figure 3.5 ToF-SIMS maps (300 × 300 µm²; scale bar, 100 µm) of Au^-, Ti^+, CF^+, F^- ions of micropatterned Au/TiW substrates functionalized with F-thiol (a-c) and F-phosphonic acid (d-f).

In order to test the orthogonality of functionalization on the microscale patterned substrates, fluorine mapping was conducted using ToF-SIMS, which has been shown to be especially well-suited for the characterization of chemically patterned surfaces[34], [35]. As shown in Figure 3.5, CF^+ and F^- were imaged on micropatterned substrates after incubation with F-thiol or F-phosphonic acid. In the case of F-thiol functionalization, the F^-, CF^+ and Au^- ions originated from the same areas, whereas on the surrounding TiW the fluorine associated ions had weak intensities (Figure 3.5a-c). Opposite observations can be drawn when the substrate was incubated with F-phosphonic acids: F^- and CF^+ signals are issued from the TiW areas (Figure 3.5d-f). It demonstrates the good orthogonality of the functionalization.

3.3.3 Nanoparticles trapping

It has been shown that thiol molecules could be selectively addressed on Au areas rather than TiW ones. In the following, we demonstrate that thiol organolayers on Au can be used for the selective capture of nanoparticles on Au/TiW patterned substrates.

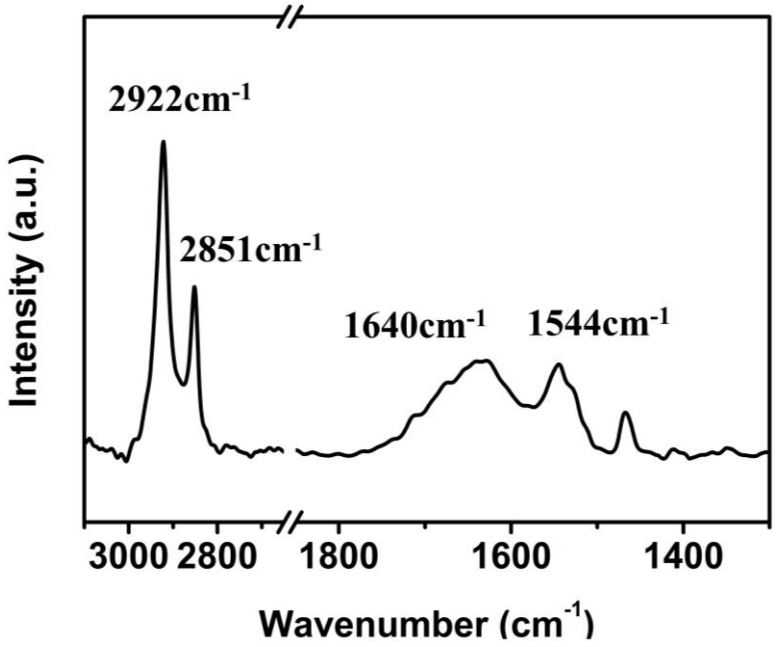

Figure 3.6 PM-IRRAS spectra of Au functionalized by MUAM.

Au/TiW micropatterned substrates were functionalized with 11-mercaptoundecylamine (MUAM). The Au area of Au/TiW surface were characterized by PM-IRRAS (Figure 3.6). The spectrum shows bands at 2922 cm^{-1} and 2851 cm^{-1} assigned to the asymmetric and symmetric vibration of CH_2. Furthermore, the position of the symmetric and asymmetric CH_2 stretching bands indicated the close-packing of the alkyl chains in the SAMs. A peak at about 1460 cm^{-1} can be assigned to the CH_2 scissor vibrations. It also showed N-H deformation vibration modes at 1640 cm^{-1} and 1544 cm^{-1}. These bands are associated with the protonated form of the primary amine group NH_3^+[36].

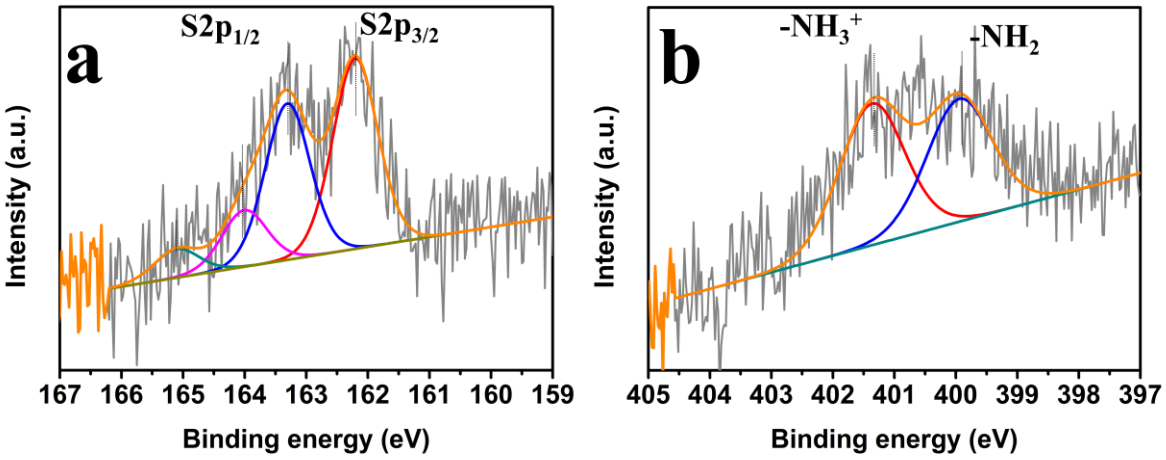

Figure 3.7 High-resolution XPS S2p (a) and N1s (b) peaks for MUAM functionalized Au.

High-resolution XPS S2p spectrum of Au areas functionalized by MUAM can be attributed to two S2p doublet with the main signals $S2p_{3/2}$ centered at 162.2 eV and 163.9 eV (Figure 3.7a). The first doublet can be assigned to sulfur bound to Au atom, and the second indicates unbound sulfur, present despite the intensive rinsing of samples[37], [38]. Due to the dissymmetry of the N1s, two contributions seems to be present on the high-resolution N1s spectra, which were associated with a free amine $-NH_2$ group at 399.8 eV and protonated amine $-NH_3^+$ group at 401.7 eV, respectively (Figure 3.7b)[39]. After functionalization by MUAM, the chemical compositions of different elements are listed in Table 3.1.

	C1s	S2p	Au4f	N1s
MUAM-Au	47.07 ± 0.6	1.26 ± 0.1	50.08 ± 0.5	1.58 ± 0.2

Table 3. 1XPS determined atomic concentrations (%) of MUAM functionalized Au.

These results in combination with the selectivity of thiol for gold vs TiW allowed the selective trapping of nanoparticles onto Au features on TiW by electrostatic interactions.

Carboxylated nanoparticles were incubated with MUAM modified micropatterned Au/TiW substrates. The experiment was conducted at pH 7.4. At this pH value, amines were expected to be protonated while carboxyl groups of the nanoparticles were expected to be deprotonated (pKa of amines and carboxylic acids are around 9-10 and 3-4 respectively). The functionalized patterned substrates were vertically immersed in carboxyl-nanoparticles solution overnight at room temperature and then rinsed with DI water. A control sample corresponding to a non-functionalized surface was also immersed in the same solution and rinsed in the same way. After washing, scanning electron microscope (SEM) images were taken and analyzed with ImageJ software to compute the specific trapping of colloids on the Au regions and non-specific adsorption on surrounding TiW.

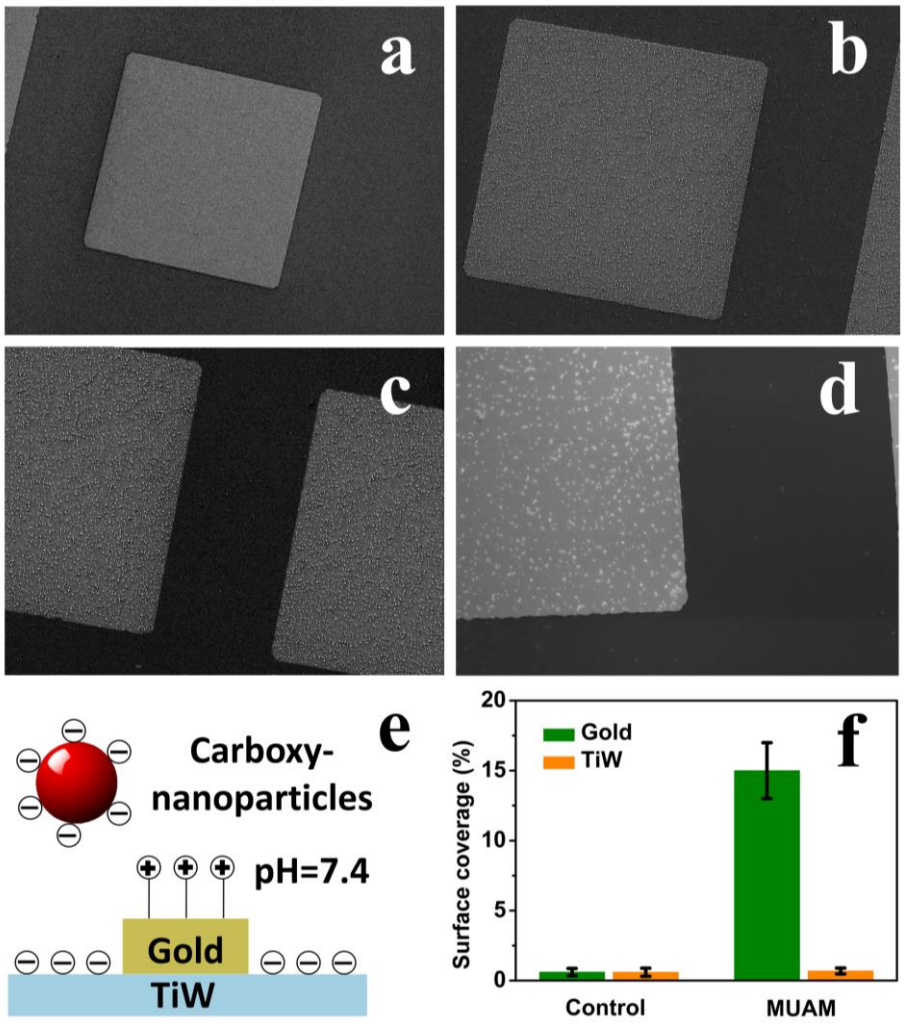

Figure 3.8 SEM images of colloid trapping based on electrostatic methods on the MUAM functionalized Au/TiW surfaces (a-d). Schematic representation of functionalized nanoparticles immobilized on the micropatterned substrates selectively functionalized by MUAM (e). Histogram presenting the surface coverage by nanoparticles on Au and TiW regions of the functionalized patterned surface *(f).*

The results of the selective trapping of nanoparticles on patterned substrates are summarized in Figure 3.8. It shows that non-specific adsorption on control sample corresponding to a non-functionalized TiW areas is generally low. Indeed, since nanoparticles deposition was performed at pH=7.4, the TiW surface as well as the carboxyl functionalized nanoparticles were expected to be negatively charged. Indeed, the point of zero charge of TiW and the pKa of carboxylic acids are around 3 and 4, respectively. Electrostatic repulsion probably accounts for the low non-specific adsorption of the colloids onto the TiW surface. Most importantly, the number of nanoparticles on MUAM modified Au areas were found to be one order of magnitude higher than the one observed on TiW. These results showed the efficiency of surface chemical functionalization to selectively anchor nanoparticles onto predefined Au regions of a heterogeneous TiW substrate.

3.4 Conclusions

In this chapter, we reported the selective and independent chemical functionalization of TiW and Au areas on Au/TiW patterned substrates thanks to the orthogonality of phosphonic acid and thiol molecules reactivity. Direct characterizations using XPS, PM-IRRAS and ToF-SIMS mapping provided evidence of the chemical orthogonality. Nanoparticles were precisely anchored on Au microscale patterns through selective chemical functionalization of the Au allowing for electrostatic trapping. The specific capturing of nanoparticles on Au was increased by one order of magnitude in respect to non-specific adsorption on TiW. This method is being developed to eventually investigate the anchoring of nano-objects or biomolecules onto large arrays of micro and nanoscale patterns.

3.5 Reference

[1] P. E. Laibinis, J. J. Hickman, M. S. Wrighton, G. M. Whitesides. Orthogonal self-assembled monolayers: alkanethiols on gold and alkane carboxylic acids on alumina. *Science*, **1989**, *245*, 845–847.

[2] T. J. Gardner, C. D. Frisbie, M. S. Wrighton. Systems for orthogonal self-assembly of electroactive monolayers on Au and ITO: an approach to molecular electronics. *J. Am. Chem. Soc.*, **1995**, *117*, 6927–6933.

[3] J. L. Wilbur, A. Kumar, H. A. Biebuyck, E. Kim, G. M. Whitesides. Microcontact printing of self-assembled monolayers: applications in microfabrication. *Nanotechnology*, **1996**, *7*, 452–457.

[4] R. Michel, I. Reviakine, D. Sutherland, C. Fokas, G. Csucs, G. Danuser, N. D. Spencer, M. Textor. A novel approach to produce biologically relevant chemical patterns at the nanometer scale: selective molecular assembly patterning combined with colloidal lithography. *Langmuir*, **2002**, *18*, 8580–8586.

[5] M. Bergkvist, N. Niamsiri, A. D. Strickland, C. A. Batt. Substrate selective patterning on lithography defined gold on silica: effect of end-group functionality on intermolecular layer formation. *Surf. Sci.*, **2008**, *602*, 2121–2127.

[6] T. A. Gschneidtner, S. Chen, J. B. Christensen, M. Käll, K. Moth-Poulsen. Toward plasmonic biosensors functionalized by a photoinduced surface reaction. *J. Phys. Chem. C*, **2013**, *117*, 14751–14758.

[7] N. Zhang, Y. Liu, J. Yang, X. Su, J. Deng, C. C. Chum, M. Hong, J. Teng. High sensitivity molecule detection by plasmonic nanoantennas with selective binding at electromagnetic hotspots. *Nanoscale*, **2014**, *6*, 1416–1422.

[8] K. Kumar, A. B. Dahlin, T. Sannomiya, S. Kaufmann, L. Isa, E. Reimhult. Embedded plasmonic nanomenhirs as location-specific biosensors. *Nano Lett.*, **2013**, *13*, 6122–6129.

[9] L. Feuz, M. P. Jonsson, F. Höök. Material-selective surface chemistry for nanoplasmonic sensors: optimizing sensitivity and controlling binding to local hot spots. *Nano Lett*., **201**2, *12*, 873–879.

[10] F. Palazon, D. Léonard, T. L. Mogne, F. Zuttion, C. Chevalier, M. Phaner-Goutorbe, É. Souteyrand, Y. Chevolot, J. P. Cloarec. Orthogonal chemical functionalization of patterned gold on silica surfaces. *Beilstein J Nanotechnol.*, **2015**, *6*, 2272–2277.

[11] R. C. Schmidt, K. E. Healy. Controlling biological interfaces on the nanometer length scale. *J. Biomed. Mater. Res. A*, **2009**, *90A*, 1252–1261.

[12] F. Palazon, P. Rojo-Romeo, C. Chevalier, T. Géhin, A. Belarouci, A. Cornillon, F. Zuttion, M. Phaner-Goutorbe, É. Souteyrand, Y. Chevolot, J. P. Cloarec. Nanoparticles selectively immobilized onto large arrays of gold micro and nanostructures through surface chemical functionalizations. *J. Colloid Interface Sci.*, **2015**, *447*, 152–158.

[13] P. Anstaett, Y. Zheng, T. Thai, A. M. Funston, U. Bach, G. Gasser. Synthesis of stable peptide nucleic acid-modified gold nanoparticles and their assembly onto gold surfaces. *Angew. Chem. Int. Ed.*, **2013**, *52*, 4217–4220.

[14] M. Palma, J. J. Abramson, A. A. Gorodetsky, E. Penzo, R. L. Gonzalez Jr., M. P. Sheetz, C. Nuckolls, J. Hone, S. J. Wind. Selective biomolecular nanoarrays for parallel single-molecule investigations. *J. Am. Chem. Soc.*, **2011**, *133*, 7656–7659.

[15] R. Michel, J. W. Lussi, G. Csucs, I. Reviakine, G. Danuser, B. Ketterer, J. A. Hubbell, M. Textor, N. D. Spencer. Selective molecular assembly patterning: a new approach to micro- and nanochemical patterning of surfaces for biological applications. *Langmuir*, **2002**, *18*, 3281–3287.

[16] L. Feuz, P. Jönsson, M. P. Jonsson, F. Höök. Improving the limit of detection of nanoscale sensors by directed binding to high-sensitivity areas. *ACS Nano*, **201**0, *4*, 2167–2177.

[17] D. Burdinski, M. Saalmink, J. P. W. G. Berg, C. Marel. Universal ink for microcontact printing *Angew. Chem. Int. Ed.*, **2006**, *26*, 4355–4358.

[18] E. Briand, V. Humblot, J. Landoulsi, S. Petronis, C. M. Pradier, B. Kasemo, S. Svedhem. Chemical modifications of Au/SiO_2 template substrates for patterned biofunctional surfaces. *Langmuir*, **2011**, *27*, 678–685.

[19] M. Palma, J. J. Abramson, A. A. Gorodetsky, E. Penzo, R. L. G. Jr, M. P. Sheetz, C. Nuckolls, J. Hone, S. J. Wind. Selective biomolecular nanoarrays for parallel single-molecule investigations. *J. Am. Chem. Soc.*, **2011**, *133*, 7656–7659.

[20] H. Cai, S. J. Wind. Improved glass surface passivation for single-molecule nanoarrays. *Langmuir*, **2016**, *32*, 10034–10041.

[21] F. Battegay, M. Fourel. Barrier material selection for TSV last, flipchip amp; 3D-UBM amp; RDL integrations. *ECTC*, **2015**, 1183–1192.

[22] C. K. Wang, S. J. Chang, Y. K. Su, C. S. Chang, Y. Z. Chiou, C. H. Kuo, T. K. Lin, T. K. Ko, J. J. Tang. GaN MSM photodetectors with TiW transparent electrodes. *Mater. Sci. Eng. B*, **2004**, *112*, 25–29.

[23] A. Roshanghias, G. Khatibi, R. Pelzer, J. Steinbrenner. On the effects of thickness on adhesion of TiW diffusion barrier coatings in silicon integrated circuits. *Surf. Coat. Technol.*, **2014**, *259*, 386–392.

[24] S. K. Bhagat, N. D. Theodore, T. L. Alford. Thermal stability of tungsten–titanium diffusion barriers for silver metallization. *Thin Solid Films*, **2008**, *516*, 7451–7457.

[25] S. Wang, S. Suthar, C. Hoeflich, B. Burrow. Diffusion barrier properties of TiW between Si and Cu. *J. Appl. Phys.*, **1993**, *73*, 2301–2320.

[26] H. C. Chiua, C. H. Chen, C. W. Yang, H. L. Kao, F. H. Huang, S. W. Peng. Highly thermally stable in situ SiN_X passivation AlGaN/GaN enhancement-mode high electron mobility transistors using TiW refractory gate structure. *J. Vac. Sci. Technol. B*, **2013**, *31*, 051212 1–4.

[27] J. C. Chiou, K. C. Juang, M. C. Chen. TiW (N) as diffusion barriers between Cu and Si. *J. Electrochem. Soc.*, **1995**, *142*, 2326–2331.

[28] J. L. Alay, H. Bender, G. Brijs, A. Demesmaeker, W. Vandervorst. Quantitative analysis of W(N), TiW and TiW(N) matrices using XPS, AES, RBS, EPMA and XRD. *Surf Interface Anal.*, **1991**, *17*, 373–382.

[29] J. C. Chiou, M. C. Chen. Thermal Stability of $Cu/CoSi_2$ Contacted p^+n Shallow Junction with and without TiW Diffusion Barrier. *J. Electrochem. Soc.*, **1994**, *141*, 2804–2810.

[30] T. J. Daou, S. Begin-Colin, J. M. Greneche, F. Thomas, A. Derory, P. Bernhardt, P. Legare, G. Pourroy. Phosphate adsorption properties of magnetite-based nanoparticles. *Chem. Mater.*, **2007**, *19*, 4494–4505.

[31] D. Toulemon, B. P. Pichon, X. Cattoën, M. W. C. Man, S. Begin-Colin. 2D assembly of non-interacting magnetic iron oxide nanoparticlesvia “click” chemistry. *Chem. Commun.*, **2011**, *47*, 11954–11956.

[32] T. Patois, A. E. Taouil, F. Lallemand, L. Carpentier, X. Roizard, J. Y. Hihn, V. Bondeau-Patissier, Z. Mekhalif. Microtribological and corrosion behaviors of 1H,1H,2H,2H-perfluorodecanethiol self-assembled films on copper surfaces. *Surf. Coat. Technol.*, **2010**, *205*, 2511–2517.

[33] F. Laffineur, D. Auguste, F. Plumier, C. Pirlot, L. Hevesi, J. Delhalle, Z. Mekhalif. Comparison between $CH_3(CH_2)_{15}SH$ and $CF_3(CF_2)_3(CH_2)_{11}SH$ monolayers on electrodeposited silver. *Langmuir*, **2004**, *20*, 3240–3245.

[34] T. K. Claus, S. Telitel, A. Welle, M. Bastmeyer, A. P. Vogt, G. Delaittre, C. Barner-Kowollik. Light-driven reversible surface functionalization with anthracenes: visible light writing and mild UV erasing. *Chem. Commun.*, **2017**, *53*, 1599–1602.

[35] T. Pauloehrl, A. Welle, K. K. Oehlenschlaeger, C. Barner-Kowollik. Spatially controlled surface immobilization of nucleophiles via trapping of photo-generated thioaldehydes. *Chem. Sci.*, **2013**, *4*, 3503–3507.

[36] E. E. Bedford, S. Boujday, V. Humblot, F. Gu, C. M. Pradier. Effect of SAM chain length and binding functions on protein adsorption: β-Lactoglobulin and apo-transferrin on gold. *Colloids Surf. B Biointerfaces*, **2014**, *116*, 489–496.

[37] C. D. Bain, E. B. Troughton, Y. T. Tao, J. Evall, G. M. Whitesides, R. G. Nuzzo. Formation of monolayer films by the spontaneous assembly of organic thiols from solution onto gold. *J. Am. Chem. Soc.*, **1989**, *111*, 321–335.

[38] R. G. Nuzzo, B. R. Zegarski, L. H. Dubois. Fundamental studies of the chemisorption of organosulfur compounds on gold (111). Implications for molecular self-assembly on gold surfaces. *J. Am. Chem. Soc.*, **1987**, *109*, 733–740.

[39] Z. Yang, Y. Chevolot, T. Géhin, V. Dugas, N. Xanthopoulos, V. Laporte, T. Delair, Y. Ataman-Önal, G. Choquet-Kastylevsky, É. Souteyrand, E. Laurencea. Characterization of three amino-functionalized surfaces and evaluation of antibody immobilization for the multiplex detection of tumor markers involved in colorectal cancer. *Langmuir*, **2013**, *29*, 1498–1509.

Chapter 4

Orthogonal chemical functionalization of $Au/SiO_2/TiW$ patterned substrates

4 Orthogonal chemical functionalization of Au/SiO_2/ TiW patterned substrates

4.1 Introduction

The increasing number of applications of nanotechnology stresses the importance of designing nanoscale features of various chemical, biochemical or physical properties[1]–[4]. In this scope, some strategies have been developed to achieve chemical patterns. In this scope, some strategies have been developed. For example, microcontact printing transfers organic compounds on defined positions of a substrate by stamping[5], [6]. Self-assembled monolayer can be patterned by electron or extreme UV irradiation lithography[7], [8]. However, on multi-material patterned substrates, one can take advantage of each material for different chemical functions, to achieve site selective chemical functionalization. The so-called orthogonal chemical functionalization was first proposed by G. M. Whitesides et al. in 1989[9]. It offers a versatile method for controlling the interfacial properties of each material on patterned substrates. Orthogonal chemical functionalization is based on the combination of 1) top-down fabrication (e.g. optical or electronic lithography, nanoimprint) enabling to implement spatially resolved patterns of different inorganic materials on a substrate; and 2) bottom-up formation of organolayers by spontaneous assembly of molecules on each material. Each inorganic pattern made of a given material exhibits a specific affinity for one or several molecules bearing particular chemical moieties. If the chosen molecules are truly selective of each chosen material, it becomes possible to modify the surface chemical characteristics of each type of pattern[10]. In this situation, geometric precision of spatial addressing is mainly driven by the resolution of the lithographic technology used for fabricating the inorganic patterns. Moreover, the method takes advantage of alignment possibilities associated with lithography: it enables to locate in an absolute positioning of the patterns on a given substrate. It is therefore possible to envisage absolute positioning of nano-objects on predefined positions, with a submicronic precision.

Various combinations of chemical compounds (thiols, silanes, phosphonic acids) and inorganic substrates (Au, SiO_2, metal oxides) have been reported for site selective chemical functionalization. For instance, Au/SiO_2 patterned substrates are the most common used template, and selective attachment of thiols to gold and silanes to SiO_2 is exploited[11]–[16]. Au/metal oxides (TiO_2, Al_2O_3) substrates[17], [18] functionalized with thiols and phosphonic acids have also been achieved thanks to the selective attachment of the phosphonic acids to metal oxides. However, it is worth noting that most of the studies are focused on the building of two different organolayers on two-material patterned substrates. As far as we know, there rare reports about building three different organolayers on a three-material patterned substrate. Among various inorganic materials of interest, TiW used as a barrier layer material

has already been reported in electronic devices. It is fully compatible with microelectronic integrations and can be used as a potential functional membrane in nanoelectronic transducer[19]–[27]. TiW thin films can be implemented on a production scale with stable and reproducible chemical characteristics. TiW is therefore a material to be considered for implementing complexe heterogeneous systems, such as nanoelectronic sensors. In chapter 2, we show that TiW bearing surface bound hydroxyl groups could be modified with a stable phosphonic acid layer. On the same type of hydroxylated TiW substrate, a monovalent silane layer exhibited a poor stability in adequate conditions. A challenge arises from the fact that there may be a competitive anchoring of silane and phosphonic acid on TiW covered with a native oxide layer.

In this work, we report in what conditions three-material substrates can be orthogonally functionalized with three molecules. Au/SiO_2/TiW patterned substrates were functionalized with thiol, phosphonic acid and monovalent silane. This was assessed by X-ray photoelectron spectroscopy (XPS), infrared spectroscopy (IR), time-of-flight secondary ion mass spectrometry (ToF-SIMS) mapping and contact angle on three-material substrates bearing either macroscopic features (1 cm) and microscopic features (100 μm) of each material.

4.2 Experimental section

4.2.1 Materials and patterns

Chemicals are of reagent grade commercially available. 1H,1H,2H,2H-Perfluorodecanethiol (F-thiol) 97% was purchased from Sigma-Aldrich. (1H,1H,2H,2H-Tridecafluorooct-1-yl)phosphonic acid (F-phosphonic acid) 95% was obtained from SiKÉMIA. (Heptadecafluoro-1,1,2,2-tetrahydrodecyl)dimethylchlorosilane (F-silane) 95% was purchased from abcr. Dichloromethane (DCM) 99.9% was purchased from Sigma-Aldrich then degassed and dried over molecular sieves. Isopropanol 99.9% was purchased from Fluka. The ultrapure water used for all the experiments was obtained by VEOLIA water system.

Macroscale patterned Au/SiO_2/TiW substrates S1, S2 and S3 were prepared using the following protocol: one third of the TiW substrate was covered by Au film. Another third of the substrate was covered by SiO_2 film. The remaining third of the substrate remained unchanged as uncovered TiW.

Microscale patterned Au/SiO_2/TiW substrates S4, S5 and S6 were prepared using a two-steps UV lithography process. Ti (5 nm) and Au (45 nm) were deposited by electron beam evaporation. SiO_2 (50 nm) was deposited by magnetron sputtering. After lift-off, the samples were cleaned by oxygen plasma treatment (HARRICK) at the oxygen flow rate of 14 mL/min, RF power level of 38 W for 5 min to ensure that no residual resist remained on the surface. The patterned substrates pictures are shown in Figure 4.1. UV lithography process and materials deposition conditions are shown in Annex B.

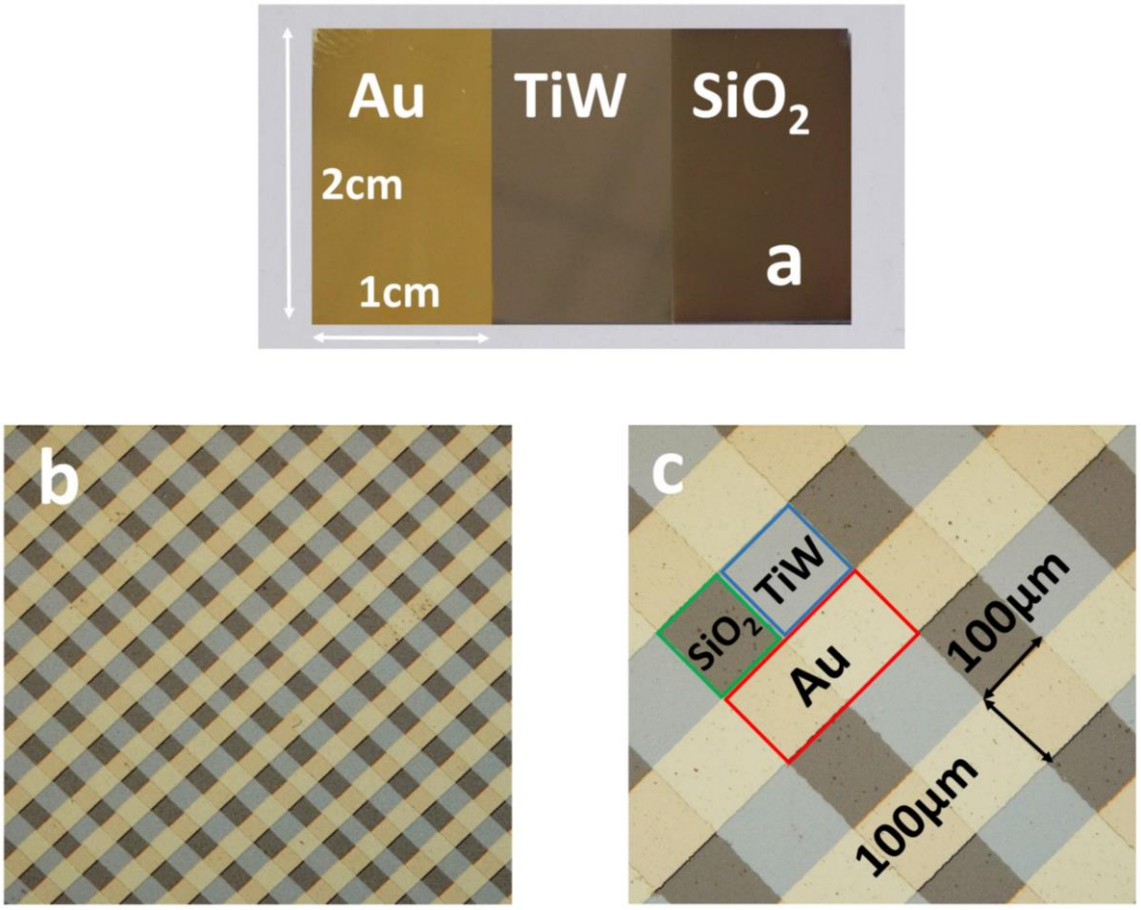

Figure 4.1 Optical photos of macropatterned substrates S1 S2 and S3 (a). Optical photos of micropatterned substrates S4 S5 and S6 (b). Enlarged version of (b).

4.2.2 Chemical functionalization

Patterned substrates S1 and S4 were functionalized by F-thiol using the following protocol: substrates were immersed in 25 ml dried DCM containing 100 µl F-thiol (14 mM) for 48 hours. Then the samples were rinsed with DCM for 5 min under ultrasound (Branson, 42 kHz, 100 W) followed by a stream of ultrapure water and dried with nitrogen flow.

Patterned substrates S2 and S5 were functionalized by F-phosphonic acid using the following protocol: substrates were immersed in 20 ml ultrapure water containing 8.5 mg F-phosphonic acid (1mM) for 16 hours. The substrates were then rinsed with isopropanol for 5 min under ultrasound (Branson, 42 kHz, 100 W) followed by a stream of ultrapure water and dried with nitrogen flow.

Patterned substrates S3 and S6 were functionalized by F-silane using the following protocol: substrate was immersed in 25 mL dried DCM containing 10 µL F-silane (1 mM) for 48 hours. Then the substrates were rinsed with DCM for 5 min under ultrasound (Branson, 42 kHz, 100 W) followed by a stream of ultrapure water and dried with nitrogen flow. After F-silane grafting, substrates were immersed in 70 °C ultrapure water for 15 min. After removing the samples were rinsed in ultrapure water and dried with nitrogen flow.

4.2.3 Characterization

X-ray Photoelectron Spectroscopy (XPS). XPS measurements on macropatterned substrates S1, S2 and S3 were performed using a focused monochromatized X-ray source (Al Kα 1486.6 eV). Spectrum acquisitions were performed under ultrahigh vacuum conditions (UHV, 10^{-9} Torr). Take-off angle was 90° relative to the substrate surface. The pass energies were 100 eV and 20 eV for wide-scan and high-resolution elemental scans, respectively. The data reduction was performed with CasaXPS software. The dimensions of TiW and Au patterns were largely higher than XPS beam, so that each material of a same substrate could be characterized individually. For each substrate, at least three measurements were performed on different locations of a same material, thus providing triplicate quantitative data for respectively TiW and Au of the same substrate.

Contact angle measurements were performed on macroscopic substrates S1, S2, S3 with a contact angle meter (Digidrop Goniometer, GBX, France) using the sessile drop method with deionized water. At least five 0.6 µL deionized water droplets were used per material zones on each substrate. For each material of a same substrate, obtained contact angle values correspond to the average of the five droplets contact angle values.

The attenuated total reflectance Fourier transform infrared (ATR-FTIR) spectra were recorded on macroscopic substrates S1, S2, S3 using a Thermo Nicolet 6700 spectrometer equipped with an MCT detector cooled with liquid nitrogen. All spectra were obtained from averages of 256 scans at a resolution of 4 cm^{-1}. The dimensions of TiW, SiO_2 and Au macropatterns were largely higher than FTIR beam, so that each material of a same substrate could be characterized individually.

Time-of-flight secondary ion mass spectrometry (ToF-SIMS) mapping measurements were performed on micropatterned substrates S4, S5, S6 with a Physical Electronics TRIFT III instrument (Physical Electronics, Chanhassen, MN) operated with a pulsed Au ion gun (ion current of 2 nA) over a 500 µm × 500 µm area. The ion dose was kept below the static conditions limits. Data were analyzed using WinCadence software. Mass calibration was performed on hydrocarbon secondary ions. For each substrate, at least three measurements were performed on different locations, thus providing triplicate quantitative data and images.

4.3 Results and discussions

Each substrate was exposed to only one type of molecule to assess the ability of one molecule to specifically bind to one single material, and not to bind with the other two materials of the substrate.

4.3.1 Orthogonality of macroscale substrates

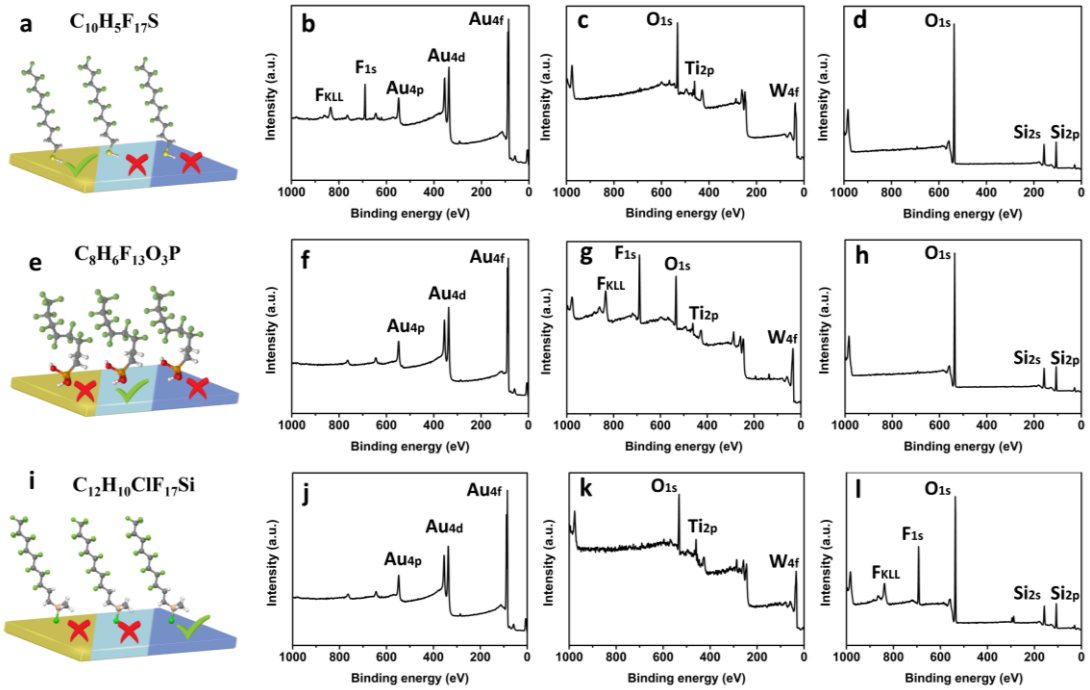

Figure 4.2 (a) Sketch of a macropatterned Au and SiO_2 on TiW substrate after reaction with F-thiol. Corresponding XPS survey spectra of Au (b), TiW (c) and SiO_2 (d) show that thiol only bonds to gold. (e) Sketch of a macropatterned Au and SiO_2 on TiW substrate after reaction with F-phosphonic acid. Corresponding XPS survey spectra of Au (f), TiW (g) and SiO_2 (h) show that phosphonic acid only binds to TiW. (i) Sketch of a macropatterned Au and SiO_2 on TiW substrate functionalized by F-silane. Corresponding XPS survey spectra of Au (j), TiW (k) and SiO_2 (l) show that silane only binds to SiO_2.

Organolayers were implemented on macroscale patterned substrates. The macropatterned Au and SiO_2 on TiW substrates were functionalized by F-thiol (Figure 4.2a), F-silane (Figure 4.2e) or F-phosphonic acid (Figure 4.2i) and were analyzed using XPS. Survey and high resolution spectra were recorded for each area corresponding to Au, TiW and SiO_2. Figure 4.2b-d showed the XPS survey spectra of Au, TiW and SiO_2 areas of macropatterned substrates after incubation with F-thiol. On gold, the presence of fluorine was clearly evidenced by the F1s and F_{KLL} peaks, showing the presence of the perfluorinated thiol. On the contrary, fluorine peaks could not be observed by XPS on TiW and SiO_2. This suggested that F-thiol was specifically grafted on the Au and not on TiW and SiO_2. After incubation of the macroscale patterned substrates with F-phosphonic acid, F1s and F_{KLL} peaks were only observed on TiW. Such peaks were not observed on Au and SiO_2 (Figure 4.2f-h). Phosphonic acids modified selectively the TiW surface. After incubation with F-silane, intense F1s and F_{KLL} peaks were observed on SiO_2. However, low intensity F1s peaks were also observed on TiW (Figure 4.3a). Nevertheless, after immersion in 70 °C water for 15 min, the F1s peaks disappeared on TiW, but did not decrease on SiO_2 (Figure 4.2j-l). Indeed, according to chapter 2, the grafting of monovalent silane molecules on TiW is some-how labile. Therefore,

site selective functionalization of SiO_2 on Au/SiO_2/TiW substrate can be achieved providing that the monofunctional silane molecules can be removed from TiW by hydrolysis of the Si-O-M bond.

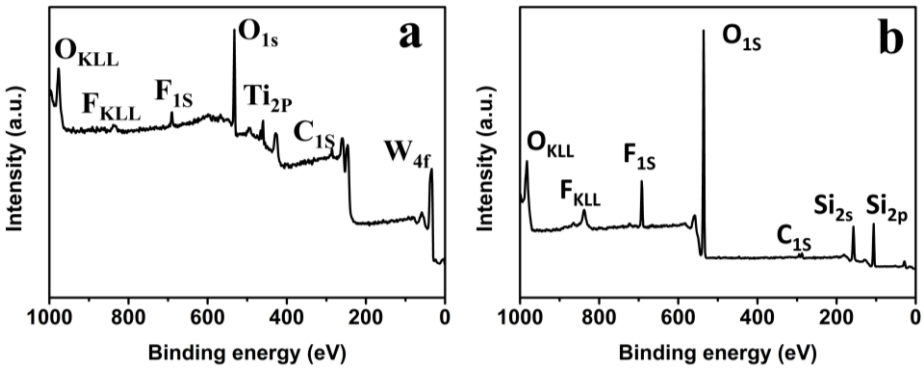

Figure 4.3 XPS survey spectra of TiW (a) and SiO_2 (b) regions on macropatterned substrates functionalized by F-silane before immersion in 70°C ultrapure H_2O.

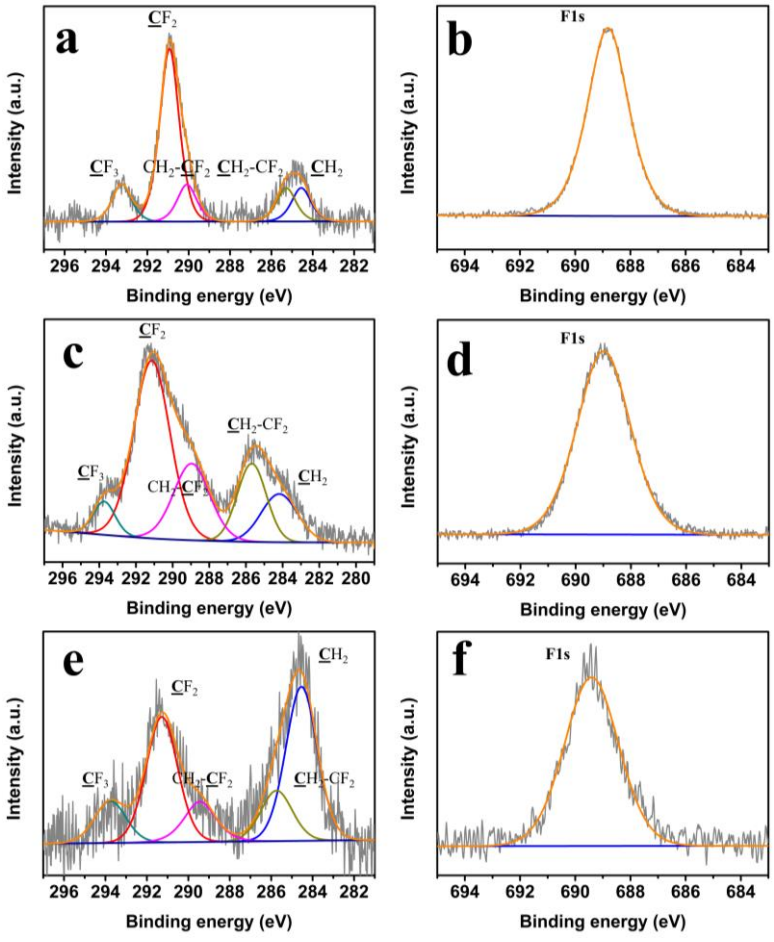

Figure 4.4 High-resolution XPS C1s and F1s spectrum of F-thiol functionalized Au (a, b), F-phosphonic acid functionalized TiW (c, d) and F-silane functionalized SiO_2 (e, f).

High-resolution XPS spectrum of F1s and C1s confirmed that the fluorine component observed in each case originated from perfluoromolecules as expected (Figure 4.4). These results suggested that orthogonal chemical functionalization is possible.

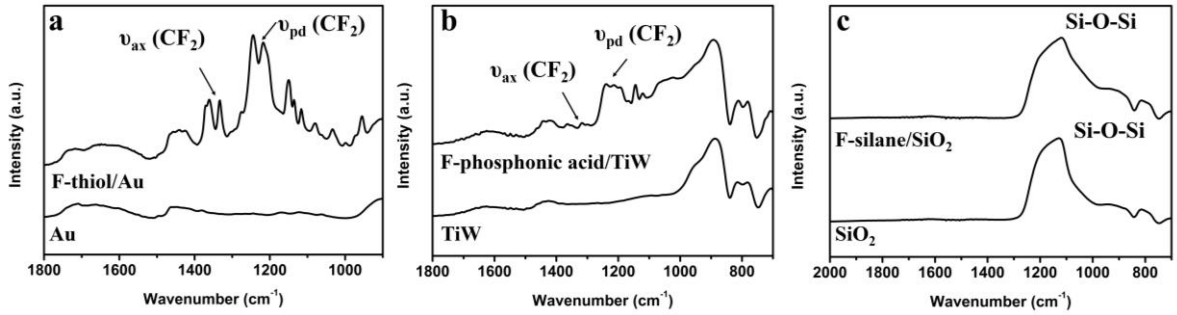

Figure 4.5 ATR-FTIR spectrum of (a) F-thiol functionalized Au, (b) F-phosphonic acid functionalized TiW, (c) F-silane functionalized SiO_2.

ATR-FTIR spectra were recorded on macroscale patterned substrates after incubation with F-thiol, F-phosphonic acid or F-silane. After incubation with F-thiol, the spectra obtained for TiW and SiO_2 areas remained unchanged. However, the spectra corresponding to the Au area displayed clear signatures of C-F (Figure 4.5a). The band at around 1239 cm^{-1} and 1350 cm^{-1} were attributed to the perpendicular CF_2 stretching bands $\upsilon_{pd}CF_2$ and to the axial CF_2 stretching vibration bands $\upsilon_{ax}CF_2$, respectively[28], [29]. Similarly, after incubation with F-phosphonic acid, the spectra of Au and SiO_2 remained unchanged. The TiW displayer clear IR signatures of the symmetric and asymmetric CF_2 vibrations ($\upsilon_{pd}CF_2$ and $\upsilon_{ax}CF_2$) at 1240 cm^{-1} and 1354 cm^{-1}, respectively (Figure 4.5b). A broad peak at from 1080 cm-1 to 1100 cm-1 was attributed to the P-O bend[30], [31]. After incubation with F-silane, the spectra of SiO_2 did not have any obvious C-F signatures (Figure 4.5c). It maybe resulted from that typical CF_2 vibration band is overlapped with Si-O-Si vibrations bands.

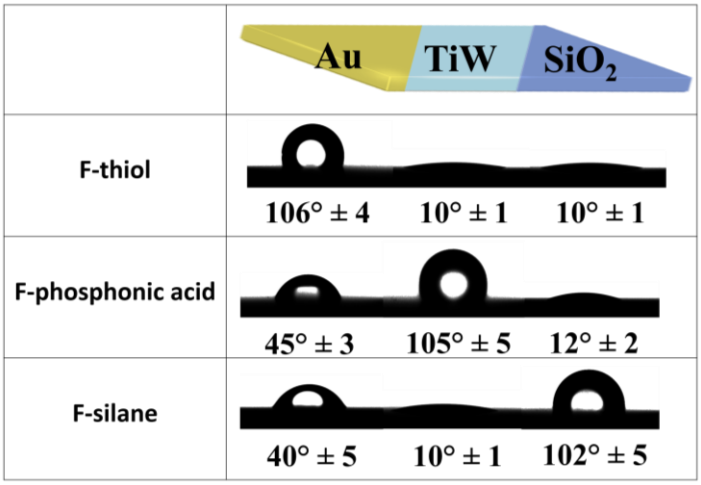

Figure 4.6 Contact angles of macropatterned substrates functionalized by F-thiol, F-phosphonic acid, F-silane. By comparison, contact angles of bare Au, TiW and SiO_2 were respectively 43°, 12° and 10°.

Water contact angles were measured at each region of patterned substrates as shown in Figure 4.6. The water contact angles of Au, TiW and SiO_2 regions on the control patterned substrate immersed in the pure solvent without molecules (thiol, silane or phosphonic acid) were 43°, 12° and 10°, respectively. After incubation of the patterned substrates in the F-thiol, the water

contact angle of Au increased to around 106°. The water contact angles of TiW and SiO_2 areas did not have obvious changes. The 106° angle observed on gold was attributed to the formation of a perfluoroalkyl hydrophobic layer on Au[29]. After incubation the patterned substrates with F-phosphonic acid, the water contact angle on TiW increased to around 105° due to the formation of hydrophobic F-phosphonic acid layer[32]. Meanwhile, the water contact angles of Au and SiO_2 areas remained similar to the original values. Incubation the patterned substrates with F-silane lead to a water contact angle on SiO_2 of 102°, 40° on the TiW areas and Au. However, after immersion in 70°C H_2O for 15 minutes, this water contact angle measured on TiW decreased to nearly 10° due to the hydrolysis of the Si-O-M bond.

4.3.2 Orthogonality of microscale substrates

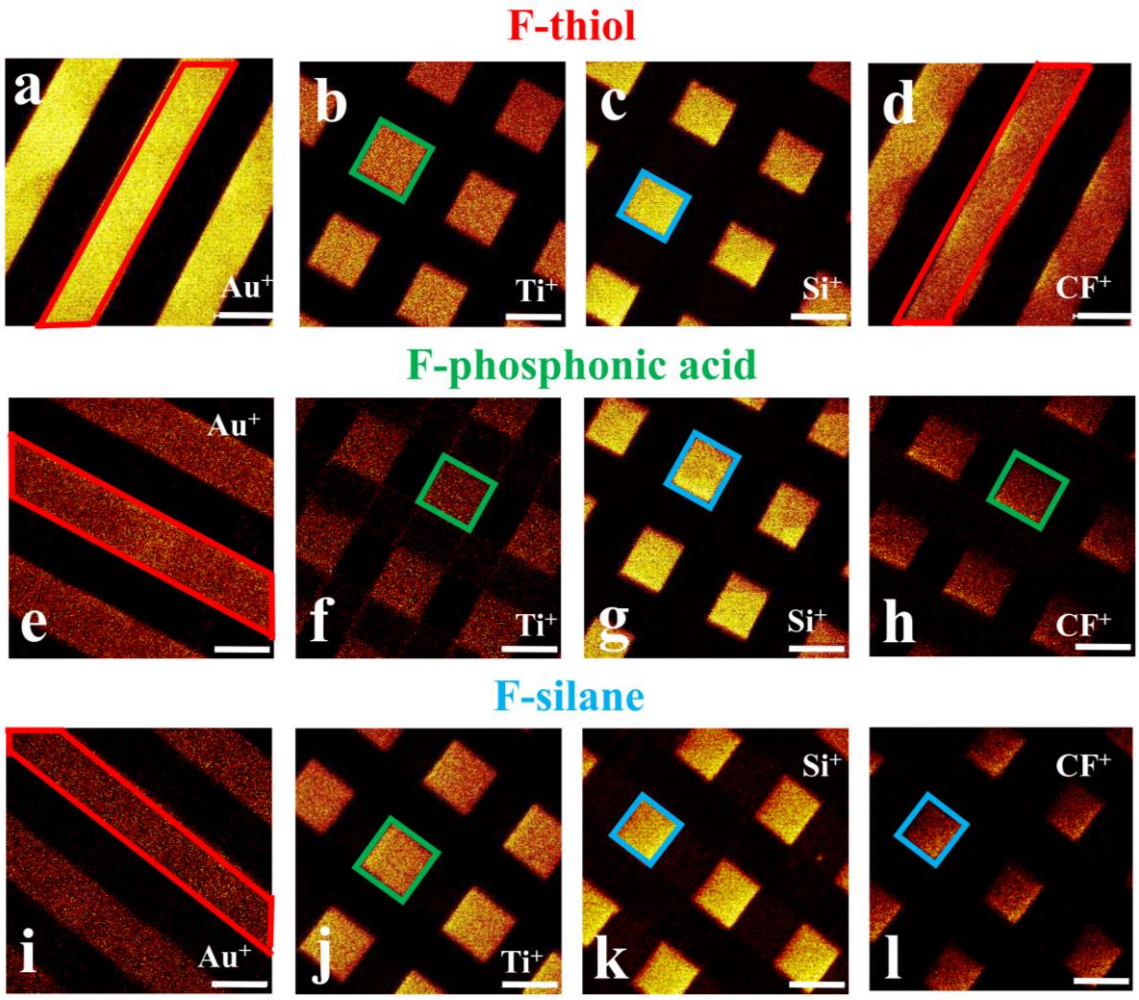

Figure 4.7 Au^+, Ti^+, Si^+, CF^+ ToF-SIMS mapping of patterned Au/SiO_2/TiW substrates functionalized by F-thiol (a-d), F-phosphonic acid (e-h), F-silane (i-l), scale bars (100 μm).

Functionalization of microscale patterned substrates was implemented and imaged by ToF-SIMS after incubation with F-thiol (Figure 4.7a-d), F-phosphonic acid (Figure 4.7e-h) or F-silane (Figure 4.7i-l) [33], [34].

After incubation with F-thiol, CF^+ (m/z = 31.00) and Au^+ (m/z = 196.97) originated from the same areas whereas CF^+ signals had low intensities for the areas where Ti^+ (m/z = 47.95) and Si^+ (m/z = 27.98) were originating. It suggests that F-thiol was selectively immobilized on Au. Similarly, ToF-SIMS imaging of the F-phosphonic acid or F-silane functionalized substrates showed that CF^+ was localized with Ti^+ or Si^+ ions, respectively.

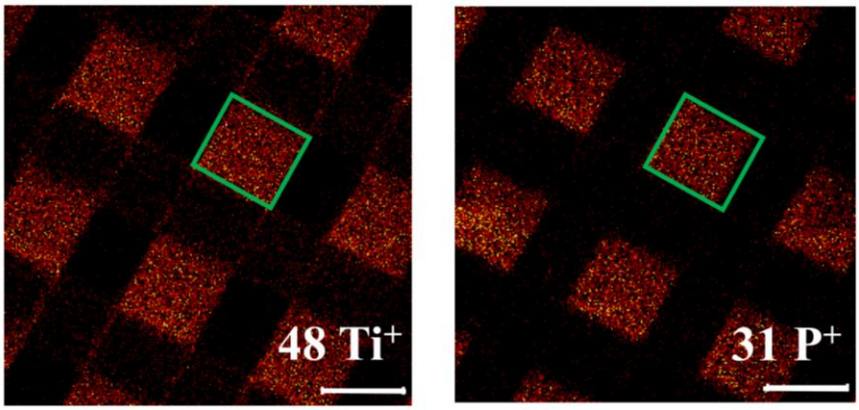

Figure 4.8 Ti^+ and P^+ ToF–SIMS mapping of patterned Au/SiO_2/TiW substrates functionalized with F-phosphonic acid. The scale bars are 100 µm.

Furthermore, on the F-phosphonic acid derivatized substrate, the P^+ (m/z = 30.97) signal is in registration with Ti^+ signal, which also suggested the selective grafting of phosphonic acid on TiW only (Figure 4.8). The results above demonstrate the good orthogonality of the functionalization.

4.3.3 Orthogonality outlook of three functionalization reactions

Experimental results show it is possible to specifically locate 1) F-thiol on Au; 2) F-phosphonic acid on TiW; 3) F-silane on SiO_2. When one of these three reactions are implemented on a substrate bearing the three materials Au, TiW and SiO_2, no trace of adsorption of the used molecule is detected on the other two materials. The next step of this work will consist in performing these three reactions on a same three-material substrate. We plan to sequentially test the functionalization of Au/TiW/SiO_2 substrate with consecutive reactions, in this order: F-thiol => F-silane (followed by 70°C water washing) => F-phosphonic acid. F-silane on SiO_2 has a good stability versus 70° water washing. We expect a good stability of F-thiol organolayer on gold versus 70° water washing.

4.4 Conclusions

In this chapter, the orthogonal chemical functionalization of building three different organolayers on a patterned substrate integrated with three inorganic materials was developed and assessed. We reported functionalization procedures of patterned Au and SiO_2 on TiW substrates with thiols, phosphonic acid and monovalent silane, respectively. Monovalent silane molecules desorbed from the TiW but remind on SiO_2 by a simple washing step. The

direct chemical characterization using XPS, water contact angle and ToF-SIMS mapping provided evidence of the orthogonality. Our work proposed to be implemented different fields of nanotechnology, especially in the development of localized surface plasmon resonance (LSPR) based biosensors.

4.5 References

[1] R. C. Schmidt, K. E. Healy. Controlling biological interfaces on the nanometer length scale. *J. Biomed. Mater. Res. A*, **2009**, *90A*, 1252–1261.

[2] W. Shi, T. Xu, L. Xu, Y. Chen, Y. Wen, X. Zhang, S. Wang. Cell micropatterns based on silicone-oil-modified slippery surfaces. *Nanoscale*, **2016**, *8*, 18612–18615.

[3] A. A. Popova, K. Demir, T. G. Hartanto, E. Schmitt, P. A. Levkin. Droplet-microarray on superhydrophobic–superhydrophilic patterns for high-throughput live cell screenings. *RSC Adv.*, **2016**, *6*, 38263–38276.

[4] A. Ruediger, F. Rosei. AFM extends its reach. *Nat. Nanotechnol*., **2010**, *5*, 388–389.

[5] J. L. Wilbur, A. Kumar, H. A. Biebuyck, E. Kim, G. M. Whitesides. Microcontact printing of self-assembled monolayers: applications in microfabrication. *Nanotechnology*, **1996**, *7*, 452–457.

[6] C. J. Pan, H. Qin, Y. D. Nie, H. Y. Ding. Control of osteoblast cells adhesion and spreading by microcontact printing of extracellular matrix protein patterns. *Colloids Surf. B Biointerfaces*, **2013**, *104*, 18–26.

[7] A. Turchanin, A. Tinazli, M. El-Desawy, H. Großmann, M. Schnietz, H. H. Solak, R. Tampé, A. Gölzhäuser. Molecular self-assembly, chemical lithography, and biochemical tweezers: a path for the fabrication of functional nanometer-scale protein arrays. *Adv. Mater*., **2008**, *20*, 471–477.

[8] A. Turchanin, M. Schnietz, M. El-Desawy, H. H. Solak, C. David, A. Gölzhäuser. Fabrication of molecular nanotemplates in self-assembled monolayers by extreme-ultraviolet-induced chemical lithography. *Small*, **2007**, *3*, 2114–2119.

[9] P. E. Laibinis, J. J. Hickman, M. S. Wrighton, G. M. Whitesides. Orthogonal self-assembled monolayers: alkanethiols on gold and alkane carboxylic acids on alumina. *Science*, **1989**, *245*, 845–847.

[10] T. J. Gardner, C. D. Frisbie, M. S. Wrighton. Systems for orthogonal self-assembly of electroactive monolayers on Au and ITO: an approach to molecular electronics. *J. Am. Chem. Soc.*, **1995**, *117*, 6927–6933.

[11] M. Bergkvist, N. Niamsiri, A. D. Strickland, C. A. Batt. Substrate selective patterning on lithography defined gold on silica: effect of end-group functionality on intermolecular layer formation. *Surf. Sci.*, **2008**, *602*, 2121–2127.

[12] F. Palazon, D. Léonard, T. L. Mogne, F. Zuttion, C. Chevalier, M. Phaner-Goutorbe, É. Souteyrand, Y. Chevolot, J. P. Cloarec. Orthogonal chemical functionalization of patterned gold on silica surfaces. *Beilstein J Nanotechnol.*, **2015**, *6*, 2272–2277.

[13] E. Briand, V. Humblot, J. Landoulsi, S. Petronis, C. M. Pradier, B. Kasemo, S. Svedhem. Chemical modifications of Au/SiO_2 template substrates for patterned biofunctional surfaces. *Langmuir*, **2011**, *27*, 678–685.

[14] K. Maeda, N. Okabayashi, S. Kano, S. Takeshita, D. Tanaka, M. Sakamoto, T. Teranishi, Y. Majima. Logic operations of chemically assembled single-electron transistor. *ACS Nano*, **2012**, *6*, 2798–2803.

[15] M. Palma, J. J. Abramson, A. A. Gorodetsky, E. Penzo, R. L. G. Jr, M. P. Sheetz, C. Nuckolls, J. Hone, S. J. Wind. Selective biomolecular nanoarrays for parallel single-molecule investigations. *J. Am. Chem. Soc.*, **2011**, *133*, 7656–7659.

[16] H. Cai, S. J. Wind. Improved glass surface passivation for single-molecule nanoarrays. *Langmuir*, **2016**, *32*, 10034–10041.

[17] D. Burdinski, M. Saalmink, J. P. W. G. Berg, C. Marel. Universal ink for microcontact printing. *Angew. Chem. Int. Ed.*, **2006**, *26*, 4355–4358.

[18] L. Feuz, P. Jönsson, M. P. Jonsson, F. Höök. Improving the limit of detection of nanoscale sensors by directed binding to high-sensitivity areas. *ACS Nano*, **201**0, *4*, 2167–2177.

[19] F. Battegay, M. Fourel, Barrier material selection for TSV last, flipchip & 3D-UBM & RDL integrations. *ECTC*, **2015**, 1183–1192.

[20] C. K. Wang, S. J. Chang, Y. K. Su, C. S. Chang, Y. Z. Chiou, C. H. Kuo, T. K. Lin, T. K. Ko, J. J. Tang. GaN MSM photodetectors with TiW transparent electrodes. *Mater. Sci. Eng. B*, **2004**, *112*, 25–29.

[21] A. Roshanghias, G. Khatibi, R. Pelzer, J. Steinbrenner. On the effects of thickness on adhesion of TiW diffusion barrier coatings in silicon integrated circuits. *Surf. Coat. Technol.*, **2014**, *259*, 386–392.

[22] S. K. Bhagat, N. D. Theodore, T. L. Alford. Thermal stability of tungsten–titanium diffusion barriers for silver metallization. *Thin Solid Films*, **2008**, *516*, 7451–7457.

[23] S. Wang, S. Suthar, C. Hoeflich, B. Burrow. Diffusion barrier properties of TiW between Si and Cu. J. *J. Appl. Phys.* **1993**, *73*, 2301–2320.

[24] H. C. Chiua, C. H. Chen, C. W. Yang, H. L. Kao, F. H. Huang, S. W. Peng. Highly thermally stable in situ SiN_X passivation AlGaN/GaN enhancement-mode high electron mobility transistors using TiW refractory gate structure. *J. Vac. Sci. Technol. B,* **2013**, *31*, 051212 1–4.

[25] J. C. Chiou, K. C. Juang, M. C. Chen. TiW (N) as diffusion barriers between Cu and Si. *J. Electrochem. Soc.*, **1995**, *142*, 2326–2331.

[26] J. L. Alay, H. Bender, G. Brijs, A. Demesmaeker, W. Vandervorst. Quantitative analysis of W(N), TiW and TiW(N) matrices using XPS, AES, RBS, EPMA and XRD. *Surf Interface Anal.,* **1991**, *17*, 373–382.

[27] J. C. Chiou, M. C. Chen. Thermal Stability of $Cu/CoSi_2$ Contacted p^+n Shallow Junction with and without TiW Diffusion Barrier. *J. Electrochem. Soc.,* **1994**, *141*, 2804–2810.

[28] F. Laffineur, D. Auguste, F. Plumier, C. Pirlot, L. Hevesi, J. Delhalle, Z. Mekhalif. Comparison between $CH_3(CH_2)_{15}SH$ and $CF_3(CF_2)_3(CH_2)_{11}SH$ monolayers on electrodeposited silver. *Langmuir,* **2004**, *20*, 3240–3245.

[29] T. Patois, A. E. Taouil, F. Lallemand, L. Carpentier, X. Roizard, J. Y. Hihn, V. Bondeau-Patissier, Z. Mekhalif. Microtribological and corrosion behaviors of 1H,1H,2H,2H-perfluorodecanethiol self-assembled films on copper surfaces. *Surf. Coat. Technol.,* **2010**, *205*, 2511–2517.

[30] T. J. Daou, S. Begin-Colin, J. M. Greneche, F. Thomas, A. Derory, P. Bernhardt, P. Legare, G. Pourroy. Phosphate adsorption properties of magnetite-based nanoparticles. *Chem. Mater.,* **2007**, *19*, 4494–4505.

[31] D. Toulemon, B. P. Pichon, X. Cattoën, M. W. C. Man, S. Begin-Colin. 2D assembly of non-interacting magnetic iron oxide nanoparticlesvia “click” chemistry. *Chem. Commun.,* **2011**, *47*, 11954–11956.

[32] A. R. McNeill, A. R. Hyndman, R. J. Reeves, A. J. Downard, M. W. Allen. Tuning the band bending and controlling the surface reactivity at polar and nonpolar surfaces of ZnO through phosphonic acid binding. *ACS Appl. Mater. Interfaces*, **2016**, *8*, 31392–31402.

[33] T. K. Claus, S. Telitel, A. Welle, M. Bastmeyer, A. P. Vogt, G. Delaittre, C. Barner-Kowollik. Light-driven reversible surface functionalization with anthracenes: visible light writing and mild UV erasing. *Chem. Commun.,* **2017**, *53*, 1599–1602.

[34] T. Pauloehrl, A. Welle, K. K. Oehlenschlaeger, C. Barner-Kowollik. Spatially controlled surface immobilization of nucleophiles via trapping of photo-generated thioaldehydes. *Chem. Sci.*, **2013**, *4*, 3503–3507.

General conclusion

Conclusion générale

Ce travail de thèse a été centré sur l'étude du TiW, un matériau fortement maitrisé par l'industrie de la nanoélectronique, mais encore très peu étudié en termes de fonctionnalisation de surface.

Nous avons dans un premier temps étudié la formation de différentes couches organiques sur un substrat de TiW plan et homogène : nous avons exploré dans quelles conditions il est possible de fonctionnaliser le TiW avec un cathécol, un silane, et un acide phosphonique. Nous nous sommes appuyés sur des analyses XRD, AFM, ATR-FTIR, XPS, ToF-SIMS pour caractériser le matériau et les couches organiques formées à sa surface. Le substrat de TiW a été systématiquement pré-traité par plasma oxygène, ce qui a simultanément supprimé une majorité des contaminants organiques de surface, et hydroxylé la surface du TiW. Après fonctionnalisation, des lavages progressifs dans de l'eau à 70°C ont été employés pour évaluer la robustesse des couches formées avec les trois types de molécules. Ces premiers travaux ont montré que les trois types de couches organiques présentent des stabilités différentes : après 15 min de lavage, environ 95 % de la couche de silane semble supprimée ; environ 70% de la couche d'acide phosphonique reste conservée et stable sur une heure de lavage ; la couche de dopamine se dégrade progressivement quand on poursuit les lavages sur une heure, et 50% de la dopamine fixée avant lavage reste présente après une heure de lavage.

La faible stabilité du silane utilisé semble attribuable à son caractère de silane monofonctionnel. Les couches de silane trifonctionnel immobilisées sur TiW sont décrites comme stables dans la littérature, mais l'emploi d'un silane lié à la surface du TiW par une seule liaison covalente, sans polymérisation latérale, conduit à une couche labile. Les liaisons Si-O-Ti ou Si-O-W semblent donc peu robustes.

Les couches d'acide phosphonique semblent mieux résister que les couches de silane. Cette stabilité peut être attribuée à la robustesse de l'interaction entre phosphonate et oxyde de tungstène, via la stabilité des liaisons P-O-Ti ou P-O-W.

La dopamine présente une stabilité intermédiaire entre silane et acide phosphonique. Nous faisons l'hypothèse que la dopamine est fixée sur forme de deux types de complexe avec la surface : un complexe monodentate et un complexe bidentate. Le complexe bidentate est considéré comme stable dans la littérature, alors que le complexe monodentate peut être progressivement désorbé de la surface par les lavages.

Nous nous sommes appuyés sur ces premiers résultats pour explorer la fonctionnalisation orthogonale de substrats de TiW recouverts d'autres matériaux. L'acide phosphonique présentant la meilleure affinité pour le TiW, nous avons mis en œuvre une fonctionnalisation de surfaces TiW+or, avec (1) un acide phosphonique d'une part, et (2) un alkythiol d'autre part. L'objectif était d'identifier (1) si l'acide phosphonique se fixe spécifiquement sur le TiW,

et pas sur l'or ; et (2) si l'alkythiol se fixe spécifiquement sur l'or, et pas sur TiW. Des analyses spectroscopiques ont été effectuées d'abord sur des substrats macroscopiques avec des zones de TiW et d'or dont la taille était de l'ordre du centimètre. Par la suite, nous avons élaboré sur substrat de TiW des motifs d'or d'une centaine de micromètre de taille caractéristique. Dans les deux cas, les caractérisations ont pu montrer que dans le cas (1) l'acide phosphonique est présent sur TiW, et non détectable sur or ; dans le cas (2) l'alkylthiol est présent sur or, et non détectable sur TiW. De cette manière, un premier niveau d'orthogonalité a été démontré. Il a été possible de capturer spécifiquement des carboxynanoparticules sur des motifs d'or fonctionnalisés par un thiol comportant une terminaison amine primaire. En milieu pH 7.4, les particules se sont spécifiquement fixées sur les zones d'or, comportant des amines protonées en surface. Les particules ont été environ dix fois moins adsorbées sur le TiW. Nous envisageons deux perspectives à ce travail: il s'agirait à terme de tester l'orthogonalité des réactions quand un mélange de thiol et d'acide phosphonique est utilisé pour fonctionnalisé le substrat TiW+or en une étape. Il s'agirait aussi de tester si la réduction en taille des motifs élaborés a un effet sur l'efficacité de la fonctionnalisation. Pour démontrer l'intérêt de fonctionnalisation de surface de nanotransducteurs, il sera nécessaire de tester la fonctionnalisation de motifs fabriqués à l'échelle nanométrique.

Enfin, nous avons étudié pour la première fois s'il est envisageable de mettre en œuvre trois réactions orthogonales avec trois molécules différentes, sur une surface composée de trois matériaux : TiW, or et silice. Dans ce travail, les surfaces TiW+or+silice ont été traitées avec respectivement (1) un acide phosphonique ; (2) un silane ; (3) un alkykthiol. Nous avons montré que dans nos conditions d'élaboration, il est possible de greffer sélectivement chacune des trois molécules sur un seul des trois matériaux, sans contaminer les autres matériaux : dans le cas (1) l'acide phosphonique se fixe seulement sur TiW ; dans le cas (2) le silane se fixe seulement sur la silice, après lavage à l'eau à 70°C ; dans le cas (3) le thiol se fixe seulement sur l'or. Ces résultats ont été obtenus à l'échelle macroscopique, et à l'échelle micronique. La suite envisagée pour ce travail consisterait d'abord à tester comment fonctionnaliser de manière séquentielle un même substrat TiW+or+silice avec un alkylthiol, un silane et un acide phosphonique. L'ordre des fonctionnalisations respectives et des lavages devrait être choisi en tenant compte des résultats de la présente thèse.

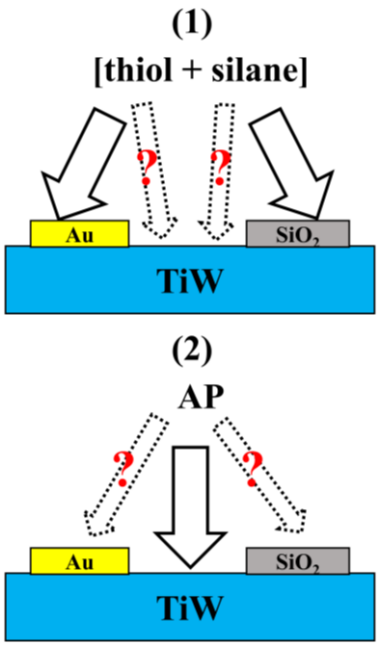

Figure C.1 Fonctionnalisation en deux étapes: mélange thiol+silane puis acide phosphonique.

Dans un deuxième temps, il s'agirait de tester s'il est possible de réduire le nombre d'étapes de fonctionnalisation. Il est problable qu'il est possible d'utiliser un mélange [alkylthiol+silane] pour mener une première réaction orthogonale, suivie d'un lavage à l'eau à 70°C pour désorber le silane de du TiW (Figure C.1). Il sera important de tester si le silane reste stable sur la silice avec ce lavage. L'acide phosphonique pourrait alors être déposé dans un deuxième temps pour se fixer sur TiW. Enfin, on pourra explorer comment se comporte un mélange des trois molécules [acide phosphonique + silane + thiol] dans un même solvant, pour fonctionnaliser en une étape une surface TiW+or+silice (Figure C.2). Comprendre comment acide phosphonique et silane entrent en compétition pour se fixer sur la silice serait un des enjeux de ce travail.

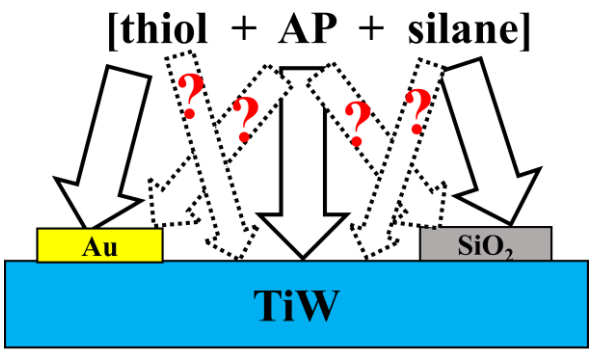

Figure C.2 Fonctionnalisation en une seule étape avec un mélange [thiol+silane+acide phosphonique].

Enfin, la suite de ce travail consistera à utiliser ce type de surfaces multimatériaux fonctionnalisées pour y greffer des biomolécules ou des nano-objets, en vue de réaliser des dispositifs avec de nouvelles propriétés.

Annexes

Annexes

A Characterization tools

A.1 Contact angle

The contact angle is based on the measure of the angle formed by a liquid drop on a solid surface in contact with a gas environment. The interfacial tension between the three phases should satisfy Young's equation:

$$\gamma_{SG} = \gamma_{SL} + \gamma_{LG} \cos\theta_C$$

Υ_{SG} is solid-gas interfacial tension, Υ_{SL} is solid-liquid interfacial tension, Υ_{LG} is liquid-gas interfacial tension and θ_c is contact angle (Figure A.1).

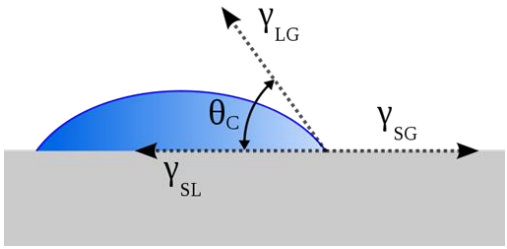

Figure A.1 Contact angle at liquid-gas-solid interface (source: wikipedia).

Contact angles are generally used for wettability studies. The liquid used in a contact angle experiment is often ultrapure water which interacts with the surface mostly by hydrogen binding. In this case, the smaller the contact angle is, the higher the hydrophilicity of the solid is. More generally, the use of distinct liquids may be useful to probe different interactions such as ionic or Van der Waals forces. The water wettability of a solid surface is related to the presence and composition of SAMs. Thus, contact angle measurements are usually used as the primary data to prove the success of the functionalization[1]–[3]. A simple setup for contact angle measurement is composed of a syringe to deposit a droplet of controlled volume onto surfaces and a camera to capture an image of the droplet and calculate the contact angle.

A.2 Ellipsometry

Ellipsometry is an optical technique for investigating the dielectric properties (complex refractive index or dielectric function) of thin films (Figure A.2). Ellipsometry does not directly measure optical constants, it measures the change of polarization upon reflection or transmission and compares it to a model. It is very sensitive to the change in the optical response of incident radiation that interacts with the material being investigated. After computer modeling, it could tell us the thickness of thin films, which can be used as a method for SAMs characterization. Ellipsometry is rarely used as the sole characterization method of

a SAM but rather followed by other spectroscopy (XPS, IR) to explore the chemical composition of the surface in more detail[2]–[4].

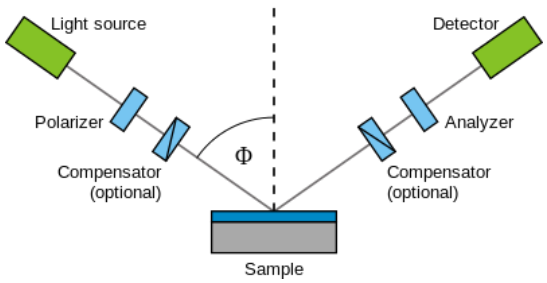

Figure A.2 Schematic setup of an Ellipsometry experiment.

A.3 XPS

X-ray photoelectron spectroscopy (XPS) is a sensitive and quantitative technique widely used to measure the elemental composition, chemical state and electronic state of the elements within a sample. The sample surface is exposed to photons (E_{photon}) in the X-ray range (typical Al K_α X-rays, E_{photon}=1486.6 eV). These photons interact with core-level electrons of the atom presents on the surface up to 10 nm depth. The excited photoelectrons expelled from the surface with different kinetic energies (E_k) depending on the binding energy (E_b). E_b is independent on the E_{photon} of the X-rays and only depends on its parent element and atomic energy level. The E_b of each of the emitted electrons can be determined by using an equation that is based on the work of Ernest Rutherford:

$$E_b = E_{photon} - (E_k + W)$$

W is the spectrometer work function, E_{photon} is determined by the X-rays source (1486.6 eV of Al K_α) and E_k is the measured kinetic energy. The XPS analyzer counts the number of photoelectrons at different Ek. The XPS analyzer counts the number of electrons (per unit time) reaching the detector with a given E_k. Thus the data are presented as a graph of relative intensity (counts/s) versus binding energy of electron, which is referred to as XPS spectrum (Figure A.3). Obviously, only electrons whose binding energy is inferior to the energy of the input X-ray photons can be detected. Three kinds of information can be obtained from XPS spectrum: (1) the nature of the elements within the 10 nm thickness of the surface based on binding energy of each peak; (2) the relative percentage of each element based on the peak area of the element; (3) the chemical or electronic state of the element based on the "chemical shift". So-called "chemical shift" refers to the fact that electrons at the same quantic state (same orbital) of the same element have slightly different binding energies depending on the chemical environment or electric state of the given atom. For example, the binding energy of C1s orbital of a carbon atom in an alkyl chain C-C-C (C1s peak around 284.6 eV) is different from that of C1s orbital of a carbon atom in a PEG chain C-C-O (C1s peak around 287.0 eV)[5]. The binding energy of C1s orbital of a carbon atom in an alkyl chain C-C-C (C1s

peak around 284.6 eV) is different from that of C1s orbital of a carbon atom in a carboxylic acid chemical group O=C-O (C1s peak around 289.0 eV)[6].

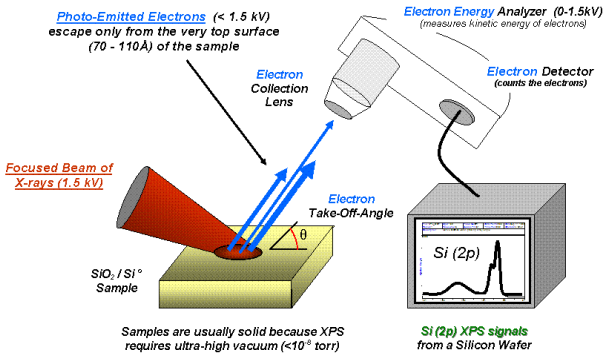

Figure A.3 Basic components of a XPS system (source: wikipedia).

A.4 AES

Auger electron spectroscopy (AES) is a common analytical technique used in the study of surfaces, which provides quantitative elemental and chemical state information from surfaces with the average depth of approximately 5 nm. AES is accomplished by exciting a surface with a finely focused electron beam (typically 2-10keV). Such electrons have sufficient energy to ionize all levels of the lighter elements, and higher core levels of the heavier elements. The Auger process is initiated by creation of a core hole. The ionized atom after the removal of the core hole electron is in a highly-excited state and will causing another electron falls from a higher level to fill an initial core hole by one of two routes: (1) emission of X-ray fluorescence; (2) causing another electron from a higher level emitted from the, which is called Auger electron. An electron energy analyzer is used to measure the energy of the emitted Auger electrons. From the kinetic energy and intensity of an Auger peak, the elemental identity and quantity of a detected element can be determined. In some cases chemical state information is available from the measured peak position and observed peak shape[7].

A.5 ToF-SIMS

Time-of-Flight Secondary Ion Mass Spectrometry (TOF-SIMS) provides elemental, chemical state and molecular information from surfaces of solid materials[8], [9]. It is a very sensitive (typically around 1-2nm depth) surface analysis method that can be used to characterize SAMs and monitor its formation kinetics. TOF-SIMS is accomplished by exciting a samples surface with a finely focused primary ion beam (ionized gold clusters or fullerenes), which causes secondary ions and ion clusters to be emitted from the samples surface. These secondary ions are then accelerated with a constant voltage onto a time-of-flight mass spectrometer that separates the different species according to their mass-to-charge ratio (m/z) which can be determined by computing the “time of flight”. A time-of-flight analyzer is used

to measure the exact mass of the emitted secondary ions. From the exact mass and intensity of the peaks, the identity of an element or molecular fragments can be determined. In addition, by grating a fine-focused ion beam over the surface, like an electron beam in an electron microprobe, mass resolved secondary ion images (chemical maps) can be obtained simultaneously.

A.6 IR spectroscopy

Infrared spectroscopy (IR) is used for qualitative identification of the presence of functional groups in organic and inorganic compounds[10]. It is based on the absorption of infrared photons by chemical bonds. Molecules are made up of atoms linked by chemical bonds. The vibration of a diatomic molecule can be approximated by the vibration of a spring with two spherical masses attached. This characteristic vibrations are called natural frequency of vibration. If the frequency of the applied IR radiation is identical to the natural frequency of bond vibration, some of the intensity of the light is absorbed by the bond. The intensity of the absorption is proportional to the magnitude of the dipole change. Thus, when a surface is on the optical pathway of the mid-infrared region (ca. $4000cm^{-1}$-$400cm^{-1}$), it will absorb part of the incident light at specific wavenumbers. By plotting the absorption of the sample versus the wavenumber of the light it can obtains the infrared spectrum of the surface with characteristic peaks of the different molecular bonds in the sample. The two fundamental vibrational modes found in mid-IR region are stretching ($4000cm^{-1}$-$1500cm^{-1}$), and bending vibrations (below $1500cm^{-1}$). These modes occur in different regions of the infrared spectra and therefore, relate to different vibrational energies. Stretching vibrations require more energy and occur at larger wavenumbers, usually toward the functional region. Bending vibrations occur at lower energy and are found at lower wavenumbers, usually toward the fingerprint region.

Instead, most IR spectrometers are Fourier-Transform Infrared Spectroscopy (FTIR) based on Michelson interferometer. In this configuration, the general layout of a spectrometer starts at its source. The high intensity, broad band source energy is projected into the Michelson interferometer. The interferometer consists of a beam splitter which reflects half of the energy to a stationary mirror and half to the moving mirror, creating thus constructive and destructive interferences on the beam that reaches the sample. The moving mirror scans back and forth producing a path length difference with respect to the stationary mirror. This path length difference is sampled in time with respect to the internal laser, allowing for the precise mirror position from scan to scan. The reflected beams then combine back at the beam splitter and are reflected into the sample compartment. The sample may absorb some of the modulated energy from the interferometer. The detector measures the intensity of the modulated energy to produce an interferogram. This interferogram is later translated into a spectrum by a Fourier Transformation, hence the name of the technique (Figure A.4). The spectral resolution is dependent on the amplitude of the moving mirror in the Michelson Interferometer.

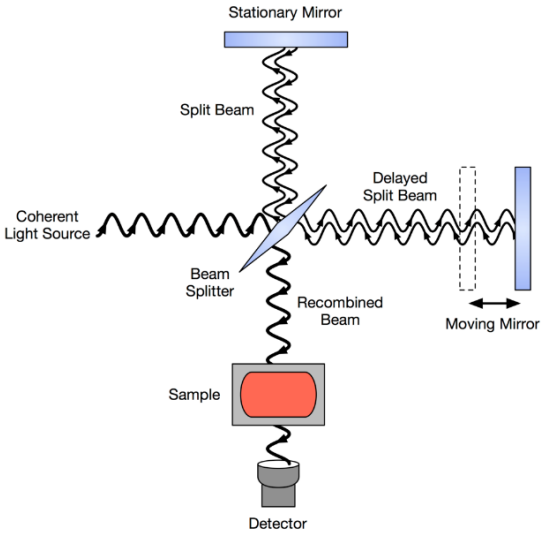

Figure A.4 Schematic diagram of FTIR (source: wikipedia).

A.7 ATR-FTIR

Attenuated total reflection (ATR) is a sampling technique used in conjunction with infrared spectroscopy which enables samples to be examined directly in the solid or liquid state without further preparation. IR beam is directed into a crystal of relatively higher refractive index (mostly >2). Then IR beam reflects from the internal surface of the crystal and creates an evanescent wave which projects orthogonally in to the sample in intimate contact with the ATR crystal. The evanescent waves penetrate the sample at each reflection point. Some of the energy of evanescent wave is absorbed by the sample and reflected radiation is returned to the detector (Figure A.5). Typical materials for ATR crystals include germanium, zinc selenide, and diamond. The shape of the crystal depends on the type of spectrometer and nature of the sample.

ATR generally allows qualitative or quantitative analysis of samples with little or no sample preparation, which greatly speeds sample analysis. The main benefit of ATR sampling comes from the very thin sampling path length and depth of penetration of the IR beam into the sample. This contrasts with FTIR sampling by transmission where the sample must be diluted with IR transparent salt, pressed into a pellet or pressed to a thin film, prior to analysis to prevent totally absorbing bands in the infrared spectrum. ATR is also very useful in determining the SAMs grafted on a surface. For examples, SAMs of phosphonates on metal oxides could be evidenced[11], [12].

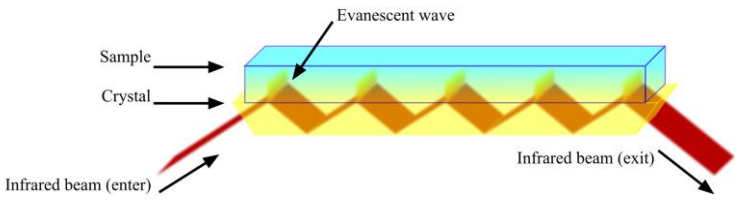

Figure A.5 A multiple reflection ATR system (source: wikipedia).

A.8 PM-IRRAS

Polarization Modulation-Infrared Reflection-Adsorption Spectroscopy (PM-IRRAS) is a surface sensitive spectroscopy technique for studying thin films or monolayer on metallic substrate[13]–[15]. The advantage of PM-IRRAS is that it makes the characterization of single molecule layers and molecule orientation possible. In addition, the interfering effect of water vapor and CO_2 can fairly be eliminated.

In fact, there is difference in reflectivity of interfaces for p-polarized (perpendicular to surface) and s-polarized (planar to surface) light. The phase shift of the s-polarized light is nearly 180° for all the angles of incidence, the net amplitude of this IR radiation is nearly zero on the surface so this polarization is not sensitive to the substrate surface. In contrast, the phase shift of the p-polarized light depends upon the angle of incidence and the net amplitude of the field usually shows a maximum at grazing incidence angle (Figure A.6). However, the instrument noise, CO_2 and water interference make it difficult to extract signals. In a typical PM-IRRAS setup, the incident beam is polarized by a ZnSe photo elastic modulator (PEM), which switched the polarization from p to s at a high frequency. It allows the acquisition of two signals simultaneously: the sum (R_p+ R_s) and difference ($|R_p$-$R_s|$) reflectivity. The difference of two reflectivity provides the surface feature information. The modulated reflectivity is independent on the isotropic adsorption from gas or bulk water. By taking the ratio of these two signals: $\frac{\Delta R}{R} = (R_p - R_s)/(R_p + R_s)$ one could obtain a spectrum of the surface without the contribution of isotropic absorptions from the environment, having a better surface-sensitivity without the need of acquiring a background spectrum.

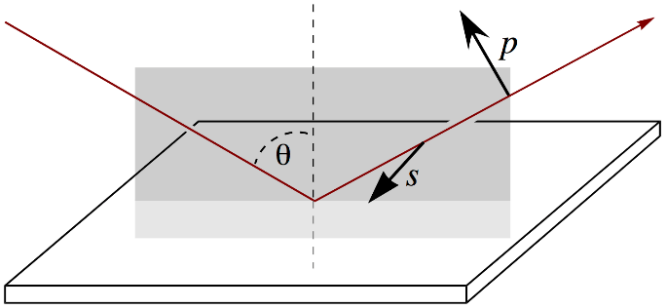

Figure A.6 Schematic illustration of the p and s polarization radiation (source: wikipedia).

A.9 Raman

Raman spectroscopy is a spectroscopic technique used to observe vibrational, rotational, and other low-frequency modes in solid, liquid and gaseous samples. Raman spectroscopy is commonly used in chemistry to provide vibration modes of chemical bonds by which molecules can be identified[16]. Raman spectroscopy is a spectroscopic technique based on inelastic scattering of infrared photons, usually from a laser source. The laser light interacts with molecules, resulting in the energy of the laser photons being changed and shifted up or

down, which is called Raman scattering. The shift in energy gives information about the vibrational modes in the molecules. Surface-enhanced Raman spectroscopy (SERS) is an important development of advanced Raman spectroscopy that can be very useful in the characterization of SAMs[17], [18]. SERS enhances Raman scattering by molecules adsorbed on metal surfaces or by nanostructures such as plasmonic hot spots, which may detect single molecules.

A.10 AFM

Atomic force microscopy (AFM) is a high-resolution scanning probe microscopy. AFM has been widely used for surface study. It can work on different kinds of materials, while STM requires conducting surfaces. Furthermore, it can be performed under normal pressure and different conditions (vacuum, air or liquid), while SEM need to be operated under high vacuum. AFM is constructed by a microscopic cantilever with a nanoscale tip (silicon, silicon oxide or silicon nitride) used to scan sample surfaces. The cantilever is tens to hundreds of micrometers in size, whose height is controlled by piezoelectric materials and its deflection is monitored by a laser beam and photodiode (Figure A.7).

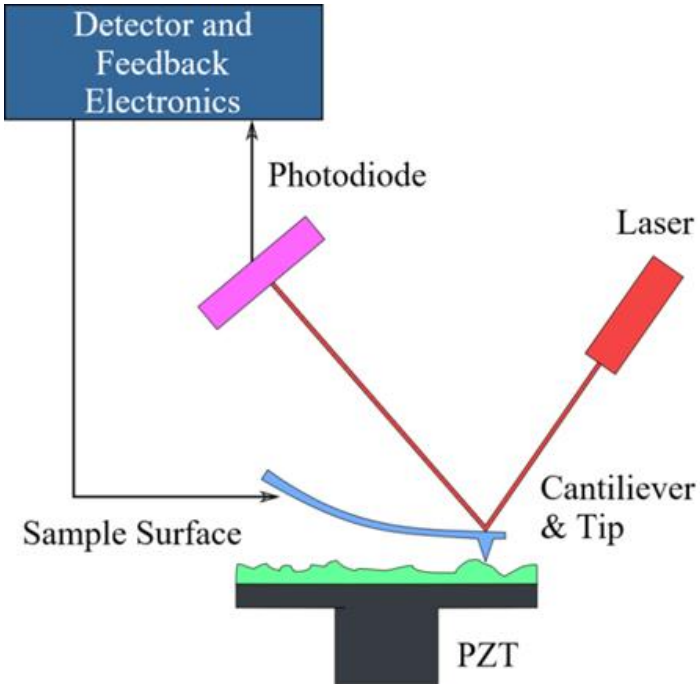

Figure A.7 Atomic force microscopy (source: wikipedia).

The working modes of AFM are contact mode and tapping mode. In contact mode, the tip contacts the surface and the topography of the surface is obtained from its deflection when it moves on the sample surface all the time. In tapping mode, the tip does not contact the surface, but is set to oscillate near its resonant frequency above the surface. The topography of the surface is obtained from changes in the amplitude of oscillations when the tip moves over the sample surface. In both cases, instead of measuring directly the deflection or change in amplitude of the oscillations, AFM is usually set-up to maintain these parameters constant by

a feedback loop, so that it is the signal necessary to maintain them that, indirectly, gives the topography of the surface. AFM has been widely used to characterize different SAMs[19]–[21].

A.11 STM

With the advent of the scanning tunneling microscope (STM) in the 1980s (Gerd Binnig and Heinrich Rohrer at IBM Zürich), it has become feasible to explore in real space the surfaces at the atomic. A STM is 0.1 nm lateral resolution and 0.01 nm depth resolution. With this resolution, individual atoms within materials could be routinely imaged and manipulated. The basic principle of an STM is based on the concept of quantum tunneling. When a voltage bias is applied and a sharp metal tip is brought close (3-5 Å) to the sample surface, an overlap occurs between the tip and sample wave functions, decaying exponentially into the junction gap. The bias voltage V_t can allow electrons to tunnel through the vacuum between them. The resulting tunneling current is a function of tip position, applied voltage, and the local density of states of the sample. Information is obtained by monitoring the current with the tip position scans across the surface, and is usually displayed in image form (Figure A.8).

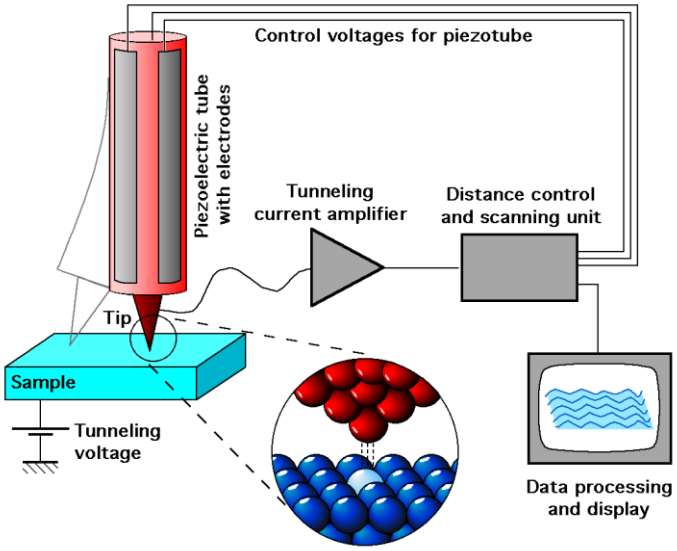

Figure A.8 Scanning tunneling microscope (source: wikipedia).

STM has been widely used to well characterize metal surfaces such as alkanethiol SAMs on gold, which has special advantage for the early fundamental studies of SAMs formation showing evidence of different low coverage and high coverage phases and crystalline arrangements as well as defects[19], [22]–[25].

A.12 TERS

Tip-enhanced Raman spectroscopy (TERS) relies on the enhancement and spatial confinement of light in the close vicinity of the point of a plasmonic sharp tip, typically coated with gold. TERS is the combination of Raman Spectroscopy and a suitable scanning

probe microscopy, such as AFM or STM (Figure A.9)[26]. By raster scanning the tip of microscopy, it can obtain nanoimages with high spatial resolution. Indeed, a far-field beam is coupled to a tip to irradiate only a tiny region (ca. 10nm x 10nm) of the sample that delivers extremely high spatial resolution in nanoimaging. TERS is promising because it combines unique spatial resolution with spectral signatures for identification of different molecules. J. Stadler et al. shows TERS can clearly distinguish domains of different thiolate isomers deposited on a surface through microcontact printing and back-filling[27].

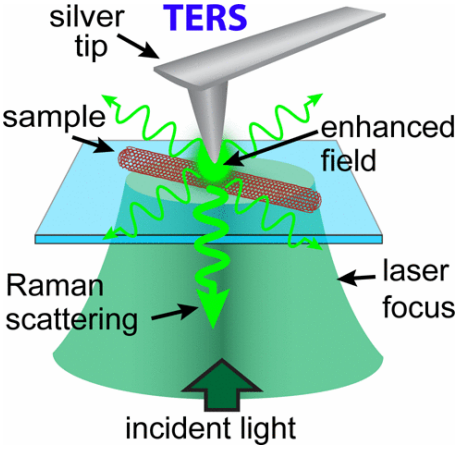

Figure A.9 Tip-enhanced Raman spectroscopy[26].

B Pattern fabrication

B.1 Lithography

The current evolution of nanotechnology stresses the importance of patterned substrates with different materials. Patterned substrates has many photoelectronic or bioelectronic applications such as localized surface plasmon resonance biosensors[28] and colloidal nano-objects trapping[29]. Lithography is the most widespread technique in micro and nanofabrication to allow the patterned substrates with different micro and nanostructures[30]–[33]. Lithography is the transfer of geometric shapes on a mask to a smooth surface. In modern manufacturing, photolithography uses UV radiation to image the mask on a substrate using photoresist layers. Other methods are electron beam, focused ion beam, and scanning probe lithography. In the following paragraphs, we will briefly present UV lithography and the materials and methods used during this work. This work has been possible thanks to NanoLyon platform at INL.

B.2 UV lithography

UV lithography is perhaps the most commonly used photolithography technique in operation today. UV lithography is mainly used for large-scale, high-throughput and low-resolution patterns. The main advantage of photolithography is that many microstructures over a large area (several cm^2) can be exposed simultaneously. However, resolution is limited by

diffraction, so that photolithography is mainly employed for typical sizes over 1µm. As the name implies, the crux of UV lithography centers around the properties and attributes of UV light (λ = 300nm-400nm). UV light is shined through a mask onto a photoresist covered wafer. The mask stops some of the light from proceeding onto the resist covered surface. This allows the motif on the mask to be transferred to the photoresist. An overview of UV lithography is in Figure B.1.

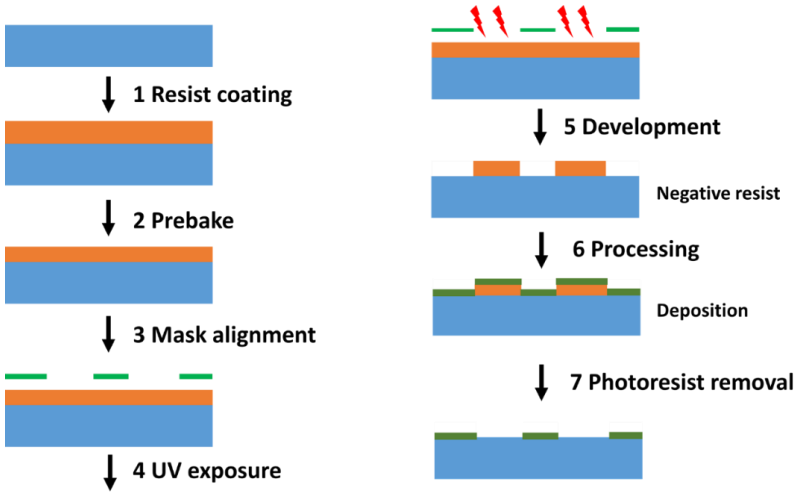

Figure B.1 UV lithography process.

1 Resist coating: Photoresist is deposited by spin coating on the substrate. Simply put, the substrate is spun rapidly inside a vacuum, while being coated with the photoresist. The photoresist bonds uniformly to the surface, with the excess flying off during spinning.

2 Prebake: The prebake is a simple process of heating the surface in a convection oven or through a heated plate placed below the surface. The purpose of prebake is to evaporate the coating solvent and to densify the resist after spin coating.

3 Mask alignment: A photomask is a desired pattern that can be transferred onto a surface by means of light waves. The mask creates a sort of shadow between the light and the surface. Less light passes through sections blocked by the mask. The mask must be aligned correctly in reference to the surface. This procedure is accomplished by hand using certain marks on the mask and the surface, or by using an automatic pattern recognition device.

4 UV exposure: The photoresist, surface, and mask are subjected to UV light via a UV lamp.

5 Development: During the development stage, chemicals are applied to the surface causing either a positive photoresist reaction or a negative photoresist reaction.

6 Processing: The openings created in the resist are then used for processing. There are two primary techniques for patterning additive and subtractive processes. (1) Etch back: photoresist is applied overtop of the layer to be patterned and unwanted material is etched away. (2) Lift off: patterned layer is deposited over top of the photoresist and unwanted material is lifted off when resist is removed.

7 Photoresist removal: Photoresists are removed from the substrates. Simple solvents are generally sufficient for polymers whose solubility in a developer (basic solvent). Plasma etching with O_2 is also effective for removing organic polymer.

B.3 Materials and methods used during this work

This section presents the protocols used for the top-down substrate patterning: Au/TiW and Au/SiO_2/TiW. All the processes were conducted at INL Nanolyon platform with the help of Radoslaw Mazurczyk or Christelle Yeromonahos.

(1) Au/TiW patterned substrate

(a) Photolithography

1. Spin-coat the AZ 5214 (negative) resist at 5500 rpm for 30 s.
2. Bake at 110 °C for 60 s.
3. Expose to UV through mask for 4 s.
4. Bake at 110 °C for 90s.
5. Expose whole sample (flood exposure) to UV for 30s.
6. Develop in TMAH (Metal-Ion Free (MIF) 726) for 60 s under constant agitation.
7. Stop development by soaking in ultrapure water.

(b) Gold deposition

Gold e-beam evaporation was conducted in a Leybold© e-beam evaporator.

1. Introduce sample in evaporation chamber and pump to a pressure of 1.5×10^{-6} Torr (27 K).
2. Switch on the cooling system.
3. Deposition of chromium adhesion layer.

(a) Set voltage to 6 kV.
(b) Increase current until the deposition rate, monitored by a QCM, reaches ca. 1Å=s (a cache is “hiding” the substrate so far so that no deposition occurs on it).
(c) Remove cache and wait until the deposited layer reaches 2-3 nm thickness.
(d) Place cache back, decrease current slowly to 0, switch off voltage and wait for the socket containing the chromium to cool down.
(e) Change socket to the one containing the gold.

4. Deposition of gold layer.

(a) Set voltage to 6 kV.
(b) Increase current until the deposition rate, monitored by a QCM, reaches ca. 2Å=s (a cache is “hiding” the substrate so far so that no deposition occurs on it).
(c) Remove cache and wait until the deposited layer reaches 45-50 nm thickness.
(d) Place cache back, decrease current slowly to 0, switch off voltage and wait for the socket to cool down.

(c) Lift off

The deposited substrates were cleaned with acetone until all the remained resist lift off from substrates.

(2) **Au/SiO_2/TiW patterned substrate.**

(a) First photolithography

1. Spin-coat the AZ 5214 (negative) resist at 5500 rpm for 30 s.
2. Bake at 110 °C for 60 s.
3. Expose to UV through mask (Figure B.2) for 4 s.
4. Bake at 110 °C for 90 s.
5. Expose whole sample (flood exposure) to UV for 30 s.
6. Develop in TMAH (Metal-Ion Free (MIF) 726) for 60s under constant agitation.
7. Stop development by soaking in ultrapure water.

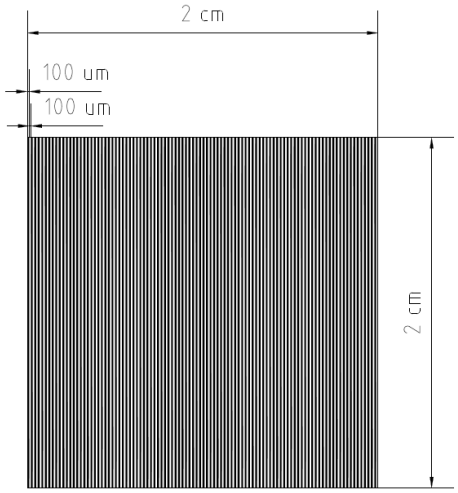

Figure B.2 Mask for photolithography.

(b) Gold deposition

Gold e-beam evaporation was conducted in a Leybold© e-beam evaporator.

1. Introduce sample in evaporation chamber and pump to a pressure of 1.5×10^{-6} Torr (27 K).
2. Switch on the cooling system.
3. Deposition of chromium adhesion layer.

(a) Set voltage to 6 kV.

(b) Increase current until the deposition rate, monitored by a QCM, reaches ca. 1Å=s (a cache is “hiding” the substrate so far so that no deposition occurs on it).

(c) Remove cache and wait until the deposited layer reaches 2-3 nm thickness.

(d) Place cache back, decrease current slowly to 0, switch off voltage and wait for the socket containing the chromium to cool down.

(e) Change socket to the one containing the gold.

4. Deposition of gold layer.

(a) Set voltage to 6 kV.

(b) Increase current until the deposition rate, monitored by a QCM, reaches ca. 2Å=s (a cache is "hiding" the substrate so far so that no deposition occurs on it).

(c) Remove cache and wait until the deposited layer reaches 45-50 nm thickness.

(d) Place cache back, decrease current slowly to 0, switch off voltage and wait for the socket to cool down.

(c) Lift off

The deposited substrates were cleaned with acetone until all the remained resist lift off from substrates.

(d) Second photolithography

1. Spin-coat the AZ 5214 (negative) resist at 5500 rpm for 30 s.
2. Bake at 110 °C for 60 s.
3. Expose to UV through mask (Rotate 90 degrees) for 4 s.
4. Bake at 110 °C for 90 s.
5. Expose whole sample (flood exposure) to UV for 30 s.
6. Develop in TMAH (Metal-Ion Free (MIF) 726) for 60s under constant agitation.
7. Stop development by soaking in ultrapure water.

(e) SiO_2 sputtering

SiO_2 was deposited by magnetron sputtering (AC450, Ar 42.7 sccm, O_2 7.5 sccm, RF power 70W, V_{bias} 140V, 5 x 10^{-3} mbar). Two-steps photolithography and materials deposition process are shown in Figure B.3.

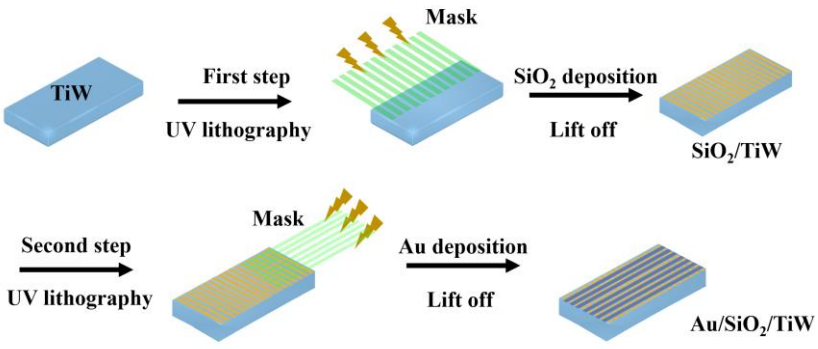

Figure B.3 Two-steps photolithography and materials deposition process.

(f) Lift off

The deposited substrates were cleaned with acetone until all the remained resist lift off from substrates.

C References

[1] M. Lestelius, B. Liedberg, P. Tengvall. In vitro plasma protein adsorption on ω-functionalized alkanethiolate self-assembled monolayers. *Langmuir*, **1997**, *13*, 5900–5908.

[2] H. F. Chieh, F. C. Su, J. D. Liao, S. C. Lin, C. W. Chang, M. R. Shen. Attachment and morphology of adipose-derived stromal cells and exposure of cell-binding domains of adsorbed proteins on various self-assembled monolayers. *Soft Matter*, **2011**, *7*, 3808–3817.

[3] S. V. Atre, B. Liedberg, D. L. Allara. Chain length dependence of the structure and wetting properties in binary composition monolayers of OH- and CH_3-terminated alkanethiolates on gold. *Langmuir*, **1995**, *11*, 3882–3893.

[4] M. D. Porter, T. B. Bright, D. L. Allara, C. E. D. Chidsey. Spontaneously organized molecular assemblies. 4. Structural characterization of n-alkyl thiol monolayers on gold by optical ellipsometry, infrared spectroscopy, and electrochemistry. *J. Am. Chem. Soc*., **1987**, *109*, 3559–3568.

[5] L. Li, S. Chen, J. Zheng, B. D. Ratner, S. Jiang. Protein adsorption on oligo(ethylene glycol)-terminated alkanethiolate self-assembled monolayers: the molecular basis for nonfouling behavior. *J. Phys. Chem. B*, **2005**, *109*, 2934–2941.

[6] A. Manakhov, P. Kiryukhantsev-Korneev, M. Michlíček, E. Permyakova, E. Dvořáková, J. Polčák, Z. Popov, M. Visotinef, D. V. Shtansky. Grafting of carboxyl groups using CO_2/C_2H_4/ Ar pulsed plasma: theoretical modeling and XPS derivatization. *Appl. Surf. Sci.*, **2018**, *435*, 1220–1227.

[7] S. N. Raman, L. LaVanier, J. Moskito, D. Madamba. Auger electron spectroscopy - history and applications in materials characterization with emphasis on medical devices. *Microsc. Microanal.*, **2018**, *24*, 1030–1031.

[8] L. Houssiau, P. Bertrand. ToF–SIMS study of organosilane self-assembly on aluminum surfaces. *Appl. Surf. Sci.*, **2001**, *175–176*, 351–356.

[9] L. Houssiau, P. Bertrand. TOF–SIMS study of alkanethiol adsorption and ordering on gold. *Appl. Surf. Sci.*, **2001**, *175–176*, 399–406.

[10] B. Stuart. Infrared spectroscopy. *Kirk-Othmer Encyclopedia of Chemical Technology*, **2015**, 1–18.

[11] C. Luengo, M. Brigante, J. Antelo, M. Avena. Kinetics of phosphate adsorption on goethite: Comparing batch adsorption and ATR-IR measurements. *J. Colloid Interface Sci.*, **2006**, *300*, 511–518.

[12] S. J. Parikh, J. Chorover. ATR-FTIR spectroscopy reveals bond formation during bacterial adhesion to iron oxide. *Langmuir*, **2006**, *22*, 8492–8500.

[13] M. Gliboff, L. Sang, K. M. Knesting, M. C. Schalnat, A. Mudalige, E. L. Ratcliff, H. Li, A. K. Sigdel, A. J. Giordano, J. J. Berry, D. Nordlund, G. T. Seidler, J. L. Brédas, S. R. Marder, J. E. Pemberton, D. S. Ginger. Orientation of phenylphosphonic acid self-assembled monolayers on a transparent conductive oxide: a combined NEXAFS, PM-IRRAS, and DFT Study. *Langmuir*, **2013**, *29*, 2166–2174.

[14] H. Lavoie, B. Desbat, D. Vaknin, C. Salesse. Structure of rhodopsin in monolayers at the air-water interface: a PM-IRRAS and X-ray reflectivity study. *Biochemistry (Mosc.)*, **2002**, *41*, 13424–13434.

[15] M. A. Ramin, G. Le Bourdon, N. Daugey, B. Bennetau, L. Vellutini, T. Buffeteau. PM-IRRAS investigation of self-assembled monolayers grafted onto SiO_2/Au substrates. *Langmuir*, **2011**, *27*, 6076–6084.

[16] L. Opilik, T. Schmid, R. Zenobi. Modern Raman imaging: vibrational spectroscopy on the micrometer and nanometer scales. *Annu. Rev. Anal. Chem.*, **2013**, *6*, 379–398.

[17] C. Blum, T. Schmid, L. Opilik, S. Weidmann, S. R. Fagerer, R. Zenobi. Understanding tip-enhanced Raman spectra of biological molecules: a combined Raman, SERS and TERS study. *J. Raman Spectrosc.*, **2012**, *43*, 1895–1904.

[18] T. Schmid, L. Opilik, C. Blum, R. Zenobi. Nanoscale chemical imaging using tip-enhanced Raman spectroscopy: a critical review. *Angew. Chem. Int. Ed.*, **2013**, *52*, 5940–5954.

[19] S. Chen, L. Li, C. L. Boozer, S. Jiang. Controlled chemical and structural properties of mixed self-assembled monolayers of alkanethiols on Au (111). *Langmuir*, **2000**, *16*, 9287–9293.

[20] K. Tamada, M. Hara, H. Sasabe, W. Knoll. Surface phase behavior of n-alkanethiol self-assembled monolayers adsorbed on Au (111): an atomic force microscope study. *Langmuir*, **1997**, *13*, 1558–1566.

[21] F. Tantakitti, J. Burk-Rafel, F. Cheng, R. Egnatchik, T. Owen, M. Hoffman, D. N. Weiss, D. M. Ratner. Nanoscale clustering of carbohydrate thiols in mixed self-assembled monolayers on gold. *Langmuir*, **2012**, *28*, 6950–6959.

[22] T. Sawaguchi, Y. Sato, F. Mizutani. In situ STM imaging of individual molecules in two-component self-assembled monolayers of 3-mercaptopropionic acid and 1-decanethiol on Au (111). *J. Electroanal. Chem.*, **2001**, *496*, 50–60.

[23] G. Xu, D. P. Woodruff, N. Bennett, M. Elliott, J. E. Macdonald. STM study of molecule double-rows in mixed self-assembled monolayers of alkanethiols. *Langmuir*, **2010**, *26*, 8174–8179.

[24] R. K. Smith, S. M. Reed, P. A. Lewis, J. D. Monnell, R. S. Clegg, K. F. Kelly, L. A. Bumm, J. E. Hutchison, P. S. Weiss. Phase separation within a binary self-assembled monolayer on Au (111) driven by an amide-containing alkanethiol. *J. Phys. Chem. B*, **2001**, *105*, 1119–1122.

[25] P. A. Lewis, R. K. Smith, K. F. Kelly, L. A. Bumm, S. M. Reed, R. S. Clegg, J. D. Gunderson, J. E. Hutchison, P. S. Weiss. The role of buried hydrogen bonds in self-assembled mixed composition thiols on Au (111). *J. Phys. Chem. B*, **2001**, *105*, 10630–10636.

[26] P. Verma. Tip-enhanced Raman spectroscopy: technique and recent advances. *Chem. Rev.*, **2017**, *117*, 6447–6466.

[27] J. Stadler, T. Schmid, L. Opilik, P. Kuhn, P. S. Dittrich, R. Zenobi. Tip-enhanced Raman spectroscopic imaging of patterned thiol monolayers. *Beilstein J. Nanotechnol.*, **2011**, *2*, 509–515.

[28] S. S. Aćimović, M. P. Kreuzer, M. U. González, R. Quidant. Plasmon near-field coupling in metal dimers as a step toward single-molecule sensing. *ACS Nano*, **2009**, *3*, 1231–1237.

[29] F. Palazon, V. Monnier, Y. Chevolot, É. Souteyrand, J. P. Cloarec. Nanotraps: different approaches for the precise placement of micro and nano-objects from a colloidal dispersion onto nanometric scale sites of a patterned macroscopic surface. *J. Colloid Sci. Biotechnol.*, **2013**, *2*, 249–262.

[30] J. Melngailis, A. A. Mondelli, I. L. Berry, R. Mohondro. A review of ion projection lithography. *J. Vac. Sci. Technol. B Microelectron. Nanometer Struct. Process. Meas. Phenom.*, 1998, 16, 927–957.

[31] Y. Xia, G. M. Whitesides. Soft Lithography. *Angew. Chem. Int. Ed.*, **1998**, *37*, 550–575.

[32] S. Y. Chou, P. R. Krauss, P. J. Renstrom. Imprint lithography with 25-nanometer resolution. *Science*, 1996, 272, 85–87.

[33] B. Wu, A. Kumar. Extreme ultraviolet lithography: A review. *J. Vac. Sci. Technol. B Microelectron. Nanometer Struct. Process. Meas. Phenom.*, **2007**, *25*, 1743–1761.

Jian ZHANG

Email: jian.zhang@doctorant.ec-lyon.fr
jianzhang_ecl@163.com
Tel: +33 6 65 61 13 10
Address: 36 Avenue Guy de Collongue, 69134 Ecully Cedex, France

Education

10/2015 - 11/2018: PhD in Materials Chemistry
University of Lyon, Ecole Centrale de Lyon (ECL), Institut des Nanotechnologies de Lyon (INL), UMR CNRS 5270, Ecully, France.

09/2012 - 07/2015: MSc in Materials Science
National Center for Nanoscience and Technology (NCNST), Beijing Institute of Nanoenergy and Nanosystems (BINN), Chinese Academy of Sciences, Beijing, China.

09/2008 - 07/2012: BSc in Materials Science and Engineering
Northwestern Polytechnical University (NPU), Xi'an, China.

Research experience

10/2015 - 11/2018: PhD thesis: Orthogonal chemical functionalization of titanium tungsten (TiW) based multi-material surfaces. University of Lyon, Ecole Centrale de Lyon (ECL), Institut des Nanotechnologies de Lyon (INL).

09/2012 - 07/2015: MSc thesis: Electrochemical biosensors based on hybrid nanomaterials/ graphite microfiber electrodes. National Center for Nanoscience and Technology (NCNST), Beijing Institute of Nanoenergy and Nanosystems (BINN).

01/2012 - 07/2012: BSc research internship: Separation behavior study of Al-Cu-Mn alloy during solid-solution aging treatment in Materials Science and Engineering. Northwestern Polytechnical University (NPU).

Publications

Manuscripts in preparation:

(1) **J. Zhang**, C. Yeromonahos, D. Léonard, T. Géhin, C. Botella, G. Grenet, A. Benamrouche, J. Penuelas, S. Monfray, Y. Chevolot, J. P. Cloarec. Surface chemical functionalization of titanium tungsten substrate with silane, phosphonic acid or ortho-dihydroxyaryl based organolayers.

(2) **J. Zhang**, D. Léonard, R. Mazurczyk, C. Yeromonahos, V. Monnier, T. Géhin, S. Monfray, Y. Chevolot, J. P. Cloarec. Orthogonal chemical functionalization of patterned Au/TiW substrate for selective immobilization of nanoparticles.

(3) **J. Zhang**, C. Yeromonahos, R. Mazurczyk, D. Léonard, T. Géhin, S. Monfray, Y. Chevolot, J. P. Cloarec. Orthogonal chemical functionalization of Au/SiO_2/TiW patterned substrates.

Published papers:

(1) **J. Zhang**, A. Li, X. Yu, W. Guo, Z. Zhao, J. Qiu, X. Mou, J. P. Claverie, H. Liu. Scaly graphene oxide/graphite fiber hybrid electrodes for DNA biosensor. *Advanced Materials Interfaces*, 2015, **2**, 1500072.

(2) **J. Zhang**, X. Yu, W. Guo, J. Qiu, X. Mou, A. Li, H. Liu. Construction of titanium dioxide nanorod/graphite microfiber hybrid electrodes for high performance electrochemical glucose biosensor. *Nanoscale*, 2016, **8**, 9382.

(3) A. Li, **J. Zhang** (contributed equally), J. Qiu, Z. Zhao, C. Wang, C. Zhao, H. Liu. A novel aptameric biosensor based on the self-assembled DNA–WS_2 nanosheet architecture. *Talanta*, 2017, **163**, 78.

(4) X. Yu, **J. Zhang** (contributed equally), Z. Zhao, W. Guo, J. Qiu, X. Mou, A. Li, J. P. Claverie, H. Liu. NiO-TiO_2 p–n heterostructured nanocables bridged by zero-bandgap rGO for highly efficient photocatalytic water splitting. *Nano Energy*, 2015, **16**, 207.

(5) A. Li, **J. Zhang**, X. Yu, J. Li, J. Qiu, Z. Zhao, W. Guo, J. P. Claverie, X. Mou, H. Liu. An impedimetric-fluorescence double-checking biosensor with enhanced reliability based on graphene oxide. *Advanced Materials Interfaces*, 2015, **2**, 1500279.

(6) X. Yu, Z. Zhao, **J Zhang**, W Guo, L Li, H Liu, Z. Wang. One-step synthesis of ultrathin nanobelts-assembled urchin-like anatase TiO_2 nanostructures for highly efficient photocatalysis. *CrystEngComm*, 2017, **19**, 129.

(7) X. Yu, Z Zhao, **J Zhang**, W Guo, J Qiu, D Li, Z Li, X Mou, L Li, A Li, H Liu Rutile nanorod/anatase nanowire junction array as both sensor and power supplier for high-performance, self-powered, wireless UV photodetector. *Small*, 2016, **12**, 2759.

(8) X. Yu, L. Wang, **J. Zhang**, W. Guo, Z. Zhao, Y. Qin, X. Mou, A. Li, H. Liu. Hierarchical hybrid nanostructures of Sn_3O_4 on N doped TiO_2 nanotubes with enhanced photocatalytic performance. *J. Mater. Chem. A*, 2015, **3**, 19129.

(9) X. Yu, X. Han, Z. Zhao, **J. Zhang**, W. Guo, C. Pan, A. Li, H. Liu, Z. Wang. Hierarchical TiO_2 nanowire/graphite fiber photoelectrocatalysis setup powered by a wind-driven nanogenerator: a highly efficient photoelectrocatalytic device entirely based on renewable energy. *Nano Energy*, 2015, **11**, 19.

(10) S. Wang, J. Qiu, W. Guo, X. Yu, J. Nie, **J. Zhang**, X. Zhang, Z. Liu, X. Mou, L. Li, H. Liu. A nanostructured molybdenum disulfide film for promoting neural stem cell neuronal differentiation: toward a nerve tissue-engineered 3D scaffold. *Advanced Biosystems*, 2017, **1**, 1600042.

Conference and Workshops

- **J. Zhang**, C. Yeromonahos, D. Léonard, R. Mazurczyk, T. Géhin, S Monfray, Y. Chevolot, J. P. Cloarec. *Journees du groupe de recherche bio-ingenierie des interfaces*, **Oral** presentation (25-26, June, 2018, Besançon, France).
- **J. Zhang**, C. Yeromonahos, D. Léonard, R. Mazurczyk, V. Monnier, T. Géhin, S. Monfray, Y. Chevolot, J. P. Cloarec. *8th International Colloids Conference*, **Young Investigator Perspectives Oral** presentation (10-13, June, 2018, Shanghai, China).
- **J. Zhang**, Y. Chevolot, C. Yeromonahos, C. Botella, G. Grenet, T. Géhin, A. Benamrouche, J. Penuelas, D. Léonard, S. Monfray, J. P. Cloarec. *Journees du groupe de recherche bio-ingenierie des interfaces*, **Poster** presentation (27-28, June, 2017, Bordeaux, France).
- Workshop "XPS analysis: from measurements to scientific answers" (26-30, September, 2016, Roscoff, France).
- **J. Zhang**, X. Yu, W. Guo, Z. Zhao, J. Qiu, A. Li, H. Liu. *First International Conference on Nanoenergy and Nanosystems*, **Poster** presentation (08-10, December, 2014, Beijing, China).

dernière page de la thèse

AUTORISATION DE SOUTENANCE

Vu les dispositions de l'arrêté du 25 mai 2016,

Vu la demande des directeurs de thèse

Messieurs J-P. CLOAREC et Y. CHEVOLOT

et les rapports de

Mme C. JOLIVALT
Professeur - Laboratoire de Réactivité de Surfaces - UMR 7197 Sorbonne Université-CNRS - UPMC - 4 place Jussieu - 75005 PARIS

et de

M. L. VELLUTINI
Maître de Conférences HDR - Institut des Sciences Moléculaires - Université de Bordeaux - Bâtiment A12 - 351 cours de la libération - 33405 TALENCE

Monsieur ZHANG Jian

est autorisé à soutenir une thèse pour l'obtention du grade de **DOCTEUR**

Ecole doctorale MATERIAUX

Fait à Ecully, le 6 novembre 2018

P/Le directeur de l'E.C.L.
La directrice des Etudes

ECOLE CENTRALE DE LYON
Service Scolarité
ECULLY

M-A. GALLAND

Abstract: The development of nanotechnologies makes it possible to manufacture the micro or nanometric-sized patterns with various materials (dielectrics, metals, semiconductors). These heterogeneous surfaces are commonly used in the electronics industry for the production of nanoelectronic structures and components: transistors, memories or sensors. The concept of orthogonal chemical functionalization was first proposed by George M. Whitesides to modify the surfaces composed of different materials at the macroscopic scale. In this context, this PhD work aimed at exploring the orthogonal chemical functionalization approach on a predefined patterned titanium tungsten (TiW) surface by lithography producing. Pattern materials (Au, SiO_2) are chosen to have different chemical properties, which can be functionalized with completely independent reactions. To achieve this aim, we have studied three different chemical groups for the formation of organolayers (silane, catechol, phosphonic acid) on TiW for the first time. The three layers were characterized (XPS, IR, ToF-SIMS) and the stability of the formed organolayers was also addressed. Then we developed and ascertained the orthogonal chemical functionalization of patterned Au/TiW and Au/SiO_2/TiW surfaces. It proposes a novel strategy for the orthogonal functionalization on a triple-material patterned surface. In addition, the capture of nanoparticles by electrostatic interaction at specific location on Au/TiW patterned substrate was successfully implemented to prove the interest of such method for colloids trapping.

Keywords: TiW; Au/TiW; Au/SiO_2/TiW; orthogonal chemical functionalization.

Résumé: Avec le développement de nouveaux dispositifs apparait le besoin d'être capable de contrôler la chimique de surfaces de substrats multi-échelle et multi-matériaux. Plusieurs techniques font appel à de la chimie localisée via différentes technologies. Une approche consiste à exploiter les différences de réactivités chimiques entre les différents matériaux du substrat et différents groupements chimiques de manière à fonctionnaliser sélectivement chaque matériaux pour former des couches minces organiques de type « Self Assembled Monolayer »: Ce principe proposée par Pr. G. M. Whitesides est appelé chimie orthogonale. Dans le cadre de cette thèse, le but ultime était de réaliser la fonctionnalisation chimique orthogonale de substrats dont la surface était composée de SiO_2/Au/TiW La première étape de ce travail a été de déterminer pour la première fois la fonction chimique la plus adaptée pour la fonctionnalisation de TiW. Pour se faire nous avons comparé la chimie des silanes, des acides phosphoniques et des catéchols. Après caractérisations (XPS, ToF-SIMS, IR) des différentes couches, la voie des acides phosphoniques semblait être celle donnant lieu à la couche la plus stable. Ensuite nous avons étudié l'orthogonalité sur de substrats bi-matériaux (SiO_2/TiW ou Au/TiW), et enfin sur substrat dont la surface était constituée de Au/SiO_2/TiW.

Mots clés: fonctionnalisation chimique orthogonale; chimie des interfaces.